Insights into the role of lipoteichoic acids in *Bacillus subtilis*- a new function for MprF

Aurélie Guyet[1]*, Amirah Alofi[1], Richard A. Daniel[1]*

[1] Centre for Bacterial Cell Biology, Baddiley-Clark Building, Biosciences Institute, Faculty of Medical Sciences, Newcastle University, Richardson Road, Newcastle upon Tyne NE2 4AX, United Kingdom.

*For correspondence Email: aurelie.guyet@newcastle.ac.uk and richard.daniel@newcastle.ac.uk Tel. +44 1912 083239.

Running title: MprF alters lipoteichoic acid production

Abstract

In *Bacillus subtilis,* the cell is protected from the environment by a cell envelope, which comprises of layers of peptidoglycan that maintain the cell shape and anionic teichoic acids polymers whose biological function remains unclear. In *B. subtilis*, loss of all Class A Penicillin-Binding Proteins (aPBPs) which function in peptidoglycan synthesis is conditionally lethal. Here we show that this lethality is associated with an alteration of the lipoteichoic acids (LTA) and the accumulation of the major autolysin LytE in the cell wall. We provide the first evidence that the length and abundance of LTA acts to regulate the cellular level of LytE. Importantly, we identify a novel function for the aminoacyl-phosphatidylglycerol synthase MprF which acts to modulate LTA biosynthesis in *B. subtilis* and in the pathogen *Staphylococcus aureus*. This finding has implications for our understanding of antimicrobial peptide resistance (particularly daptomycin) in clinically relevant bacteria and MprF-associated virulence in pathogens, such as methicillin resistant *S. aureus*.

Keywords: *Bacillus*/ LTA/ LytE/ MprF/ PBP1

13 **Introduction**

14 Gram-positive bacteria have a common cell envelope architecture that contributes to
15 maintaining cell shape and protects the cell from environmental changes. The best
16 characterised component of the cell envelope is the peptidoglycan (PG) which forms a mesh
17 like structure enclosing the cell membrane. Anionic polymers are either covalently attached to
18 PG N-acetylmuramic acids and known as wall-teichoic acids (WTA) or are tethered to the
19 external face of the membrane and named lipoteichoic acids (LTA) (Hanson and Neely, 2012,
20 Percy and Grundling, 2014, Schneewind and Missiakas, 2016, Rajagopal and Walker, 2017).
21 It is unclear whether LTA are localized in a periplasm-like space between the membrane and
22 PG or extend through the PG layers (Neuhaus and Baddiley, 2003, Erickson, 2021).
23 Peptidoglycan is synthetised by glycosyltransferases (GTases) which catalyse the addition of a
24 disaccharide pentapeptide precursor (lipid II), to the nascent PG chain while transpeptidase
25 (TPase) enzymes cross-link a proportion of the pentapeptides to adjacent PG strands (Pazos
26 and Vollmer, 2021, Straume et al., 2021). In the absence of the bifunctional transmembrane
27 GTase and TPase enzymes, known as class A Penicillin-Binding Proteins (aPBPs), *B. subtilis*
28 cells are viable but the cells are longer and thinner and are prone to lysis (McPherson and
29 Popham, 2003, Kawai et al., 2009b). The viability of *B. subtilis* lacking all aPBPs (referred as
30 *Δ4*) depends on the functionality of the essential protein RodA, that was recently identified to
31 function as a PG glycosyltransferase (Meeske et al., 2016, Emami et al., 2017). The *Δ4* strain
32 is conditionally lethal on PAB agar medium unless supplemented with magnesium (Kawai et
33 al., 2009b). It is thought that this divalent cation alters the structure of the wall by binding to
34 teichoic acids or PG and by doing so, might alter the activity of cell wall hydrolases, the
35 enzymes that modify and sculpt synthesised PG to allow the cell to elongate and divide
36 (Neuhaus and Baddiley, 2003, Do et al., 2020, Wilson and Garner, 2021).

37 In rod-shaped *B. subtilis* 168*,* LTA and WTA are composed of polyglycerolphosphate
38 (polyGroP) generated by specific biosynthetic pathways (**Fig 1A**) (Neuhaus and Baddiley,
39 2003, Percy and Grundling, 2014, Schneewind and Missiakas, 2016, Rajagopal and Walker,
40 2017). Importantly, *B. subtilis* is not able to survive the loss of both LTA and WTA synthesis
41 (Schirner et al., 2009) and these teichoic acids have roles in cell separation-division (Schirner
42 et al., 2009, Wormann et al., 2011) and cell elongation (Soldo et al., 2002), respectively. The
43 net anionic charge of these polymers can be altered by D-alanylation, a process proposed to
44 regulate autolysin activity and cell wall ion homeostasis (Neuhaus and Baddiley, 2003,
45 Schneewind and Missiakas, 2016).
46 The teichoic acids located in the wall and the membrane phospholipids produced by MprF both
47 impact on the negative net charge of the bacterial cell envelopes (**Fig 1A**) (Peschel et al., 2001,
48 Slavetinsky et al., 2017). The transmembrane protein MprF is the only enzyme known to
49 synthesise and translocate aminoacyl-phosphatidylglycerol (aaPGol), in particular lysyl-PGol
50 (**Fig 1A**) (Staubitz and Peschel, 2002, Johnson and Grossman, 2016, Atila et al., 2016, Ernst
51 and Peschel, 2019). MprF plays a role in the virulence of bacterial pathogens (Ernst and
52 Peschel, 2019, Nowak et al., 2021) and in *B. subtilis,* it confers resistance against positively
53 charged antimicrobial peptides such as nisin and daptomycin through mechanisms that are not
54 yet characterized (Salzberg and Helmann, 2008, Hachmann et al., 2009).
55 Phosphatidylglycerol is also consumed by LTA-synthases LtaS ('house-keeping'), YfnI
56 ('stress') and YqgS ('sporulation') (Schirner et al., 2009, Wormann et al., 2011) (**Fig 1A**).
57 These transmembrane LTA-synthases have an extracellular catalytic domain that uses PGol to
58 generate a polyGroP polymer on a lipid anchor (Percy and Grundling, 2014, Schneewind and
59 Missiakas, 2016). The lipid anchor is usually a diglucosyldiacylglycerol (Glc_2DAG) produced
60 by UgtP on the internal surface of the cell membrane (Jorasch et al., 1998) (**Fig 1A**). As a *ugtP*
61 mutant still produces LTA (Lazarevic et al., 2005), it suggests that polyGroP polymers are

62 anchored to the lipid diacylglycerol (DAG) as shown in *Staphylococcus aureus ΔugtP*
63 (Grundling and Schneewind, 2007a, Hesser et al., 2020b).
64 In *S. aureus,* LTA is essential and seems to promote autolytic activity (Oku et al., 2009), while
65 WTA is dispensable but appears to restrict autolytic activity (Hanson and Neely, 2012,
66 Rajagopal and Walker, 2017). Contrary to *B. subtilis*, *S. aureus* has only one LTA-synthase
67 (LtaS) whose absence is (conditionally) essential (Coe et al., 2019) and can be complemented
68 by *B. subtilis ltaS* (Grundling and Schneewind, 2007b). A recent *in vitro* study showed that *S.*
69 *aureus* LtaS is processive and that the LTA polymer elongation is directly regulated by the
70 identity and concentration of lipid starter units. The use of Glc_2DAG as a preferred starter unit
71 led to the formation of shorter polymer (Hesser et al., 2020b) while the use of PGol resulted in
72 the synthesis of longer polymers. It is not clear if this mechanism might be conserved in *B.*
73 *subtilis* however, in absence of *B. subtilis* LtaS, YfnI expression and LTA length increase
74 (Wormann et al., 2011, Hashimoto et al., 2013).
75 Through characterising *B. subtilis* strains lacking peptidoglycan GTase activity (Emami et al.,
76 2017), we aimed to understand the cell wall stresses causing aPBP mutants to lyse on glucose
77 rich media. Collectively, our data supports the idea that in *B. subtilis* LTA length acts to
78 moderate the activity of the major autolysin LytE. The presence of glucose increases the
79 expression of LtaS, YfnI, and their activity results in an alteration of LTA production in
80 absence of major PBP1. Crucially, we identify a new role for MprF in altering LTA
81 polymerisation in *B. subtilis* and the pathogen *S. aureus*. Our results reveal that MprF acts to
82 change the cell envelope in a more dramatic way than simply increasing the positive charge on
83 the cell membrane which has implications for understanding the virulence associated to MprF
84 in Gram-positive bacteria.

85 ## Results

86 **MprF alters cell viability in absence of *ponA* or *mbl***

87 In *Bacillus subtilis*, the absence of all aPBPs (*Δ4* for *ΔponA ΔpbpD ΔpbpF ΔpbpG* mutant) is
88 conditionally lethal on glucose-rich PAB agar medium unless supplemented with magnesium
89 (Kawai et al., 2009b, Emami et al., 2017). The suppressive effect of divalent magnesium has
90 been observed in other cell-wall deficient mutants (Murray et al., 1998, Claessen et al., 2008,
91 Kawai et al., 2009b, Schirner et al., 2009) and it is not well understood. To identify the cell
92 wall factors able to suppress *Δ4* lethality, we applied a random transposition mutagenesis to a
93 strain deleted for the vegetative aPBPs (**Tables EV1-3**). Mapping of the transposon in strain
94 SWA11a revealed its insertion in the gene *mprF*, encoding a lysyl-phosphatidylglycerol
95 (LysPGol) synthase known to participate in phospholipids metabolism (**Fig 1A**) (Staubitz and
96 Peschel, 2002, Salzberg and Helmann, 2008). Introduction of a null *mprF* deletion into *Δ4*,
97 confirmed that *Δ4 ΔmprF* was viable on nutrient agar (NA) with glucose and on PAB agar (**Fig
98 1B, Appendix Fig S1A**). In absence of *ponA* encoding the major aPBP (PBP1), the single
99 mutant is viable and yet its growth and the colony morphology is seen to improve in absence
100 of *mprF* (**Fig 1B, Fig EV1**).

101 We reasoned that if MprF activity is detrimental to *Δ4,* its overexpression should be deleterious
102 to *ΔponA*. Indeed, overexpression of MprF (MprF ↑) was lethal to *ponA*-deleted strains on NA-
103 glucose (**Fig 1B**). On NA, both *ΔponA* and *Δ4* strains grew slowly (**Fig 1B**) but no obvious
104 effect was observed for 168CA and *Δ3* aPBPs (i.e. *ΔpbpD ΔpbpF ΔpbpG*). Consistently, the
105 overexpression of MprF caused the cells of *ΔponA* and *Δ4* to lyse in nutrient broth (NB)
106 (**Appendix Fig S1B**).

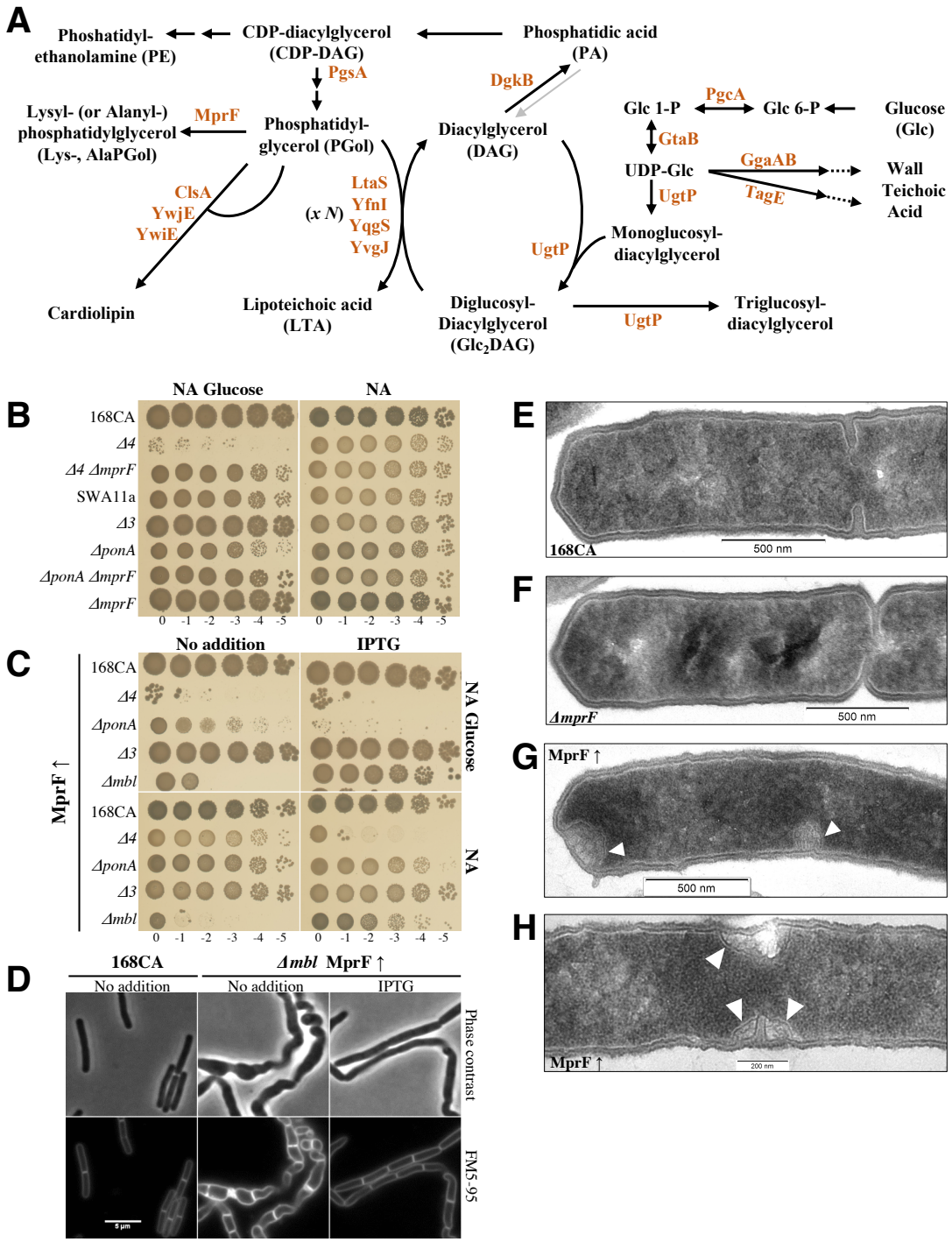

Figure 1. MprF alters cell viability of *B. subtilis* class A PBPs and *mbl* mutants.

A A schematic representation of the biosynthetic links between lipoteichoic acid, phospholipids and glucolipids in *B. subtilis*, adapted from previous studies (Matsuoka et al., 2011, Schneewind and Missiakas, 2016). Lipoteichoic acid (LTA) consist of glycerolphosphate units anchored to the membrane by a glycolipid. In absence of cytoplasmic UgtP, LTA polymer is linked to the membrane by a diacylglycerol (DAG), instead of a diglucosyldiacylglycerol (Glc_2DAG). When grown in LB at 37°C, the majority of *B. subtilis* phospholipids are phosphatidylglycerol (PGol) (37.5% ± 6.2), phosphatidylethanolamine PE (30.5% ± 3.8), Glc_2DAG (9.6% ± 4.7) and lysyl-phosphatidylglycerol (LysPGol, 7.8% ± 3.7) produced by MprF (Matsuoka et al., 2011). Recently, L- and N- succinyl-LysPGol, and also L- and D-AlaPGol were identified in *B. subtilis* (Atila et al., 2016). Grey arrow indicates a reaction step that might be bidirectional.

B Ten-fold spot growth assays of strains *B. subtilis* wild type 168CA, AG157 (*ΔponA ΔpbpD ΔpbpF ΔpbpG* renamed *Δ4*), AG223 (*Δ4 ΔmprF*), SWA11a (*ΔponA ΔpbpD ΔpbpF mprF::TnYLB-1 lacA*), AG417 (*ΔpbpD*

ΔpbpF ΔpbpG renamed *Δ3*), RE101 (*ΔponA*), AG193 (*ΔponA ΔmprF)* and AG181 (*ΔmprF*). Plates (here Glc 1%) were incubated at 37°C for 24 h and images taken.
C The effect of *mprF* overexpression (MprF ↑) is assay in different strain backgrounds using an IPTG-inducible *mprF* construct. Plates (here Glc 1%) were incubated at 37°C for 24 h and scanned. Strains tested were AG304 (MprF ↑), AG317 (*Δ4* MprF ↑), AG311 (*ΔponA* MprF ↑), AG421 (*Δ3* MprF ↑) and AG322 (*Δmbl* MprF ↑).
D Phase-contrast and membrane dye (FM5-95) microscopy images of *B. subtilis* 168CA and AG322 (*Δmbl* MprF ↑) strains grown in NB ± IPTG (0.1 mM) to mid-exponential phase at 37°C. Scale bar indicates 5 µm.
E-H Transmission electron microscopy (TEM) images show cross-sections of (F) wild type 168CA, (G) AG181 (*ΔmprF)* and (H-I) AG304 strain (MprF ↑) grown in nutrient broth (and IPTG for AG304). Arrows indicate abnormal cell wall structures that seem specific to the strain MprF ↑. All images were taken at 15,000x magnification and processed in Fiji with scale bars attached.
Data information. Strains phenotype was tested at least three times, TEM experiment was carried out one time. Supporting information for this figure is presented in **Appendix Figures S1-S3**

107 The identification of *ΔmprF* as a suppressor suggested that increased negative charge on the
108 membrane could contribute to the rescue of *Δ4* growth. This seemed to contradict the long-
109 standing hypothetical role of magnesium in altering the cell envelope by neutralizing anionic
110 polymers and/or autolysis activity (Neuhaus and Baddiley, 2003, Hanson and Neely, 2012). To
111 determine if electrostatic change in the wall was the suppressive effect we deleted *dltAB* in *Δ4,*
112 as the Dlt proteins add positive charges to the LTA polymers by D-alanylation (Perego et al.,
113 1995, Wood et al., 2018). However, the new mutant was unable to grow on glucose rich media
114 (our unpublished observations).
115 To understand if the effect of MprF was specific to *Δ4*, we altered MprF expression in known
116 magnesium dependent mutants. The *B. subtilis Δmbl* mutant requires an elevated level of
117 magnesium for growth compared to *ΔmreB* (**Appendix Fig S2**). MreB, Mbl and MreBH are
118 actin-like isologues which help maintain cell shape by controlling the cell wall synthesis
119 (Kawai et al., 2009a) and the major autolytic enzymes CwlO and LytE (Mbl for CwlO and
120 MreB/BH for LytE) (Dominguez-Cuevas et al., 2013). Interestingly, we identified that MprF
121 overexpression rescued the growth of *Δmbl* on NA-glucose and NA **(Fig 1C**). In addition,
122 morphology defects were less pronounced, changing towards a wide rod-like shape and cell
123 chains were less often twisted (**Fig 1D**).
124 To explain our genetic findings in *Δmbl* background, we had to consider that MprF might play
125 a role in cell wall metabolism. This idea seemed to be supported by our observations made by

126 transmission electron microscopy (TEM) in a wild type background overexpressing MprF (**Fig**
127 **1GH, Appendix Fig S3**). Here cells exhibited an increase in cell wall thickness (e.g. cell poles
128 with a 'dented' shape, lateral walls with septum misplacement), a defect similar to that
129 observed in cell division mutants. However the change in cell morphology of the strain deleted
130 for *mprF* was less significant (**Fig 1F**).
131 Lethality of *B. subtilis* Δ*mbl* is suppressed by the deletion of the major LTA-synthase LtaS
132 (Schirner et al., 2009) and in a single mutant *ΔltaS*, the LTA-synthase YfnI synthesises longer
133 LTA polymers (Wormann et al., 2011). This suggested that the overexpression of MprF in
134 Δ*mbl* has contributed to diminish cellular level of PGol (through a different pathway, **Fig 1A**)
135 (Johnson and Grossman, 2016) or MprF possibly functions in LTA synthesis.

136 **Conditional essentiality of UgtP in the absence of MprF and the Class A PBPs**
137 To comprehend the effect of MprF-loss in a strain lacking aPBPs, we carried out a transposon
138 screen in *Δ4 ΔmprF* pLOSS-P_{spac}-*ponA* strain (Emami et al., 2017) (AG200, **Table EV2**).
139 Strain AG200BK#42 which stabilized the plasmid carried a transposon inserted in the gene
140 *gtaB*. GtaB catalyses a cytoplasmic conversion of Glucose-1-P to UDP-Glc, where the latter
141 ultimately contributes to LTA synthesis and WTA modification (**Fig 1A**). Subsequent
142 mutagenesis in backgrounds *Δ4* and *Δ4 ΔmprF* confirmed the lethal (NA-glucose) and sick
143 (NA) phenotypes in absence of GtaB (**Fig 2A**).
144 To determine if this was related to LTA synthesis or WTA modification, we deleted
145 sequentially, in the *Δ4* or *Δ4* pLOSS-P_{spac}-*ponA* backgrounds, each enzyme whose function is
146 immediately upstream or downstream of GtaB (**Fig 1A)**. Characterisation of the resulting
147 strains (**Table S2**) showed that only deletion of *ugtP*, the enzyme which produces the Glc_2DAG
148 lipid anchor for LTA, had a similar effect to that of *gtaB*. Strain *Δ4 ΔmprF ΔugtP* was unable
149 to grow on NA glucose (**Fig 2A**), a phenotype common to *ΔponA ΔgtaB* and *ΔponA ΔugtP*
150 (**Appendix Fig S4**). On NA, *Δ4 ΔgtaB* and *Δ4 ΔugtP* grew very slowly (**Fig 2A,** right panel).

151 LysPGol content increases in *ΔugtP* cells (Johnson and Grossman, 2016) which could explain

152 the similarity of phenotype of *Δ4 ΔugtP* and *Δ4* MprF ↑ (i.e. slow growing on NA) but not the

153 dominant effect of *ΔugtP* on *Δ4 ΔmprF.* In *S. aureus,* it has been observed that *ΔugtP* (*ypfP*)

154 and *ΔgtaB* mutants produce long LTA (Grundling and Schneewind, 2007a). Thus this context

155 and our results reinforced the idea that MprF may have a role in LTA synthesis.

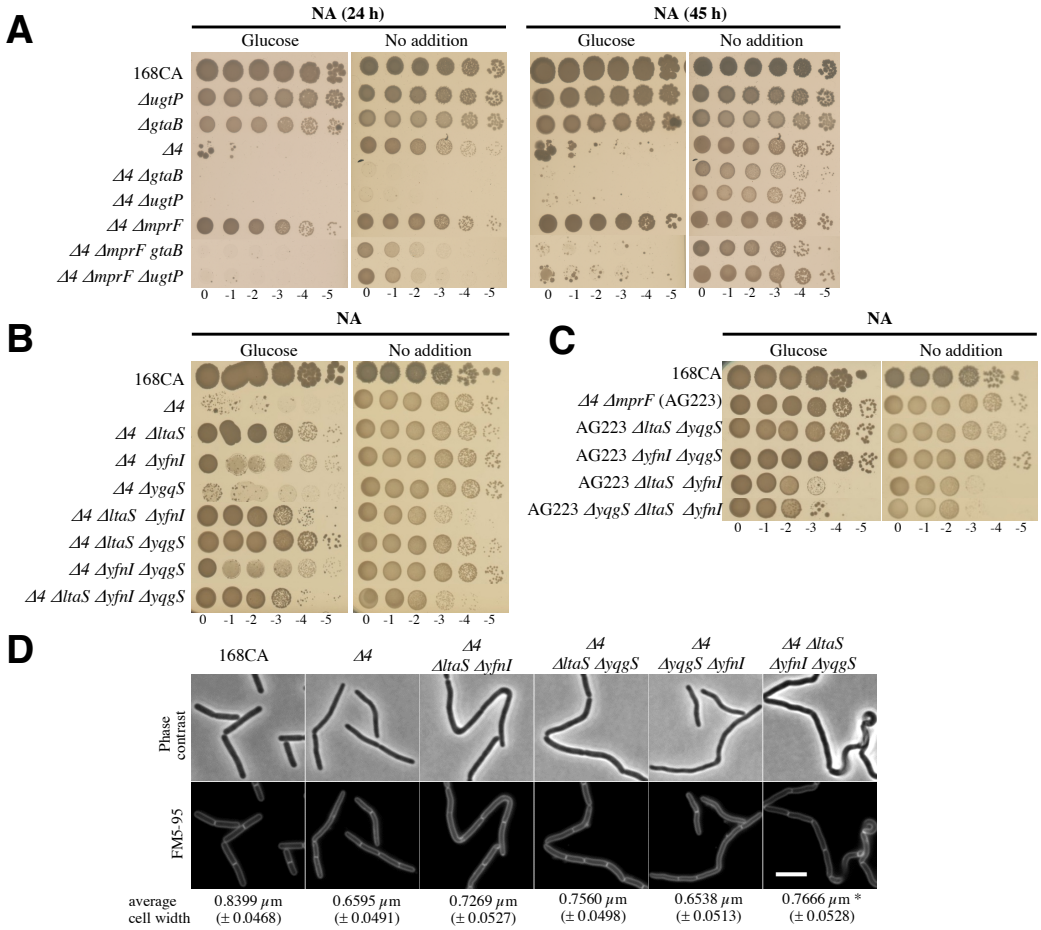

Figure 2. LtaS causes cell morphogenesis defect of an all-class A PBP mutant.

A Absence of *gtaB* or *ugtP* causes severe growth defect in absence of class A PBPs and MprF. Strains were grown exponentially in NB with 20 mM $MgS0_4$, then were washed and diluted in NB prior to preparing a 10-fold serial dilution in NB spotting on the NA and NA glucose (0.5%) plates which were incubated at 37°C and imaged after 24 h and 45 h. Strains were also spotted on same media supplemented with 10 mM $MgS0_4$ to confirm all the strains dilution spots could grow, at 17 h of incubation only *Δ4 ΔgtaB* and *Δ4 ΔugtP* displayed colonies of smaller size at that time point (data not shown). Strains tested: *B. subtilis* wild type (168CA), PG253 (*ΔugtP*), SM08 (*ΔgtaB*), AG157 (*Δ4*), AG290NopLOSS (*Δ4 ΔgtaB*), AG443 (*Δ4 ΔugtP*), AG223 (*Δ4 ΔmprF*), AG636 (*Δ4 ΔmprF gtaB::TnYLB-1*) and AG632 (*Δ4 ΔmprF ΔugtP*).

B Spot dilution growth assays for the following strains: *B. subtilis* wild type 168CA, AG157 (*Δ4*), AG342 (*Δ4 ΔltaS*), AG343 (*Δ4 ΔyfnI*), AG344 (*Δ4 ΔyqgS*), AG370 (*Δ4 ΔltaS ΔyfnI*), AG372 (*Δ4 ΔltaS ΔyqgS*), AG377 (*Δ4 ΔyfnI ΔyqgS*) and AG380 (*Δ4 ΔltaS ΔyfnI ΔyqgS*). Samples were inoculated onto NA ± Glc 1% and, incubated at 37°C for 24 h.

C Ten-fold serial dilutions were prepared for *B. subtilis* wild type 168CA, AG223 (*Δ4 ΔmprF*), AG389 (AG223 *ΔltaS ΔyqgS*), AG390 (AG223 *ΔyfnI ΔyqgS*), AG399 (AG223 *ΔltaS ΔyfnI*) and AG400 (AG223 *ΔyqgS ΔltaS ΔyfnI*) strains. Plates (here Glc 1%) were incubated at 37°C and imaged after 24h.

D Representative microscopy images of cells of strains of (A) grown in NB at 37°C for 120 min and stained with a FM5-95 dye. Scale bar represents 5 µm. The average of cells diameter extracted from **Appendix Figure S5** is indicated. * The cells measurement was done on the straight regions of the cell chain.
Data information: Strains phenotype was tested at least three times. Supporting information is presented in **Appendix Figure S4-S6**. **Appendix Figures S4, S6** displayed results obtained in *ΔponA* background.

156 **Growth of a strain lacking all aPBPs mutant improves in absence of LtaS**

157 To verify that LTA synthesis alters *Δ4* growth, we analysed the phenotype of strains lacking
158 aPBPs and the LTA-synthase genes individually or in combination (**Fig 1A**). Surprisingly, the
159 *Δ4 ΔltaS* mutant was viable on NA-glucose as well as with the additional deletion of *yfnI* or
160 *yqgS* (**Fig 2B**). Thus, LtaS activity is also linked to the glucose-associated lethality of *Δ4.*
161 Interestingly, the absence of MprF is more advantageous to *Δ4,* as it results in a faster growth
162 and larger colonies formed on NA-glucose compared to *Δ4 ΔltaS* (**Fig EV1**). This phenotype
163 difference indicated that slightly different mechanisms helped restore the growth of *Δ4*.
164 To test this, LTA-synthase genes were systematically deleted in the *Δ4 ΔmprF* (AG223)
165 background and the viability of the strains generated determined on NA with or without
166 glucose. All the strains remained viable on NA glucose (**Fig 2C**) which indicated the effect of
167 MprF loss could be related to LTA. In support of this, in the *Δ4 ΔmprF* background the
168 combined absence of *ltaS* and *yfnI* delayed growth on NA glucose resulting in a phenotype
169 similar to that observed on NA (**Fig 2C)**. Thus, in these specific genetic backgrounds LTA
170 synthesis is not essential but desirable for cell growth.
171 Neither absence of LtaS or MprF has an effect on the filamentous thin cell morphology of *Δ4*
172 (**Appendix Fig S5**) but cell lysis is significantly decreased in NB. In the absence of all LTA-
173 synthases, *Bacillus* is viable but the strain forms filamentous and clumpy cells (Schirner et al.,
174 2009). We observed that the combined absence of LtaS, YfnI and/or YqgS in *Δ4, ΔponA* or *Δ4*
175 *ΔmprF* genetic backgrounds lead to an increase in cell diameter and cells remained attached at
176 the site of division (**Fig 2D, Appendix Fig S5-6**). However, when LtaS was the only functional
177 LTA-synthase (e.g. *Δ4 ΔyqgS ΔyfnI*, **Fig 2D**), cells were thin and comparable to *Δ4* and the

178 *ΔponA* background (**Appendix Fig S6**). Collectively, our results indicate that LtaS activity
179 accounts for the conditional lethality of *Δ4*.

180 **Impact of glucose, PBP1 and MprF on LTA synthesis.**

181 To comprehend the effect of LtaS, MprF and UgtP in the absence of aPBPs we decided to
182 analyse LTA production. We developed a Western blot protocol relying on commercially
183 available Gram-positive monoclonal LTA and polyclonal PBP2B antibodies. First we
184 determined the LTA profile for 168CA and the LTA-synthases mutants (**Fig 3A** and **Appendix**
185 **Fig S7**) grown in parallel in NB and in NB glucose (0.2%). The wild type LTA signal
186 corresponded to a mobility comparable to 7-17 kDa as previously identified (Wormann et al.,
187 2011). Interestingly, our media comparison showed that LTA-signal in *ΔltaS* cells grown in
188 NB-glucose (> 15 kDa) (**Fig 3A** left panel, 2nd lane) was distinct from that seen for growth in
189 NB (7-32 kDa) (**Fig 3A** right panel, 2nd lane). However, the LTA pattern was different when
190 YfnI was the only functional LTA-synthase (**Fig 3A**). From this analysis, short LTA (<10 kDa)
191 were more abundantly produced in NB-glucose presumably through LtaS activity, as we
192 observed an increase in short LTA in *ΔyfnI* and *ΔyfnI ΔyqgS* mutants compared to 168CA (**Fig**
193 **3A** left panel, 3rd & 5th lanes). Collectively, our results show that the regulation of LTA
194 synthesis is more complex than thought (Wormann et al., 2011) as it alters in presence of
195 glucose.

196 As the *mprF* mutation suppressed the *ΔponA* phenotype (**Fig 1B, Fig EV1, Appendix Fig 6A**)
197 we reasoned that any alteration of LTA synthesis would be detectable in a strain where only
198 the major aPBP was deleted. Moreover, *ΔponA* is impaired but viable on NA-glucose (0.5%),
199 whereas the multiple aPBP deletion strain was very lytic and did not grow under these
200 conditions (**Fig EV1**). Thus, we settled to work in *ΔponA* background and using NB glucose
201 0.2% for growth of samples for the Western blot analysis. This revealed that there was an

202 increase of short LTA in *ΔponA* cells grown in the presence of glucose (**Fig 3B** left panel, 3rd
203 lane, **Appendix Fig S8**). The LTA signal of *ΔponA ΔmprF* decreased compared to *ΔponA* (**Fig**
204 **3B** left panel, 5th lane) and the *ΔmprF* mutant in NB-glucose (**Fig 3B** left panel, 4th lane)
205 decreased compared to 168CA. However, we found that *mprF* overexpression (MprF ↑) had a
206 significant effect, increasing LTA polymer length (6th lane in **Fig 3B)**. This effect was
207 independent of YfnI, as a similar LTA profile was observed in a strain *ΔyfnI* MprF ↑ (our
208 unpublished observations, strain AG353 in **Table EV2**). The overexpression of *mprF* in *ΔponA*
209 cells, which resulted in lysis on NA-glucose (**Fig 1C**), resulted in LTA-signals that
210 corresponded to the sum of the effects of the two mutations (7th lane in **Fig 3B**).
211 Interestingly, our analysis showed that LTA production is altered in *Δmbl*, as we observed a
212 weak, short LTA-signal (second to last lane **Fig 3B**). Previously, we found that overexpression
213 of MprF rescued *Δmbl* growth (**Fig 1C**) and here we identified that it is associated to an increase
214 in LTA length and abundance (last lane **Fig 3B**). Consistently, we observed the production of
215 long LTA polymers in the suppressor strain *Δmbl ΔltaS* (our unpublished observations)
216 (Schirner et al., 2009) similar to that of *ΔltaS* (**Fig 3A**). Thus an increase in LTA length seems
217 to characterize the effect of these two *Δmbl* suppressor mutations.
218 Analysis of the suppressor *ΔltaS ΔponA* revealed the dominant effect of *ltaS* deletion, in that
219 the LTA exhibited a retarded migration (3rd lanes in **Fig 3C, Appendix Fig S9**), similar to that
220 observed in *ΔltaS* (**Fig 3C**). In absence of UgtP which produces a lipid anchor Glc_2DAG (**Fig**
221 **1A**), we observed an increase in LTA length in both media conditions, but the shift was more
222 distinct in glucose (>12 kDa, left panel 4th lane in **Fig 3C**). The latter is comparable to the LTA
223 signal detected in the *S. aureus ΔugtP* mutant grown in TSB, a glucose rich medium (Grundling
224 and Schneewind, 2007a). Analysis of *ΔponA ΔugtP,* which was conditionally lethal on NA-
225 glucose (**Appendix Fig S4**), revealed an increase of the LTA-signals and length (7-25 kDa, left

226 panel 5th lane, **Fig 3C**), a pattern reminiscent of that determined for *ΔponA* MprF↑ strain, which

227 was lethal on NA-glucose (left panel 7th lane in **Fig 3B**, **Fig 1C**).

228 To conclude we show the first evidence that MprF activity has a role in altering the length of

229 LTA, through a LtaS-dependent mechanism and has an impact on cell wall metabolism. Our

230 results highlight that the conditions leading to the lethality of *ponA* are associated with an

231 increase in the abundance and the length of LTA.

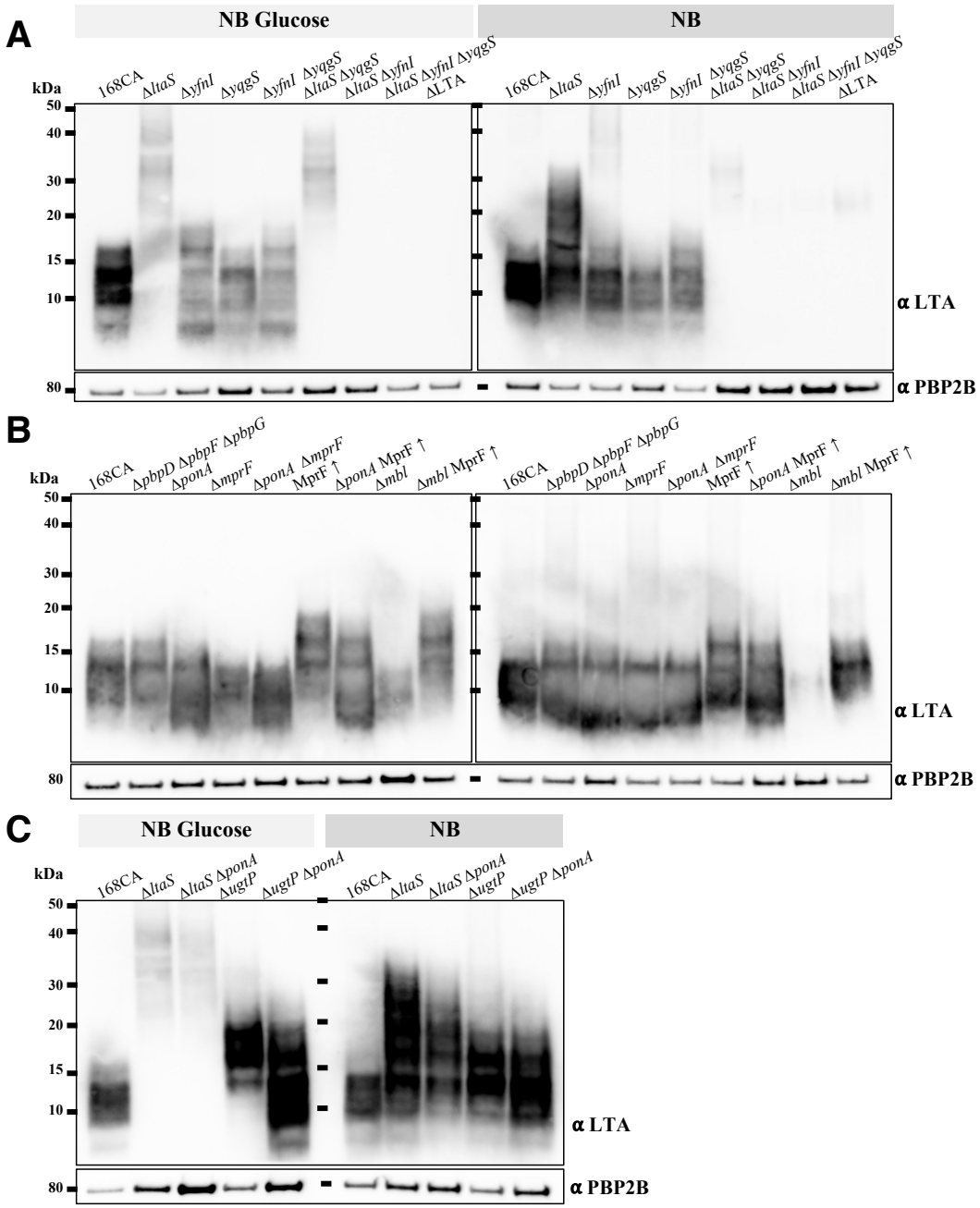

Figure 3. Analysis of lipoteichoic acid production in *B. subtilis* strains.

For each set of cultures (NB ± Glc 0.2%), samples were separated on the same Bis-Tris gradient gel. Membrane was split at ~ 60 kDa position. The lower part of the membrane was probed using a monoclonal LTA antibody and an HRP-linked anti-mouse antibody. The other membrane part was probed using polyclonal anti-PBP2B and HRP-linked anti-rabbit antibodies, to provide a sample loading control.
A Samples were prepared from strains *B. subtilis* wild type (168CA), 4285CA (*ΔltaS*), 4289CA (*ΔyfnI*), 4292CA (*ΔyqgS*), AG595 (*ΔyfnI ΔyqgS*), AG593 (*ΔltaS ΔyqgS*), AG594 (*ΔltaS ΔyfnI*), AG600 (*ΔltaS ΔyfnI ΔyqgS*) and 4620 (*ΔltaS ΔyfnI ΔyqgS ΔyvgJ*, noted here ΔLTA).
B Strains analysed: *B. subtilis* wild type, AG417 (*ΔpbpD ΔpbpF ΔpbpG*), RE101 (*ΔponA*), AG181 (*ΔmprF*), AG193 (*ΔponA ΔmprF*), AG304 (MprF ↑), AG311 (*ΔponA* MprF ↑), 4261CA *(Δmbl),* AG322 *(Δmbl* MprF ↑).
C Samples were extracted from *B. subtilis* 168CA, 4285CA (*ΔltaS*), AG383 (*ΔltaS ΔponA*), PG253 (*ΔugtP*) and AG444 (*ΔugtP ΔponA*) strains.
Data information: Representative of one of three independent experiments shown in **Appendix Figures S7-S9.** At each section A, B, C, samples were derived from the same experiment.

Overexpression of major autolysin LytE is lethal in absence of PBP1 or LtaS

Our results inferred that the conditional lethality of aPBPs mutant might be linked to an interplay between LTA length and autolysin activity. Autolysins or cell wall hydrolases help shape and recycle the peptidoglycan during cell elongation and division. *B. subtilis* expresses a larger number of them but only the loss of both PG D,L-endopeptidases CwlO and LytE is lethal (Hashimoto et al., 2012, Salzberg et al., 2013, Dobihal et al., 2019, Do et al., 2020, Wilson and Garner, 2021). Our interest in LytE derived from the facts that this major autolysin is secreted and thought to be anchored to the lateral cell wall and the septum (Dominguez-Cuevas et al., 2013). LytE abundance also increased in *ΔltaS* (Kasahara et al., 2016) and both LtaS and LytE affect colony development (Mamou et al., 2017) and cell diameter (Schirner et al., 2009, Dominguez-Cuevas et al., 2013).

We reasoned that if an imbalance of LytE activity existed in the aPBPs mutants (*Δ4* and *ΔponA*) grown in glucose-rich medium, then a deliberate increase in LytE expression should exacerbate the strain phenotype, leading to cell death. Interestingly, LytE overexpression (by IPTG induction of a $P_{hyspank}$-*lytE* allele) was found to be lethal to *ΔponA* on NA-glucose and it significantly delayed the growth of *Δ4* and *ΔponA* on NA but not that of *Δ3 ponA+* (**Fig 4A, Appendix Fig S10**). This result confirmed that an imbalance in autolytic activity was detrimental to the cell that had lost PBP1. Importantly, the overexpression of *lytE* in the *Δ4*

250 *ΔltaS, ΔponA ΔltaS* and *ΔltaS* strains was lethal, while the *Δ4 ΔmprF* and *ΔponA ΔmprF* strains

251 grew slowly (**Fig 4A**) but no change was observed for the *ΔmprF* background.

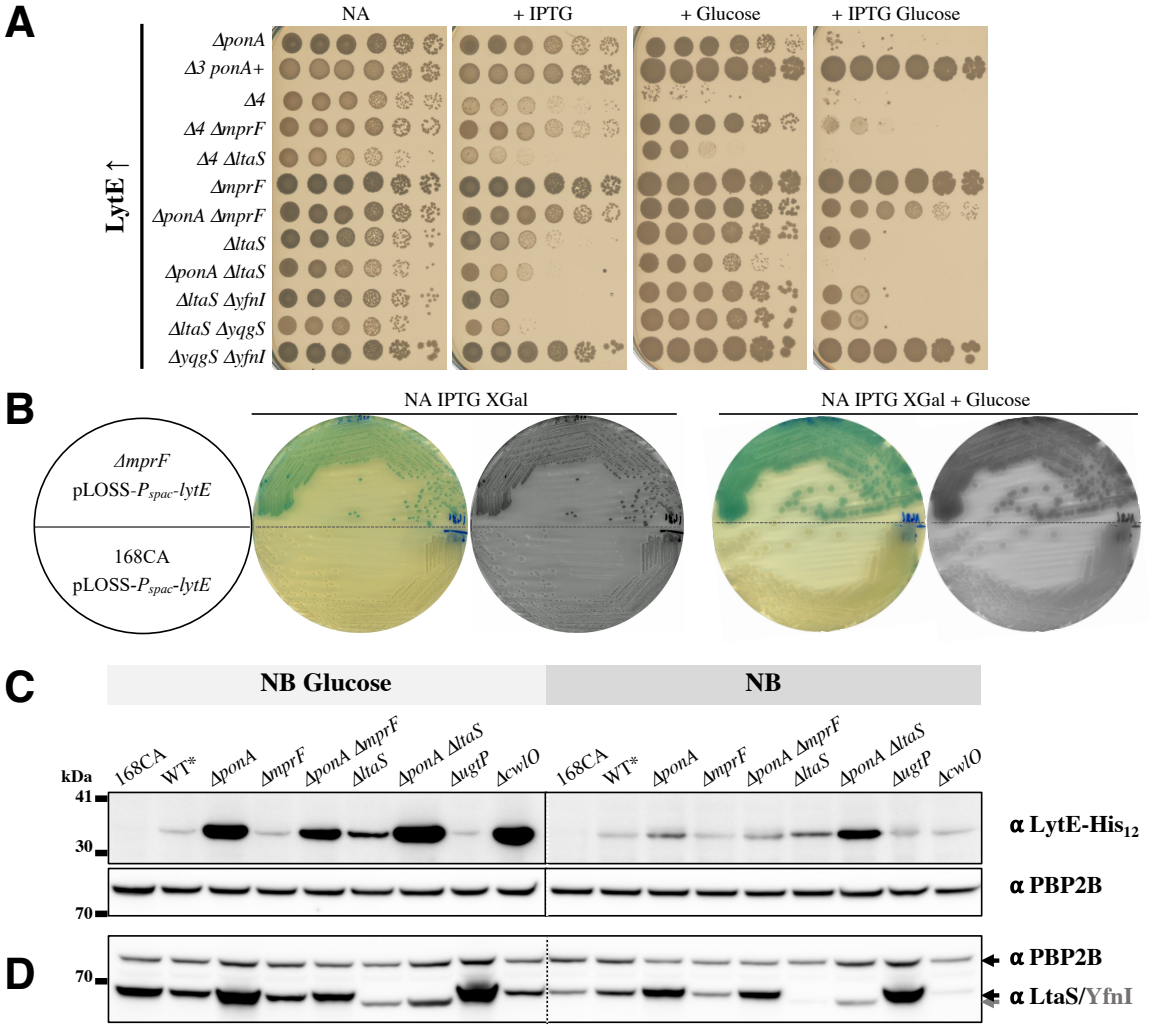

Figure 4. LytE overexpression is conditionally lethal in absence of PBP1 or LtaS.

A *lytE* overexpression was analysed in strains which integrated at the *amyE* locus an (0.1 mM) IPTG-inducible $P_{hyspank}$-*lytE,* represented here LytE ↑. The strains tested had the following relevant features: AG484 (*ΔponA* LytE ↑), AG1460 (*Δ3 ponA*$^+$ LytE ↑), AG501 (*Δ4* LytE ↑), AG502 (*Δ4 ΔmprF* LytE ↑), AG1465 (*Δ4 ΔltaS* LytE ↑), AG1478 (*ΔmprF* LytE ↑), AG1479 (*ΔponA ΔmprF* LytE ↑), AG1462 (*ΔltaS* LytE ↑), AG1480 (*ΔponA ΔltaS* LytE ↑), AG1497 (*ΔltaS ΔyfnI* LytE ↑), AG1498 (*ΔltaS ΔyqgS* LytE ↑) and AG1499 (*ΔyqgS ΔyfnI* LytE ↑). The following strains that did not display any obvious phenotype are not represented here: AG475 (168CA LytE ↑), AG1461 (*ΔlytE* LytE ↑), AG1463 (*ΔyfnI* LytE ↑), AG1492 (*ΔyqgS* LytE ↑). Plates (here Glc 0.5%)were incubated at 37°C and scanned after 24 h (this figure) and 48 h (**Appendix Figure S10**).
B Strains AG1481 (*ΔmprF* pLOSS-P_{spac}-*lytE*) and AG551 (168CA pLOSS-P_{spac}-*lytE*) were streaked on NA and NA glucose (Glc 0.5%), supplemented with IPTG (1 mM) and X-Gal from a fresh colony on NA spectinomycin. Plates were incubated at 37°C and scanned after 24 h. Blue colonies indicate the stabilisation of plasmid pLOSS-P_{spac}-*lytE* in *ΔmprF*. Grey scale images are here to help visualize white colonies.
C Detection of LytE-His$_{12}$ and PBP2B by Western blots. For simplification on this figure only the relevant background feature is displayed for the following strains (expressing LytE-His$_{12}$ under the control of its native promoter): wild-type-like AG565 (WT*), AG587 (*ΔponA*), AG1486 (*ΔmprF*), AG1487 (*ΔponA ΔmprF*), AG1489

(Δ*ltaS*), AG1488 (*ΔponA ΔltaS*), AG1535 (*ΔugtP*) and AG1541 (*ΔcwlO*). In addition, *B. subtilis* 168CA was grown in parallel (without antibiotic) and used here as a negative control for the LytE-blot. The membrane was split and incubated either with a monoclonal Penta-His and an HRP-linked anti-mouse antibodies or with a polyclonal anti-PBP2B and HRP-linked anti-rabbit antibodies. Note: a 'ladder' sample loaded after the NB-Glc (0.2%) sample set is not displayed and the image editing is symbolised by the vertical black line (see original on **Appendix Fig S11B**).
D Detection of LTA-synthases LtaS/YfnI and PBP2B by Western blots. The samples used in experiment A were loaded on a new SDS-gel and the Western blot was carry out with polyclonal anti-LtaS (able to detect YfnI, unpublished Errington's lab), anti-PBP2B antibodies, and HRP-linked anti-rabbit antibody.
Data information: One representative set of three independent Western Blot experiments is shown here and in **Appendix Figures S11-12**. Additional supporting information is presented in **Fig EV2-3** and **Appendix Figure S13**. At each section samples were derived from the same experiment.

252 This finding suggested that *ΔponA ΔltaS* and *ΔponA ΔmprF* mutants, which have distinct LTA
253 length, were differently sensitive to LytE activity. Therefore, we examined the double LTA-
254 synthase mutant backgrounds, here we found that only the strain expressing *ltaS* was viable
255 when LytE was overexpressed (**Fig 4A,** last strain). In these genetic backgrounds, the absence
256 of *mprF* or *ugtP* had no effect (our unpublished observations). Interestingly, *ΔltaS* LytE ↑ was
257 viable on NA (**Fig 4A,** 8th strain) but not on NA-glucose while we previously identified that
258 *ΔltaS* produces distinct LTA length on each of these media (**Fig 3A**). Thus, it is clear that the
259 activity of LtaS, presumably the presence of a specific LTA length, is required for the cell to
260 balance the effect of overexpression of *lytE*.
261 To comprehend the apparent tolerance of LtaS$^+$ and *ΔmprF* cells to LytE, we constructed an
262 unstable replicon pLOSS-P_{spac}-*lytE* plasmid which expresses *lytE* at a level lower than $P_{hyspank}$-
263 *lytE* (**Table EV1**). Introducing this plasmid into *ΔmprF* resulted in better stability of the
264 plasmid in all media conditions tested (AG1481 strain), including elevated magnesium. This
265 was indicated by the fact that the colonies remained blue on IPTG XGal supplemented media
266 (**Fig 4B**) whereas other strains tested showed no effect (e.g. 168CA, *ΔponA* and LTA-synthases
267 mutants, **Table EV2**) . At this stage, it is unclear if the *ΔmprF* strain's tolerance for *lytE*
268 overexpression is due to the loss of aaPGols or the production of shorter LTA or both.

269 **LTA influences LytE activity**

270 The conditional lethality observed when overexpressing *lytE* prompted us to investigate the
271 cellular levels of this autolytic enzyme in our strains. First, we engineered strains that could
272 express a recombinant protein LytE-LEMGRSH$_{12}$ (using pMUTin-*'lytE-his,* **Table EV1**) and
273 then analysed total lysates by Western blot using anti-histidine (for LytE) (**Fig 4C, Appendix**
274 **Fig S11**) or an anti-LtaS antibody raised against LtaS (74 kDa) that cross reacts with YfnI (73
275 kDa) (**Fig 4D, Appendix Fig S12**). Importantly, our results showed that LytE and LtaS/YfnI
276 accumulate in *ΔponA* cells, particularly when grown in presence of glucose (**Fig 4C-D**). Using
277 a set of strains that has integrated either pMUTin-*'ltaS-his* or pMUTin-*'yfnI-his,* we could
278 confirm that both LtaS and YfnI are more abundant in *ponA* cells (**Fig EV2, Tables EV1-3**).
279 In *ΔponA ΔmprF*, LytE and LtaS/YfnI protein levels decreased compared to *ΔponA* (**Fig 4C-**
280 **D**). No obvious change was observed in the wild-type background (WT*) and *ΔmprF* strains.
281 *ΔltaS* and *ΔponA ΔltaS* exhibited an increase in LytE and YfnI when grown in NB-glucose, an
282 effect more pronounced in the *ΔponA ΔltaS* mutant (**Fig 4C-D**, left panel). In addition,
283 comparative analysis of the whole set of LTA-synthase mutants (**Fig EV3**) revealed that
284 LtaS/YfnI signal increased in presence of glucose. In the absence of YfnI, LtaS increased
285 significantly and more importantly LytE abundance increased in the absence of LtaS.
286 To corroborate that the altered abundance of these proteins, identified in *ΔponA* cells, were
287 associated with the sick phenotype, we analysed the strains that were lytic under the same
288 growth conditions as **Fig 4C**. Our result show that there is an excess of LtaS/YfnI in *ΔponA*
289 *ΔugtP* and *ΔponA* MprF ↑ cells in NB and NB-glucose (**Appendix Fig S13 B-C,** e.g. 6-7th
290 lanes**)** and that LytE signal is higher than the wild type.
291 Finally, we looked at the effect of magnesium in presence of glucose as this cation suppresses
292 the growth defect of aPBP mutants (Kawai et al., 2009b). Our analysis showed that magnesium
293 decreased the abundance of LytE significantly in *ΔponA* and *ΔponA ΔmprF* (**Appendix Fig**

294 **S13**) but not as much in *ΔponA ΔltaS.* Perhaps, the unknown mechanism by which exogenous
295 magnesium helps the growth of some cell wall mutants might partially require LtaS activity to
296 tune LytE (Wilson and Garner, 2021).
297 Taken together, our results show a correlation between LTA length and LytE abundance in the
298 cell which suggest that LTA acts to moderate cell wall metabolism. In *ponA* mutants, this
299 function is unbalanced such that cell wall degradation is predominant.

300 **LTA production is altered in *S. aureus ΔmprF* and *Bacillus* daptomycin resistant strains**
301 MprF is conserved in the *Firmicutes* and has been shown to contribute to *S. aureus*
302 pathogenicity (Peschel et al., 2001, Slavetinsky et al., 2017). Importantly, studies of clinical
303 isolates have found that methicillin-resistant *S. aureus* strains (MRSA) resistant to daptomycin
304 (Dap^R) frequently carry nucleotide polymorphisms (SNPs) in *mprF* (Friedman et al., 2006,
305 Ernst et al., 2018). The active Ca^{2+}-Dap lipopeptide antibiotic is often used as last resort in the
306 treatment of MRSA infections and acts to interfere with membranes containing
307 phosphatidylglycerol (Muller et al., 2016, Ernst and Peschel, 2019, Gray and Wenzel, 2020,
308 Grein et al., 2020). Although some *mprF* SNPs were associated with a MprF gain of function
309 (increased Lys-PGol and decreased PGol contents), others had no clear correlation between the
310 phospholipids composition and their relative cell surface charge (Ernst and Peschel, 2019). In
311 that context, we asked whether the role of MprF in LTA production is conserved in *S. aureus*
312 and could shed new light in Dap^R MRSA. Analysis of LTA production in methicillin sensitive
313 *S. aureus* strains showed that the LTA from the *mprF* mutant migrated faster than that of the
314 wild type SA113 (**Fig 5A, Fig EV4A**). Thus, a role of MprF in modulating LTA production is
315 conserved across the studied *Firmicutes* species.
316 We, therefore, turned our interest to the Dap^R *B. subtilis* strain that carries a *pgsA A64V* allele
317 (Hachmann et al., 2011). This mutation of the essential gene *pgsA* encoding the PGol-synthase

318 (**Fig 1A**), is shown to reduce cellular PGol content and was suggested to modify LTA
319 production. Thus, we analysed LTA of *B. subtilis* 168 1A1 wild type (WT), Dap^R and Dap^R
320 *pgsA*^{WT} strains grown overnight in NB **(Fig 5B, Fig EV4 B-D)**. Our assays revealed that no
321 LTA signal was detected below 30 kDa in Dap^R strains whereas LTA signals migration
322 detected in the strains complemented for *pgsA* (Dap^R *pgsA*^{WT}) were similar to that of the wild
323 type. Thus, PgsA A64V accounts for the severe reduction in LTA production. Finally, we
324 verified that the two major LTA-synthases were still produced in Dap^R strains by Western blot
325 (**Fig 5C, Fig EV4 B-D**). A strong LtaS/YfnI signal was detected in Dap^R strains which proved
326 that one or both LTA-synthases were still expressed. In addition to the altered membrane
327 composition, the severe reduction in LTA production could also act to reduce susceptibility to
328 daptomycin.

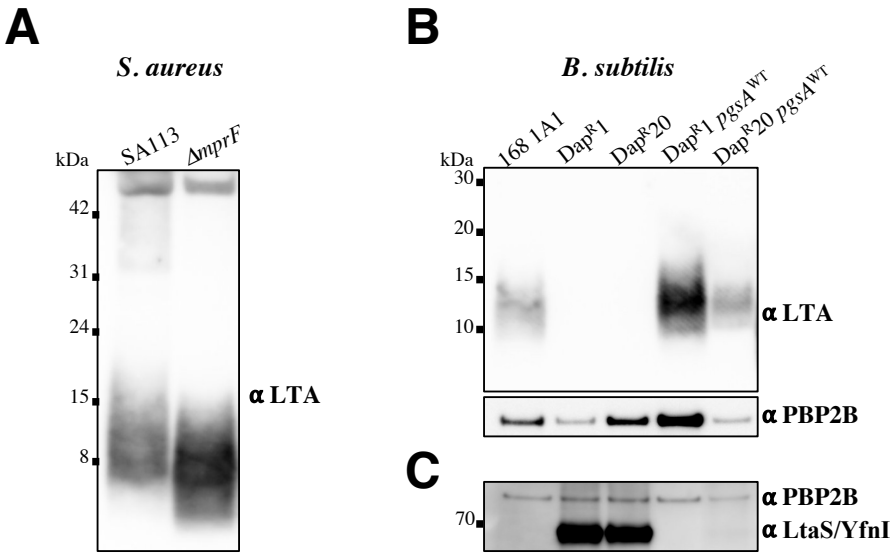

Figure 5. Altered LTA in *S. aureus* SA113 Δ*mprF* and in *B. subtilis* daptomycin resistant strains.

A Samples of methicillin-sensitive *Staphylococcus aureus* strains SA113 and SA113 *ΔmprF* (Peschel et al., 2001) were probed for LTA by Western Blot.
B Researchers identified that a modified allele of *pgsA*(*A64V*) was the major determinant of daptomycin resistance of *B. subtilis* Dap^{R}1 and Dap^{R}20 strains selected by serial daptomycin antibiotic passages (Hachmann et al., 2011). The strains 168 1A1 (wild type, WT), Dap^{R}1, Dap^{R}20, HB15516 (Dap^{R}1 *pgsA*^{WT}) and HB15507 (Dap^{R}20 *pgsA*^{WT}) were grown in NB overnight at 30°C and LTA was detected along with PBP2B productions by Western Blots. Analysis of the samples grown exponentially at 37°C using theses overnight cultures is presented in **Fig EV4**.
C shows the cellular abundance of the LTA-synthase with anti-LtaS (able to detect YfnI, unpublished Errington's lab), an anti-PBP2B and an HRP-linked anti-rabbit antibodies.
Data information: One representative set of three experiments is shown here and in **Fig EV4**.

329 **Discussion**

330 In absence of the class A PBPs (*Δ4*), *B. subtilis* is viable due to the presence of RodA, the
331 essential PG glycosyltransferase (controlled by the cell envelope stress regulator σ^M (Meeske
332 et al., 2016, Emami et al., 2017)) and yet lethal on glucose rich medium (**Fig 1B, Fig EV1**).
333 By studying either *Δ4* or *ΔponA* single mutant, we now understand that glucose presence led
334 to an increase in abundance of LtaS, YfnI (LTA-synthases) presumably causing the observed
335 change in LTA production that results in the accumulation of major autolysin LytE (**Fig 3-4**).
336 The end result being an environment unable to regulate the activity of autolysins leading to cell
337 lysis. Indeed, we have found that *Δ4* can grow on NA-glucose in the absence of LtaS or the
338 absence of MprF (**Fig 1B, 2B**). In *ΔponA,* loss of LtaS lead to the production of very long LTA
339 polymers similar to the single *ltaS* mutant (**Fig 3C**). The *ltaS* mutation is not as beneficial for
340 the growth of *Δ4* strain compared to *ΔmprF* (**Fig EV1**), which we observed reduced LTA
341 production in *ΔponA* background (**Fig 3B**). This is consistent with our finding that an increase
342 in length and abundance of LTA (overexpression *mprF*, *ΔugtP*) and/or an increase in LytE
343 coincide with glucose-mediated lethality in *ΔponA* (**Fig 1C, 3, 4A, Appendix Fig S13 B-C**).
344 The analysis of LTA-synthases mutants indicates that LtaS activity and a distinct LTA length
345 (7-17kDa) and/or abondance similar to the wild type LTA is required to prevent cell lysing
346 when *lytE* is artificial overexpressed (**Fig 4A**). Indeed, a LTA signal (7-20 kDa) is present in
347 the mutant *ΔltaS* in NB but not in NB-glucose (long LTA > 20 kDa) (**Fig 3A**) and it happens
348 that the strain *ΔltaS* LytE ↑ is unable to grow on NA-IPTG-glucose (**Fig 4A**). Moreover, the
349 mutants *ΔltaS ΔyqgS* (long LTA-only) and *ΔltaS ΔyfnI* (weak short LTA signal, **Fig 3A**) were
350 unable to grow on both media when *lytE* was overexpressed (**Fig 4A**).
351 Previous studies have suggested that LTA could inhibit autolysins activity (Neuhaus and
352 Baddiley, 2003, Hanson and Neely, 2012) but the key factors involved have not been identified.

353 Recent work in *S. aureus* showed a *ΔugtP* mutant producing long LTA is susceptible to PG
354 hydrolases (Hesser et al., 2020a) and it has been suggested that major autolysin LytA is
355 sequestered by LTA in exponential growth (Flores-Kim et al., 2019). Our results indicate that
356 LytE in *B. subtilis* exhibits similar characteristics and that the length of LTA has a role in
357 modulating LytE abundance or presumably its activity. However it is unclear how this
358 mechanism may work in relation to the localisation of the LTA in the wall relative to active
359 autolysins, particularly LytE, and remain an important question to answer.
360 In *B. subtilis* 168, expression of *lytE* is quite complex and coordinated by regulators such as σ^I
361 and WalR (Dobihal et al., 2019, Patel et al., 2020). The transcriptional regulation of *mprF* is
362 not well defined, but interestingly *B. subtilis* BSB1 *mprF* and *pgsA* expression is positively
363 correlated with that of *walKR,* the two-component response system that controls cell wall
364 metabolism, and notably *lytE* (Nicolas et al., 2012, Zhu and Stulke, 2018) (cluster A418).
365 Expression of *walKR* and *sigI* is not significantly altered in LB-glucose (Nicolas et al., 2012)
366 or in the absence of aPBPs (Emami et al., 2017) but theses regulators might play a post-
367 transcriptional role in *Δ4* that interferes with the σ^M cell wall stress response (Emami et al.,
368 2017, Patel et al., 2020). Some of the cell wall associated genes mentioned (*sigM*, *ponA*, *ltaS*,
369 *yfnI*, *mprF*, *pgsA*) are differently expressed in cells of *B. subtilis* BSB1 in LB-glucose (Nicolas
370 et al., 2012, Zhu and Stulke, 2018). Thus *B. subtilis* might need to adapt its cell wall metabolism
371 in response to glucose, this might account for the partial redundancy of function of *B. subtilis*
372 LTA-synthases. Altogether, our study brings a new perspective on the importance of LTA in
373 the cell envelope stability.
374 In this study, we have identified a new function for MprF, an enzyme known to synthetise
375 aminoacyl-phosphatidylglycerol (aaPGol) phospholipids and translocate them across the
376 membrane (**Fig 1A**). We show that MprF activity impacts the biosynthesis of LTA and this in
377 turn alters cell wall metabolism. The LTA profiles observed in the absence of *B. subtilis* MprF

378 or *S. aureus* MprF (faster mobility and/or decreased signal) and the overexpression of *B.*
379 *subtilis* MprF (smear & retarded mobility) (**Fig 3B, 5A**) suggest that MprF positively regulates
380 LTA production. Other studies have indicated that MprFs may have relaxed substrate
381 specificities across species (Slavetinsky et al., 2017, Song et al., 2021) and even synthetise
382 lysyl-glucosyl-DAG glycolipid in *Streptococcus agalactiae* (Joyce et al., 2021). Recently, it
383 has been shown that when *S. aureus* LtaS uses PGol as an alternative anchor to the glycolipid
384 produced by UgtP, the concentration of these free lipid starter units regulates the length of the
385 LTA polymerised *in vitro* (Hesser et al., 2020b). Future works could investigate whether MprF
386 produces a substrate that contributes to LTA initiation/processivity. Alternatively, MprF might
387 act to synthetise positively charged aaPGols to provide an electrostatic environment that either
388 impacts on LTA-synthase(s) activity and/or directly contributes to altering the abundance of
389 hydrolases in the wall (e.g. LytE, **Fig 4**). This might help maintain the nascent anionic LTA
390 polymers adjacent to the membrane and facilitate D-alanylation of LTA (Schneewind and
391 Missiakas, 2014), hence leading to a modification in the cell envelope charge.
392 Gain of function in MprF has been identified in methicillin-resistant *S. aureus* (MRSA) clinical
393 isolates that have acquired resistance to daptomycin (Dap), an antibiotic used as a last resort to
394 treat MRSA infections (Ernst et al., 2018, Ernst and Peschel, 2019). Over the years, MprF-
395 mediated resistance to Dap (Dap^R) has been investigated but a consensus model has yet to link
396 Dap^R to a particular domain of MprF and/or to a particular Lys-PGol content in one or both
397 membrane leaflets (Ernst and Peschel, 2019, Thitiananpakorn et al., 2020). In *B. subtilis,* our
398 analysis shows the severe decrease of LTA produced in Dap^R *pgsA* A64V (**Fig 5B**), a strain
399 with a reduced PGol content (Hachmann et al., 2011). The function of MprF in LTA synthesis
400 and the new understanding of *S. aureus* LtaS processivity (Hesser et al., 2020b) can now be
401 linked to the identification of other MRSA Dap^R isolates (*cls* encoding a cardiolipin synthase,
402 *pgsA, dlt* operon) (Gray and Wenzel, 2020). Together, these findings support the idea that a

403 modification in LTA polymerisation and D-alanylation of teichoic acid (Bertsche et al., 2013,
404 Mishra et al., 2014) could result in a cell envelope less permeable to Dap, as such not
405 necessarily linked to cell wall thickness (Yang et al., 2010). Future research simultaneously
406 analysing LTA production and cell wall composition will help redefine MprF-mediated Dap^R
407 mechanism and help appreciate the exact role of MprF in the net cell surface charge, the
408 protection against cationic antimicrobial peptides and the contribution to bacterial virulence.

409 ## Material and Methods

410 ***Plasmids, bacterial strains, and primers***

411 Plasmids and strains used in this study are listed in **Table EV1 and EV2.** Strains constructions
412 are described below or in **Table EV2** (last column). Primers used are listed in **Table EV3.**

413 ***Growth conditions and general methods***.

414 *B. subtilis* strains were grown routinely on nutrient agar (NA, Oxoid) or in nutrient broth (NB,
415 Oxoid). For some assays, strains were grown in liquid Difco antibiotic medium 3 (PAB, Oxoid)
416 and PAB agar (15 g/l agar, Oxoid). *B. subtilis* transformations were carried out as previously
417 described using SMM defined minimal medium (Anagnostopoulos and Spizizen, 1961,
418 Hamoen et al., 2002). *B. subtilis* was usually incubated at 30°C (overnight), next day cells were
419 diluted and grown at 37°C (unless specified differently). *Escherichia coli* and *Staphylococcus*
420 *aureus* strains were incubated at 37°C on NA plate or in Luria-Bertani (LB). PCR, plasmid
421 manipulations, and *E. coli* transformation were carried out using standard methods. Strains
422 were selected on NA supplemented with ampicillin (for *E. coli,* 200 µg/ml), spectinomycin (60
423 µg/ml), kanamycin (5 µg/ml), phleomycin (1 µg/ml), erythromycin (0.5 µg/ml), and
424 chloramphenicol (5 µg/ml). Various supplements were also used: IPTG (isopropyl-β-D-
425 thiogalactopyranoside, 0.1 or 1 mM), X-Gal (5-bromo-4-chloro-3-indolyl-β-D-
426 galactopyranoside, 100 µg/ml), $MgS0_4$ (between 5 mM to 25 mM as required), and glucose
427 (final concentrations up to 1%). For NA plates supplemented with 20 mM $MgSO_4$, the
428 concentration of spectinomycin, kanamycin and erythromycin antibiotics was doubled to avoid
429 growth of false positive strains. Strains with the pMUTin-'*lytE-his* integration were always
430 grown in presence of erythromycin.

431 ***Plasmids constructions***

432 To obtain pDR111-$P_{hyspank}$-*mprF* plasmid, the *mprF* (BSU_08425) coding sequence was
433 amplified using primers oAG271-272, which changed the start codon (from TTG to ATG). The
434 PCR product and pDR111 plasmid (**Table EV1**) were digested by *Sal*I and *Sph*I restriction
435 enzymes, ligated together and transformed into *E. coli* DH5α. Digestion and PCR sequencing
436 using primers oAG300-301 verified the presence of the insert.

437 To construct pDR111-$P_{hyspank}$-*ltaS*, pDR111-$P_{hyspank}$-*yfnI* and pDR111-$P_{hyspank}$-*yqgS,* each
438 LTA-synthase gene was amplified by PCR with primers pairs oAG308-309 (2064 bp),
439 oAG310-311 (2078 bp) and oAG312-313 (1990 bp), respectively. PCR products were digested
440 by *Nhe*I and *Sph*I, each ligated with the plasmid pDR111 digested with the same restriction
441 enzymes. The next steps were carried out as described for pDR111-$P_{hyspank}$-*mprF*.

442 To construct pDR111-$P_{hyspank}$-*mprF-lytE* and pDR111-$P_{hyspank}$-*lytE-mprF* plasmids for
443 coexpression of *mprF* and *lytE,* the gene *lytE* was amplified from the chromosome by PCR
444 with oAG911-912 or oAG917-918 primers, respectively. PCR reactions were set up with
445 plasmid pDR111-$P_{hyspank}$-*mprF* and with one or the other PCR-*lytE* product (PrimeSTAR GXL
446 Polymerase, TaKaRa). Recombinant plasmid-inserts were obtained by overlapping PCR and
447 *Dpn*I digestion and transformed into *E. coli* DH5α. The resulting plasmids (with duplicate RBS
448 site, 24 bp) were verified by PCRs and by plasmid sequencing using primers oAG913-916,
449 oAG919-20, oAG292 and oAG294.

450 For pLOSS-P_{spac}-*lytE, lytE* was amplified by PCR with oAG348-349 (1143 bp) primers, and
451 the PCR product inserted in pLOSS* (**Table EV1**) as a *Not*I and *BamH*I fragment. After
452 transformation, the resulting plasmid was checked by PCRs with primers oAG18-19 and finally
453 checked by sequencing.

454 To construct the plasmids pMUTin-*'lytE-his*, pMUTin-*'ltaS-his* and pMUTin-*'yfnI-his* the 3'-
455 terminus part of gene of interest gene (except for the stop codon) was amplified with primer

456 pairs oAG354-355, oAG366-367 and oAG360-361, respectively to obtain a PCR products
457 ranging from 288 to 309 bp. The PCR products and the plasmid pMUTinHis (**Table EV1**)
458 (Ishikawa et al., 2006) were digested by *Eco*RI and *Xho*I, ligated together and transformed into
459 *E. coli* DH5α. Each insertion '*lytE, 'ltaS* and *'yfnI* was verified by PCR and plasmid sequencing
460 using primers oAG368-369.
461 To construct pAM-21, plasmid pET28a (+) (Novagen) and *lytE* (from the 76th bp, removing the
462 coding sequence for the signal peptide) were amplified by PCRs using primer pairs oAA01-02
463 and oAA03-04, respectively. DNA fragments generated were assembled using NEBuilder HiFi
464 DNA assembly kit (NEB). The resulting plasmid was verified by sequencing using primers
465 oAA05-06.

466 ***Bacillus directed mutagenesis***

467 Steps leading to construction of new mutants are indicated in the last column of **Table EV2**
468 with additional details in this section. New mutants were often obtained by transformation of
469 competent cells with a clean genomic DNA extracted from another existing *B. subtilis* mutants.
470 Construction of some of the markerless class A PBPs mutants were previously described
471 (Emami et al., 2017). Additional mutants described in this study were obtained using the
472 plasmids pG+host9::*ΔponA,* pG+host10::*ΔpbpD,* pG+host10::*ΔpbpF* (**Table EV1**) (Emami et
473 al., 2017). PCR with primers oAG124 to oAG129 were consistently performed to check
474 markerless deletions were not lost (Emami et al., 2017).
475 All transformations of the background strain with, and/or leading to, deletion of *ponA, mreB,*
476 *mbl, gtaB, ugtP, ltaS* were selected for on NA medium supplemented with $MgSO_4$ (20-25 mM)
477 with the appropriate antibiotic.
478 To construct strain AG181 (*ΔmprF*), DNA fragments upstream and downstream the *mprF*
479 coding sequence were amplified by PCR using primers oAG103-104 (2390 bp) and oAG105-

480 106 (2414 bp), respectively and were digested by *Eco*RI and *Xba*I, respectively. The
481 phleomycin resistance antibiotic cassette was amplified by PCR with primers PhleoXbaIfor
482 and PhleoEcoRIrev from plasmid pIC22 and digested by both *Eco*RI and *Xba*I. The 3 digested
483 PCR-fragments were ligated to generate a linear DNA, transformed into 168CA with selection
484 for phleomycin resistance. The deletion of *mprF* was confirmed by PCR using primers
485 oAG107-108.
486 Strain AG304 (*amyE::*$P_{hyspank}$*mprF, spc*) was obtained by transformation of 168CA with
487 pDR111-$P_{hyspank}$-*mprF* plasmid (**Table EV1**). Correct recombination was confirmed by the
488 absence of amylase activity when grown on NA with 0.2% starch and by PCR (oAG300-301
489 primers). The same methods were used after transformation of other pDR111-derivatives.
490 We constructed our own *lytE* deletion mutant (Δ*lytE::cat*). For this, regions of genomic DNA
491 upstream and downstream of *lytE* were amplified by PCRs with oAG350-351 (2048 bp) and
492 oAG352-353 (2500 bp) primers pairs, respectively. These products were then digested by *Xba*I
493 or *BamH*I (**Table EV3**). The chloramphenicol resistance cassette from pCotC-GFP plasmid
494 (**Table EV1**) was amplified with primers oAG197-198. The resulting PCR products (850 bp)
495 was then digested by *Xba*I and *Bam*HI and the three DNA fragments were ligated and
496 transformed into *B. subtilis* 168CA. Strain AG547 was obtained from this transformation and
497 the deletion of *lytE* confirmed by PCR using primers oAG340-341 (**Table EV3**).
498 Strains AG565 and AG586 were obtained by integration of pMUTin-'*lytE-his* (erythromycin
499 selection) in 168CA and Δ*cwlO* (AG474 strain) background, respectively. The plasmid
500 integration (single cross-over) in *B. subtilis* resulted in expression of recombinant proteins with
501 LEMRGSH$_{12}$ tag in C-terminus, under the control of its native promoter. Since the integration
502 of this plasmid into the Δ*cwlO* background did not result in any phenotypic change it indicated
503 that the LytE-His$_{12}$ was functional, as a double mutant *lytE cwlO* is lethal (Hashimoto et al.,
504 2012). Thereafter, genomic DNA of AG565 strain was used to transform all the strains needed

505 for Western blot analysis (**Table EV2**). Of note, AG1541 strain (Δ*cwlO*) obtained by genomic
506 DNA recombination has the same genotype as AG586 strain obtained by plasmid integration.

507 ***Random transposition mutageneses***

508 Random transposition mutageneses were performed as previously described (Claessen et al.,
509 2008, Surdova et al., 2013) using the pMarB plasmid that carries the transposon TnYLB-1
510 encoding kanamycin resistance. pMarB was introduced into *B. subtilis* strains carrying pLOSS-
511 P_{spac}-*ponA* (Emami et al., 2017) (**Table EV1**), a plasmid with an unstable origin of replication
512 and *lacZ* which helps to monitor the plasmid stability by observing formation of blue or white
513 colonies. After screening the random library of mutants, genomic DNA extracted from positive
514 clones were backcrossed into the parental strain used for the transposon screen. Transposon
515 insertion sites were identified by inverse PCR using gDNA extracted from the backcrossed
516 positive clones (Surdova et al., 2013) and sequencing the resulting PCR products. Further
517 verification of the transposon's site of insertion was obtained using specific primers.
518 For the suppressor screen in *ponA pbpD pbpF* mutant background, we constructed strain
519 AG141 (**Table EV2**) which carries deletions of the three vegetative class A PBPs, *lacA* gene
520 (Surdova et al., 2013) and pLOSS-P_{spac}-*ponA* (Emami et al., 2017). The transposon mutant
521 library was screened on PAB agar supplemented with $MgSO_4$ (10 mM), X-Gal and IPTG (1
522 mM) and white colonies selected. The strain SWA11a (**Table EV2**) had a transposon in *mprF*
523 coding sequence which was verified using specific primers oAG81-82 (**Table EV3**).
524 A conditional lethal screen was also carried out in a *ponA pbpD pbpF mprF lacA* pLOSS-P_{spac}-
525 *ponA* strain (AG200, **Table EV2**). Here the transposon mutant library was screened on NA and
526 PAB supplemented with X-Gal and IPTG (1mM). Blue colonies indicating plasmid stability
527 were selected. One mutant was isolated and its genomic DNA was backcrossed into AG200

528 background. The resulting blue forming AG200BK#42 strain (**Table EV2**) was found to carry
529 a transposon in *gtaB*'s coding sequence using primers oAG165-166 (**Table EV3**).

530 ***Spot growth assays***

531 Strains were grown in NB with 20 mM $MgSO_4$ at 30°C overnight. The cultures were then
532 diluted 1:100 into fresh NB 10 mM $MgSO_4$ (or when applicable 20 mM) and grown up to mid
533 exponential phase at 37°C. Cells were harvested, washed in NB, and diluted to an $OD_{600nm} \approx$
534 0.3 in NB. Each strain sample was then serially diluted 1:10 using a 96-multiwell plate and
535 NB. Using a multichannel pipette, 5 µl of each dilution were transferred to various agar plates.
536 As a control all the serial dilutions presented in the figures were also spotted on media
537 supplemented with 10 mM or 20 mM $MgS0_4$ to ensure that growth occurred for all spots (our
538 unpublished observations). Plates were incubated at 37°C overnight and scanned at different
539 time points. Images were edited in Photoshop.

540 ***Microscopic imaging***

541 Cells were grown to exponential growth phase at 37 °C in NB medium. Before the cells were
542 mounted onto microscopic slides, the slides were covered with a thin layer of NA medium
543 supplemented with the FM5-95 membrane dye at 140 µg/ml (Invitrogen). Fluorescence
544 microscopy was carried out with a Zeiss Axiovert 200M microscope attached to a Sony Cool-
545 Snap HQ cooled CCD camera with Nikon APO x100/1.40 oil Ph3 objective lens. Images were
546 acquired using Metamorph 6 imaging software (Molecular Devices, Inc). Images were
547 analysed with ImageJ (http://rsb.info.nih.gov/ij/) and assembled with Photoshop CS software.
548 Images stained with the FM5-95 membrane dye were processed using the plugin ObjectJ in
549 ImageJ (http://rsb.info.nih.gov/ij/) to measure cell diameter and cell length of about 400 cells

550 per strain. Measurements were performed only once as cell diameter change was obvious under
551 the microscope and on the images of **Fig 2D** (details in **Appendix Figure S5**).

552 ***Transmission electron microscopy***

553 Strains were grown in NB medium (with IPTG when applicable) until reaching an OD_{600nm} of
554 about 0.4. The cell pellets were fixed in 2% glutaraldehyde in sodium cacodylate buffer at 4°C
555 for at least 24 h. Samples were spun and molten 4% agarose was added to the sample and re
556 spun. Sample were allowed to cool in the fridge for 30 min. The agarose block was removed
557 from each tube and cut into 1 mm^3 pieces. The samples were then dehydrated by microwave
558 processing using the Pelco Biowave® Pro+ incorporating the Pelco Coldspot® Pro. In the
559 vaccum chamber, samples were rinsed 3 times in buffer (150 watts for 40s), then treated in 1%
560 osmium, pulsed (100 watts for 8 min) and rinsed 3 times in distilled water (150 watts for 40s).
561 They were then taken out of the vaccum chamber and a graded series of dried acetone was
562 applied to the samples (25%, 50%,75%, and 3 times in 100%, at 150 watts for 40 s for each
563 step). This was followed by impregnation with a series of increasing concentrations of epoxy
564 resin (Taab Medium resin) in acetone (25%, 50%,75%, 3 times in 100% at 300 watts for 3 min.
565 for each step). Samples were embedded in fresh 100% resin and polymerised at 60°C for 24 h
566 in a conventional oven. Once polymerised the resin block were cut in semi-thin survey sections
567 (0.5 µm) and stained with 1% toluidine blue in 1% borax. Ultrathin sections (70 nm approx.)
568 were then cut using a diamond knife on a Leica EM UC7 ultramicrotome. The sections were
569 stretched with chloroform to eliminate compression and mounted on Pioloform-filmed copper
570 grids. Grids were stained with uranyl acetate (2%) and Lead citrate and viewed on a Hitachi
571 HT7800 transmission electron microscope using an Emsis Xarosa camera.

572 ***Samples preparation for LTA polymer detection***

573 *B. subtilis* strains were grown overnight at 30°C with shaking in NB supplemented with 5 mM
574 $MgS0_4$ (or 10 mM for *mbl* mutants). The cells were then diluted (1:60-1:80 depending on the
575 strain) to an approximate OD_{600nm} of 0.02 in prewarmed NB and NB supplemented with 0.2%
576 glucose. Strains were then incubated at 37°C shaking and grown for about 4.5 h (late
577 exponential phase). At the sampling time the OD_{600nm} of the cultures were measured before
578 harvesting 15-25 ml of culture at 3273 *g* for 10 min, using a swing out centrifuge at room
579 temperature. Pellets were washed with 200 µl of solution A (with 10 mL of Tris-HCl at 100
580 mM pH 7.4 and one cOmplete Mini EDTA-free tablet of protease inhibitor cocktail from
581 Roche) and pelleted with benchtop centrifuge. Cells pellets were then frozen in liquid nitrogen
582 and stored at -20°C until processing. Samples were resuspended in a volume of solution B (an
583 equal volume of solution A and LDS sample buffer, Life Technologies) ranging from 70 to 200
584 µl in proportion to their OD_{600nm}. Samples were boiled 30 min at 100°C, cooled down on ice
585 for 3 min and incubated each with 100 U of benzonase (E1014, Sigma) for 30 min at 37°C.
586 Samples were pelleted at 4°C, supernatants containing the extracted LTA were collected.
587 Supernatants were frozen in liquid nitrogen and kept at -25°C. For the LTA Western blots, the
588 quantity of sample loaded was normalized using the Bio-Rad Protein assays such that the final
589 OD_{595nm} was approximately 0.35. Sample sets to be compared were grown, extracted, measured
590 and normalized together for each experiment.

591 *S. aureus* strains were grown overnight at 37°C with shaking in LB. The cells were then diluted
592 (about 300-fold) to an approximate OD_{600nm} of about 0.02 and grown in LB at 37°C until
593 reaching late exponential and an OD_{600nm} of about 1. 10 ml of cultures were harvested, and
594 samples were prepared as for *B. subtilis* with the following changes: 60 µl of solution B were
595 used and about 18-20 µl of samples were loaded on SDS-PAGE with samples normalised to
596 their OD_{600nm}.

597 ***Total protein samples preparation***

598 For LytE or LtaS Western blots, cells were grown, harvested and processed in the same way
599 as the LTA-samples, with the exception that to detect the his tagged LytE, the strains were
600 grown in presence of erythromycin. An 8 ml culture sample was resuspended in 180-200 µl of
601 a solution A and sonicated until a clear lysate was obtained. Samples were centrifuged at 16,000
602 *g* for 10 min at 4°C and a volume of sample supernatant loaded on the SDS-gel, normalized
603 based on the OD_{600nm} of the cells culture collected.

604 ***SDS-PAGE, LTA and proteins Western blots, detection blots***

605 For SDS-PAGE, samples were diluted in solution B with the addition of reducing agent (1.5 µl
606 per sample) in final volume of 20 µl, heated at 70°C for 10 min, loaded on the gel (NuPAGE
607 4-12% Bis-Tris gradient Midi Gel, Life Technologies) and separated by electrophoresis. For
608 the LTA-PBP2B experiment, MES buffer, Novex Sharp prestained protein Ladder (Life
609 Technologies) and 0.2 µm Amersham Hybond sequencing PVDF membrane (GE Healthcare)
610 were used. Whereas for LytE (37 kDa) or LtaS (74 kDa) Western blots, MOPS buffer, Abcam
611 prestained mid-range protein ladder (Ab116027) and 0.45 µM Amersham Hybond PVDF
612 membrane (GE Healthcare) were used. The SDS-PAGE gels were transferred to membranes
613 using the Trans-Blot Turbo transfer system (Bio-Rad) using an in-house transfer buffer (tris
614 600 mM, glycine 600 mM, tricine 280 mM, EDTA 2.5 mM and SDS 0.05%). After transfer,
615 the membranes were washed 3x 5 min in PBS using a rocking shaker, afterwards the
616 membranes were cut where required to allow different detection methods.

617 For the LTA Western blot, membrane was cut at the 60 kDa ladder position. The bottom part
618 of the membrane was used for the LTA-blot whereas the top part was used to detect the
619 membrane protein PBP2B (79 kDa) as a loading/extraction control. All LTA Western blot steps

620 were performed at room temperature in a rolling shaker and using 50 mL falcon tubes. The
621 LTA-membranes were incubated 1h15 in PBS buffer with 3% BSA (A7030, Sigma), then 1h30
622 in fresh PBS-3% BSA with a dilution 1:1000 of Gram-positive LTA monoclonal antibody
623 (MA1-7402, Thermofischer). The membrane was then washed briefly 2 times, followed by 4x
624 8 min in PBS and then incubated in PBS-5% dried semi-skimmed milk with 1:10,000 anti-
625 mouse HRP-linked secondary antibody (A9044, Sigma) for 1 h. This was then followed by 2
626 brief and 6x 8 min washes steps prior to detection.
627 For proteins Western blots to detect LytE-His_{12} or LtaS and PBP2B, all the following steps
628 were performed at room temperature using a rocking shaker. The membranes were washed
629 after transfer in PBS-Tween20 at 0.1% (here after noted PBS-T) and blocked in PBS-T with
630 5% milk for 1h15 (i.e PBS-T-milk) at room temperature. Thereafter the LytE-His_{12}/PBP2B
631 membrane blot was cut at about 53 kDa ladder position. Membranes were placed in fresh buffer
632 PBS-T-milk for 1h (or 1h30 when performing the LTAs western blot in parallel) with the
633 polyclonal rabbit anti-PBP2B antibody (at 1:5000, lab. stock or available at Merck ABS2199),
634 the mouse monoclonal Penta-His antibody (Qiagen n°34660 stock at 200 µg/ml, used at
635 dilution 1:2000) or polyclonal rabbit anti-LtaS antibody (at 1:1000, lab. stock). Two brief
636 washing steps were performed in PBS-T followed by 3 washes of 10 min. Membranes were
637 incubated in PBS-T-milk for 1 h using 1:10000 dilutions of anti-rabbit or anti-mouse HRP-
638 linked secondary antibodies (A0545 or A9044 Sigma antibodies, respectively) as required.
639 Membranes were then washed as described at the previous step.
640 Pierce ECL Plus Western Blotting Substrate (32132, Thermo Scientific) was used for detection
641 as recommended by manufacturer. Chemiluminescence was detected using ImageQuant LAS
642 4000 mini digital imaging system (GE Healthcare) and membranes were exposed with 1 min
643 increment for 20 min. Membranes were also imaged by Epi-illumination to detect the pre-
644 stained proteins ladder on the membrane. In our conditions, quantities of LTAs samples loaded

645 were scaled down to avoid burn out of signals observed in some of the tested strains.
646 Occasionally for the LTAs blot, strains (in NB-only) can display a very weak signal above the
647 30 kDa ladder position. This phenomenon was observed by others performing *Bacillus* LTA
648 Western blots and was assumed not to be related to LTA but possibly a cross-reactivity of the
649 antibody to WTAs that also contains glycerolphosphate (Wormann et al., 2011).
650 Images were edited in ImageJ (Fiji), the same contrast enhancement was applied for the
651 membranes of the same set experiment. Three independent sets of experimental samples were
652 generated by Western blots. Contrast was sometimes added to the images, in particular to
653 observe LytE signal in low-expressing strains.

654 ***LytE purification and raising antiserum***

655 Plasmid pAM-21 was transferred into *E. coli* BL21 (DE3) strain. Newly obtained strain grew
656 at 37°C in LB kanamycin, when cell reached an approximative OD_{600nm} of 0.5 *lytE* expression
657 was induced with 1 mM IPTG for 3 h. 50 ml culture was collected by centrifugation at 9,000
658 *g* for 5 min and resuspended in 15 ml of a solution of PBS at 4 µg/ml of lysosyme. After
659 incubation for 20 min at room temperature (RT), cells were sonicated, and once clear lysate
660 was obtained cells were harvested at 3,000 *g* for 4 min. The cell pellet was resuspended in PBS
661 buffer at 8 M Urea and incubated for 30 min at RT on a rolling shaker. The cells were then
662 centrifuged at 9,000 *g* for 10 min and supernatant was collected and mixed gently with 200 µl
663 of Ni Sepharose High Performance (GE Healthcare) and incubated for 1 h in same condition
664 as above. Then the sample was washed 3 to 4 times in buffer A (50 mM Tris (pH 8) and 300
665 mM NaCl), and the last wash was done in buffer B (50 mM Tris, 300 mM NaCl, 5 mM
666 Imidazole). Sample was eluted five times in buffer C (PBS at 8 M Urea and 100mM imidazole)
667 and elution fractions were analysed by SDS-PAGE. Ice-cold acetone was added at a 4:1 volume
668 ratio to the desired eluted sample and incubated overnight at -20°C. Sample was centrifuged at
669 4 °C for 10 min at 15,000 *g* and the pellet was left to dry at RT. The pellet was suspended in

670 200 µl of PBS and 100 µg aliquot was sent to raise antiserum (Eurogentec). The LytE antiserum
671 was used in Western blot at 1:5000 dilution and with the anti-rabbit secondary antibody
672 (1:10000).

673 Acknowledgements

674 The authors thank P. Aldridge for critical reading of the manuscript. The authors thank
675 colleagues for strains or genomic DNA S. Moore, P. Dominguez-Cuevas, P. Gamba, A. Koh,
676 K. Seistrup, L. Bowman, H. Strahl and J. D. Helmann, B. M. Wendel and A. Peschel for strains
677 related to daptomycin resistance. Technical support was provided by I. Selmes, F. Davison and
678 T. Fletcher and TEM sample processing by Tracey Davey in the Electron Microscopy Research
679 Services Newcastle University (funded through the BBSRC; BB/R013942/1). The authors
680 thank J. Errington for the anti-LtaS antibody, H. Strahl and W. Vollmer for helpful discussion,
681 C. Winterhalter and S. Fenyk for advice on Western blots and P. Tiago for sharing subtiwiki
682 data. This work was funded by grants from the BBSRC (BB/G015902/1), EPSRC
683 (EP/N031962/1) (RAD and AG) and SACB (studentship for AA).

684 Author contributions

685 Conceptualization: AG; Funding acquisition, RAD; Methodology: AG; Investigation: AG and
686 AA; Methodology: AG; Project administration: RAD; Supervision: RAD; Validation: AG;
687 Visualization: AG; Writing—original draft: AG; Writing—review & editing: AG and RAD.

688 Conflict of interest

689 The authors declare that they have no conflict of interest.

690 Supporting information

691 Expanded View Figures, Expanded View Tables and Appendix are available for this
692 manuscript. This study includes no data deposited in external repositories.

693 **References**

694 ANAGNOSTOPOULOS, C. & SPIZIZEN, J. 1961. Requirements for Transformation in
695 *Bacillus subtilis*. *J Bacteriol,* 81**,** 741-6.
696 ATILA, M., KATSELIS, G., CHUMALA, P. & LUO, Y. 2016. Characterization of N-
697 Succinylation of L-Lysylphosphatidylglycerol in *Bacillus subtilis* Using Tandem
698 Mass Spectrometry. *J Am Soc Mass Spectrom,* 27**,** 1606-13.
699 BERTSCHE, U., YANG, S. J., KUEHNER, D., WANNER, S., MISHRA, N. N., ROTH, T.,
700 NEGA, M., SCHNEIDER, A., MAYER, C., GRAU, T., BAYER, A. S. &
701 WEIDENMAIER, C. 2013. Increased cell wall teichoic acid production and D-
702 alanylation are common phenotypes among daptomycin-resistant methicillin-resistant
703 *Staphylococcus aureus* (MRSA) clinical isolates. *PLoS One,* 8**,** e67398.
704 BRANDA, S. S., GONZALEZ-PASTOR, J. E., DERVYN, E., EHRLICH, S. D., LOSICK,
705 R. & KOLTER, R. 2004. Genes involved in formation of structured multicellular
706 communities by *Bacillus subtilis*. *J Bacteriol,* 186**,** 3970-9.
707 CLAESSEN, D., EMMINS, R., HAMOEN, L. W., DANIEL, R. A., ERRINGTON, J. &
708 EDWARDS, D. H. 2008. Control of the cell elongation-division cycle by shuttling of
709 PBP1 protein in *Bacillus subtilis*. *Mol Microbiol,* 68**,** 1029-46.
710 COE, K. A., LEE, W., STONE, M. C., KOMAZIN-MEREDITH, G., MEREDITH, T. C.,
711 GRAD, Y. H. & WALKER, S. 2019. Multi-strain Tn-Seq reveals common
712 daptomycin resistance determinants in *Staphylococcus aureus*. *PLoS Pathog,* 15**,**
713 e1007862.
714 DO, T., PAGE, J. E. & WALKER, S. 2020. Uncovering the activities, biological roles, and
715 regulation of bacterial cell wall hydrolases and tailoring enzymes. *J Biol Chem,* 295**,**
716 3347-3361.
717 DOBIHAL, G. S., BRUNET, Y. R., FLORES-KIM, J. & RUDNER, D. Z. 2019. Homeostatic
718 control of cell wall hydrolysis by the WalRK two-component signaling pathway in
719 *Bacillus subtilis*. *Elife,* 8.
720 DOMINGUEZ-CUEVAS, P., PORCELLI, I., DANIEL, R. A. & ERRINGTON, J. 2013.
721 Differentiated roles for MreB-actin isologues and autolytic enzymes in *Bacillus*
722 *subtilis* morphogenesis. *Mol Microbiol,* 89**,** 1084-98.
723 EMAMI, K., GUYET, A., KAWAI, Y., DEVI, J., WU, L. J., ALLENBY, N., DANIEL, R.
724 A. & ERRINGTON, J. 2017. RodA as the missing glycosyltransferase in *Bacillus*
725 *subtilis* and antibiotic discovery for the peptidoglycan polymerase pathway. *Nat*
726 *Microbiol,* 2**,** 16253.
727 ERICKSON, H. P. 2021. How Teichoic Acids Could Support a Periplasm in Gram-Positive
728 Bacteria, and Let Cell Division Cheat Turgor Pressure. *Front Microbiol,* 12**,** 664704.
729 ERNST, C. M. & PESCHEL, A. 2019. MprF-mediated daptomycin resistance. *Int J Med*
730 *Microbiol,* 309**,** 359-363.
731 ERNST, C. M., SLAVETINSKY, C. J., KUHN, S., HAUSER, J. N., NEGA, M., MISHRA,
732 N. N., GEKELER, C., BAYER, A. S. & PESCHEL, A. 2018. Gain-of-Function
733 Mutations in the Phospholipid Flippase MprF Confer Specific Daptomycin
734 Resistance. *mBio,* 9.

735 FLORES-KIM, J., DOBIHAL, G. S., FENTON, A., RUDNER, D. Z. & BERNHARDT, T.
736 G. 2019. A switch in surface polymer biogenesis triggers growth-phase-dependent
737 and antibiotic-induced bacteriolysis. *Elife,* 8.
738 FORMSTONE, A. & ERRINGTON, J. 2005. A magnesium-dependent *mreB* null mutant:
739 implications for the role of *mreB* in *Bacillus subtilis*. *Mol Microbiol,* 55**,** 1646-57.
740 FRIEDMAN, L., ALDER, J. D. & SILVERMAN, J. A. 2006. Genetic changes that correlate
741 with reduced susceptibility to daptomycin in *Staphylococcus aureus*. *Antimicrob*
742 *Agents Chemother,* 50**,** 2137-45.
743 GRAY, D. A. & WENZEL, M. 2020. More Than a Pore: A Current Perspective on the In
744 Vivo Mode of Action of the Lipopeptide Antibiotic Daptomycin. *Antibiotics (Basel),*
745 9.
746 GREIN, F., MULLER, A., SCHERER, K. M., LIU, X., LUDWIG, K. C., KLOCKNER, A.,
747 STRACH, M., SAHL, H. G., KUBITSCHECK, U. & SCHNEIDER, T. 2020. Ca^{2+}-
748 Daptomycin targets cell wall biosynthesis by forming a tripartite complex with
749 undecaprenyl-coupled intermediates and membrane lipids. *Nat Commun,* 11**,** 1455.
750 GRUNDLING, A. & SCHNEEWIND, O. 2007a. Genes required for glycolipid synthesis and
751 lipoteichoic acid anchoring in *Staphylococcus aureus*. *J Bacteriol,* 189**,** 2521-30.
752 GRUNDLING, A. & SCHNEEWIND, O. 2007b. Synthesis of glycerol phosphate
753 lipoteichoic acid in *Staphylococcus aureus*. *Proc Natl Acad Sci U S A,* 104**,** 8478-83.
754 HACHMANN, A. B., ANGERT, E. R. & HELMANN, J. D. 2009. Genetic analysis of
755 factors affecting susceptibility of *Bacillus subtilis* to daptomycin. *Antimicrob Agents*
756 *Chemother,* 53**,** 1598-609.
757 HACHMANN, A. B., SEVIM, E., GABALLA, A., POPHAM, D. L., ANTELMANN, H. &
758 HELMANN, J. D. 2011. Reduction in membrane phosphatidylglycerol content leads
759 to daptomycin resistance in *Bacillus subtilis*. *Antimicrob Agents Chemother,* 55**,**
760 4326-37.
761 HAMOEN, L. W., SMITS, W. K., DE JONG, A., HOLSAPPEL, S. & KUIPERS, O. P.
762 2002. Improving the predictive value of the competence transcription factor (ComK)
763 binding site in *Bacillus subtilis* using a genomic approach. *Nucleic Acids Res,* 30**,**
764 5517-28.
765 HANSON, B. R. & NEELY, M. N. 2012. Coordinate regulation of Gram-positive cell surface
766 components. *Curr Opin Microbiol,* 15**,** 204-10.
767 HASHIMOTO, M., OOIWA, S. & SEKIGUCHI, J. 2012. Synthetic lethality of the *lytE cwlO*
768 genotype in *Bacillus subtilis* is caused by lack of D,L-endopeptidase activity at the
769 lateral cell wall. *J Bacteriol,* 194**,** 796-803.
770 HASHIMOTO, M., SEKI, T., MATSUOKA, S., HARA, H., ASAI, K., SADAIE, Y. &
771 MATSUMOTO, K. 2013. Induction of extracytoplasmic function sigma factors in
772 *Bacillus subtilis* cells with defects in lipoteichoic acid synthesis. *Microbiology,* 159**,**
773 23-35.
774 HESSER, A. R., MATANO, L. M., VICKERY, C. R., WOOD, B. M., SANTIAGO, A. G.,
775 MORRIS, H. G., DO, T., LOSICK, R. & WALKER, S. 2020a. The length of
776 lipoteichoic acid polymers controls *Staphylococcus aureus* cell size and envelope
777 integrity. *J Bacteriol*.

HESSER, A. R., SCHAEFER, K., LEE, W. & WALKER, S. 2020b. Lipoteichoic acid polymer length is determined by competition between free starter units. *Proc Natl Acad Sci U S A,* 117**,** 29669-29676.

ISHIKAWA, S., KAWAI, Y., HIRAMATSU, K., KUWANO, M. & OGASAWARA, N. 2006. A new FtsZ-interacting protein, YlmF, complements the activity of FtsA during progression of cell division in *Bacillus subtilis*. *Mol Microbiol,* 60**,** 1364-80.

JOHNSON, C. M. & GROSSMAN, A. D. 2016. The Composition of the Cell Envelope Affects Conjugation in *Bacillus subtilis*. *J Bacteriol,* 198**,** 1241-9.

JORASCH, P., WOLTER, F. P., ZAHRINGER, U. & HEINZ, E. 1998. A UDP glucosyltransferase from *Bacillus subtilis* successively transfers up to four glucose residues to 1,2-diacylglycerol: expression of *ypfP* in *Escherichia coli* and structural analysis of its reaction products. *Mol Microbiol,* 29**,** 419-30.

JOYCE, L. R., MANZER, H. S., DA C. MENDONÇA, J., VILLARREAL, R., DORAN, K. S., PALMER, K. L. & GUAN, Z. 2021. *Streptococcus agalactiae* MprF synthesizes a novel cationic glycolipid and plays a role in brain entry and meningitis. *bioRxiv***,** 2020.12.01.406702.

KASAHARA, J., KIRIYAMA, Y., MIYASHITA, M., KONDO, T., YAMADA, T., YAZAWA, K., YOSHIKAWA, R. & YAMAMOTO, H. 2016. Teichoic Acid Polymers Affect Expression and Localization of dl-Endopeptidase LytE Required for Lateral Cell Wall Hydrolysis in *Bacillus subtilis*. *J Bacteriol,* 198**,** 1585-1594.

KAWAI, Y., ASAI, K. & ERRINGTON, J. 2009a. Partial functional redundancy of MreB isoforms, MreB, Mbl and MreBH, in cell morphogenesis of *Bacillus subtilis*. *Mol Microbiol,* 73**,** 719-31.

KAWAI, Y., DANIEL, R. A. & ERRINGTON, J. 2009b. Regulation of cell wall morphogenesis in *Bacillus subtilis* by recruitment of PBP1 to the MreB helix. *Mol Microbiol,* 71**,** 1131-44.

KOO, B. M., KRITIKOS, G., FARELLI, J. D., TODOR, H., TONG, K., KIMSEY, H., WAPINSKI, I., GALARDINI, M., CABAL, A., PETERS, J. M., HACHMANN, A. B., RUDNER, D. Z., ALLEN, K. N., TYPAS, A. & GROSS, C. A. 2017. Construction and Analysis of Two Genome-Scale Deletion Libraries for *Bacillus subtilis*. *Cell Syst,* 4**,** 291-305 e7.

LAZAREVIC, V., SOLDO, B., MEDICO, N., POOLEY, H., BRON, S. & KARAMATA, D. 2005. *Bacillus subtilis* α-phosphoglucomutase is required for normal cell morphology and biofilm formation. *Appl Environ Microbiol,* 71**,** 39-45.

LE BRETON, Y., MOHAPATRA, N. P. & HALDENWANG, W. G. 2006. *In vivo* random mutagenesis of *Bacillus subtilis* by use of TnYLB-1, a mariner-based transposon. *Appl Environ Microbiol,* 72**,** 327-33.

MAMOU, G., FIYAKSEL, O., SINAI, L. & BEN-YEHUDA, S. 2017. Deficiency in Lipoteichoic Acid Synthesis Causes a Failure in Executing the Colony Developmental Program in *Bacillus subtilis*. *Front Microbiol,* 8**,** 1991.

MATSUOKA, S., HASHIMOTO, M., KAMIYA, Y., MIYAZAWA, T., ISHIKAWA, K., HARA, H. & MATSUMOTO, K. 2011. The *Bacillus subtilis* essential gene *dgkB* is dispensable in mutants with defective lipoteichoic acid synthesis. *Genes Genet Syst,* 86**,** 365-76.

822 MCPHERSON, D. C., DRIKS, A. & POPHAM, D. L. 2001. Two class A high-molecular-
823 weight penicillin-binding proteins of *Bacillus subtilis* play redundant roles in
824 sporulation. *J Bacteriol,* 183**,** 6046-53.
825 MCPHERSON, D. C. & POPHAM, D. L. 2003. Peptidoglycan synthesis in the absence of
826 class A penicillin-binding proteins in *Bacillus subtilis*. *J Bacteriol,* 185**,** 1423-31.
827 MEESKE, A. J., RILEY, E. P., ROBINS, W. P., UEHARA, T., MEKALANOS, J. J.,
828 KAHNE, D., WALKER, S., KRUSE, A. C., BERNHARDT, T. G. & RUDNER, D.
829 Z. 2016. SEDS proteins are a widespread family of bacterial cell wall polymerases.
830 *Nature,* 537**,** 634-638.
831 MISHRA, N. N., BAYER, A. S., WEIDENMAIER, C., GRAU, T., WANNER, S.,
832 STEFANI, S., CAFISO, V., BERTUCCIO, T., YEAMAN, M. R., NAST, C. C. &
833 YANG, S. J. 2014. Phenotypic and genotypic characterization of daptomycin-resistant
834 methicillin-resistant *Staphylococcus aureus* strains: relative roles of *mprF* and *dlt*
835 operons. *PLoS One,* 9**,** e107426.
836 MULLER, A., WENZEL, M., STRAHL, H., GREIN, F., SAAKI, T. N. V., KOHL, B.,
837 SIERSMA, T., BANDOW, J. E., SAHL, H. G., SCHNEIDER, T. & HAMOEN, L.
838 W. 2016. Daptomycin inhibits cell envelope synthesis by interfering with fluid
839 membrane microdomains. *Proc Natl Acad Sci U S A,* 113**,** E7077-E7086.
840 MURRAY, T., POPHAM, D. L. & SETLOW, P. 1998. *Bacillus subtili*s cells lacking
841 penicillin-binding protein 1 require increased levels of divalent cations for growth. *J*
842 *Bacteriol,* 180**,** 4555-63.
843 NEUHAUS, F. C. & BADDILEY, J. 2003. A continuum of anionic charge: structures and
844 functions of D-alanyl-teichoic acids in Gram-positive bacteria. *Microbiol Mol Biol*
845 *Rev,* 67**,** 686-723.
846 NICOLAS, P., MADER, U., DERVYN, E., ROCHAT, T., LEDUC, A., PIGEONNEAU, N.,
847 BIDNENKO, E., MARCHADIER, E., HOEBEKE, M., AYMERICH, S., BECHER,
848 D., BISICCHIA, P., BOTELLA, E., DELUMEAU, O., DOHERTY, G., DENHAM,
849 E. L., FOGG, M. J., FROMION, V., GOELZER, A., HANSEN, A., HARTIG, E.,
850 HARWOOD, C. R., HOMUTH, G., JARMER, H., JULES, M., KLIPP, E., LE
851 CHAT, L., LECOINTE, F., LEWIS, P., LIEBERMEISTER, W., MARCH, A.,
852 MARS, R. A., NANNAPANENI, P., NOONE, D., POHL, S., RINN, B.,
853 RUGHEIMER, F., SAPPA, P. K., SAMSON, F., SCHAFFER, M., SCHWIKOWSKI,
854 B., STEIL, L., STULKE, J., WIEGERT, T., DEVINE, K. M., WILKINSON, A. J.,
855 VAN DIJL, J. M., HECKER, M., VOLKER, U., BESSIERES, P. & NOIROT, P.
856 2012. Condition-dependent transcriptome reveals high-level regulatory architecture in
857 *Bacillus subtilis*. *Science,* 335**,** 1103-6.
858 NOWAK, J., VISNOVSKY, S. B., CRUZ, C. D., FLETCHER, G. C., VAN VLIET, A. H.
859 M., HEDDERLEY, D., BUTLER, R., FLINT, S., PALMER, J. & PITMAN, A. R.
860 2021. Inactivation of the gene encoding the cationic antimicrobial peptide resistance
861 factor MprF increases biofilm formation but reduces invasiveness of *Listeria*
862 *monocytogenes*. *J Appl Microbiol,* 130**,** 464-477.
863 OKU, Y., KUROKAWA, K., MATSUO, M., YAMADA, S., LEE, B. L. & SEKIMIZU, K.
864 2009. Pleiotropic roles of polyglycerolphosphate synthase of lipoteichoic acid in
865 growth of *Staphylococcus aureus* cells. *J Bacteriol,* 191**,** 141-51.

866 PATEL, Y., ZHAO, H. & HELMANN, J. D. 2020. A regulatory pathway that selectively up-
867 regulates elongasome function in the absence of class A PBPs. *Elife,* 9.
868 PAZOS, M. & VOLLMER, W. 2021. Regulation and function of class A Penicillin-binding
869 proteins. *Curr Opin Microbiol,* 60**,** 80-87.
870 PERCY, M. G. & GRUNDLING, A. 2014. Lipoteichoic Acid Synthesis and Function in
871 Gram-Positive Bacteria. *Annu Rev Microbiol*.
872 PEREGO, M., GLASER, P., MINUTELLO, A., STRAUCH, M. A., LEOPOLD, K. &
873 FISCHER, W. 1995. Incorporation of D-alanine into lipoteichoic acid and wall
874 teichoic acid in *Bacillus subtilis*. Identification of genes and regulation. *J Biol Chem,*
875 270**,** 15598-606.
876 PESCHEL, A., JACK, R. W., OTTO, M., COLLINS, L. V., STAUBITZ, P., NICHOLSON,
877 G., KALBACHER, H., NIEUWENHUIZEN, W. F., JUNG, G., TARKOWSKI, A.,
878 VAN KESSEL, K. P. & VAN STRIJP, J. A. 2001. *Staphylococcus aureus* resistance
879 to human defensins and evasion of neutrophil killing via the novel virulence factor
880 MprF is based on modification of membrane lipids with l-lysine. *J Exp Med,* 193**,**
881 1067-76.
882 RAJAGOPAL, M. & WALKER, S. 2017. Envelope Structures of Gram-Positive Bacteria.
883 *Curr Top Microbiol Immunol,* 404**,** 1-44.
884 SALZBERG, L. I. & HELMANN, J. D. 2008. Phenotypic and transcriptomic characterization
885 of *Bacillus subtilis* mutants with grossly altered membrane composition. *J Bacteriol,*
886 190**,** 7797-807.
887 SALZBERG, L. I., POWELL, L., HOKAMP, K., BOTELLA, E., NOONE, D. & DEVINE,
888 K. M. 2013. The WalRK (YycFG) and s^I RsgI regulators cooperate to control CwlO
889 and LytE expression in exponentially growing and stressed *Bacillus subtilis* cells. *Mol*
890 *Microbiol,* 87**,** 180-95.
891 SCHIRNER, K. & ERRINGTON, J. 2009. The cell wall regulator s^I specifically suppresses
892 the lethal phenotype of *mbl* mutants in *Bacillus subtilis*. *J Bacteriol,* 191**,** 1404-13.
893 SCHIRNER, K., MARLES-WRIGHT, J., LEWIS, R. J. & ERRINGTON, J. 2009. Distinct
894 and essential morphogenic functions for wall- and lipo-teichoic acids in *Bacillus*
895 *subtilis*. *EMBO J,* 28**,** 830-42.
896 SCHNEEWIND, O. & MISSIAKAS, D. 2014. Lipoteichoic acids, phosphate-containing
897 polymers in the envelope of Gram-positive bacteria. *J Bacteriol,* 196**,** 1133-42.
898 SCHNEEWIND, O. & MISSIAKAS, D. 2016. Lipoteichoic acid synthesis and function in
899 gram-positive bacteria. *Biogenesis of Fatty Acids, Lipids and Membranes***,** 1-18.
900 SLAVETINSKY, C., KUHN, S. & PESCHEL, A. 2017. Bacterial aminoacyl phospholipids -
901 Biosynthesis and role in basic cellular processes and pathogenicity. *Biochim Biophys*
902 *Acta Mol Cell Biol Lipids,* 1862**,** 1310-1318.
903 SOLDO, B., LAZAREVIC, V. & KARAMATA, D. 2002. *tagO* is involved in the synthesis
904 of all anionic cell-wall polymers in *Bacillus subtilis* 168. *Microbiology (Reading),*
905 148**,** 2079-2087.
906 SONG, D., JIAO, H. & LIU, Z. 2021. Phospholipid translocation captured in a bifunctional
907 membrane protein MprF. *Nat Commun,* 12**,** 2927.

908 STAUBITZ, P. & PESCHEL, A. 2002. MprF-mediated lysinylation of phospholipids in
909 *Bacillus subtilis* - protection against bacteriocins in terrestrial habitats? *Microbiology,*
910 148**,** 3331-2.
911 STEINMETZ, M. & RICHTER, R. 1994. Plasmids designed to alter the antibiotic resistance
912 expressed by insertion mutations in *Bacillus subtilis*, through in vivo recombination.
913 *Gene,* 142**,** 79-83.
914 STRAUME, D., PIECHOWIAK, K. W., KJOS, M. & HAVARSTEIN, L. S. 2021. Class A
915 PBPs: It is time to rethink traditional paradigms. *Mol Microbiol*.
916 SURDOVA, K., GAMBA, P., CLAESSEN, D., SIERSMA, T., JONKER, M. J.,
917 ERRINGTON, J. & HAMOEN, L. W. 2013. The conserved DNA-binding protein
918 WhiA is involved in cell division in *Bacillus subtilis*. *J Bacteriol,* 195**,** 5450-60.
919 THITIANANPAKORN, K., AIBA, Y., TAN, X. E., WATANABE, S., KIGA, K., SATO'O,
920 Y., BOONSIRI, T., LI, F. Y., SASAHARA, T., TAKI, Y., AZAM, A. H., ZHANG,
921 Y. & CUI, L. 2020. Association of *mprF* mutations with cross-resistance to
922 daptomycin and vancomycin in methicillin-resistant *Staphylococcus aureus* (MRSA).
923 *Sci Rep,* 10**,** 16107.
924 VEENING, J. W., KUIPERS, O. P., BRUL, S., HELLINGWERF, K. J. & KORT, R. 2006.
925 Effects of phosphorelay perturbations on architecture, sporulation, and spore
926 resistance in biofilms of *Bacillus subtilis*. *J Bacteriol,* 188**,** 3099-109.
927 WILSON, S. & GARNER, E. 2021. An Exhaustive Multiple Knockout Approach to
928 Understanding Cell Wall Hydrolase Function in *Bacillus subtilis*. *bioRxiv***,**
929 2021.02.18.431929.
930 WOOD, B. M., SANTA MARIA, J. P., JR., MATANO, L. M., VICKERY, C. R. &
931 WALKER, S. 2018. A partial reconstitution implicates DltD in catalyzing lipoteichoic
932 acid d-alanylation. *J Biol Chem,* 293**,** 17985-17996.
933 WORMANN, M. E., CORRIGAN, R. M., SIMPSON, P. J., MATTHEWS, S. J. &
934 GRUNDLING, A. 2011. Enzymatic activities and functional interdependencies of
935 *Bacillus subtilis* lipoteichoic acid synthesis enzymes. *Mol Microbiol,* 79**,** 566-83.
936 YANG, S. J., NAST, C. C., MISHRA, N. N., YEAMAN, M. R., FEY, P. D. & BAYER, A.
937 S. 2010. Cell wall thickening is not a universal accompaniment of the daptomycin
938 nonsusceptibility phenotype in Staphylococcus aureus: evidence for multiple
939 resistance mechanisms. *Antimicrob Agents Chemother,* 54**,** 3079-85.
940 ZHU, B. & STULKE, J. 2018. SubtiWiki in 2018: from genes and proteins to functional
941 network annotation of the model organism *Bacillus subtilis*. *Nucleic Acids Res,* 46**,**
942 D743-D748.

Expanded View figures

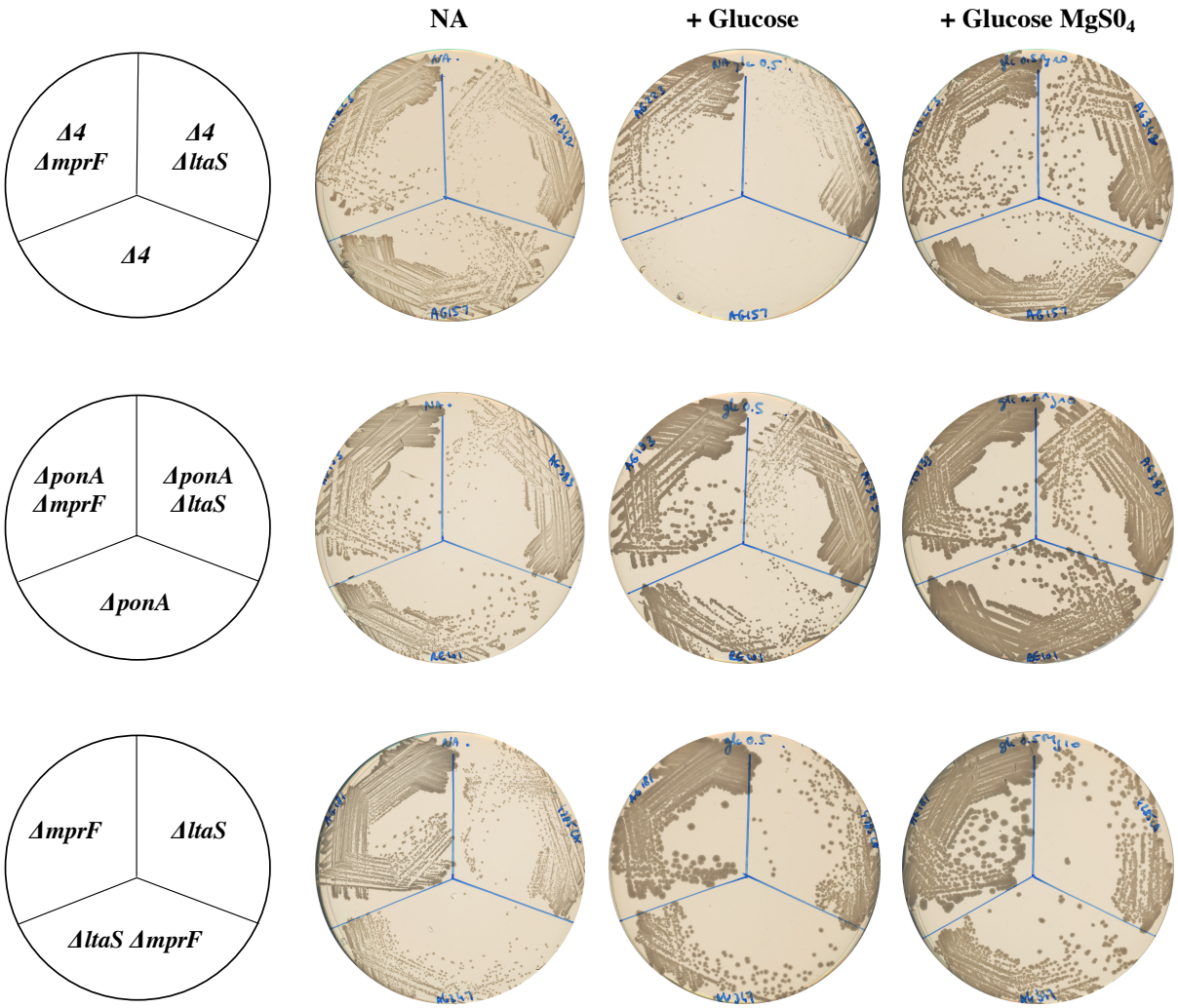

Figure EV1. Comparison of *Δ4* and *ΔponA* mutants in absence MprF or LtaS

Strains were streaked from glycerol stocks onto NA plates (supplemented with antibiotic and/or magnesium, where required). After incubation at 37°C overnight, a single colony for each strain was then streak across the set of plates shown above (with glucose 0.5%, $MgS0_4$ 10mM) and scanned after 16 h incubation at 37°C. The following strains were inoculated: AG157 (*Δ4*), AG223 (*Δ4 ΔmprF*), AG342 (*Δ4 ΔltaS*), RE101 (*ΔponA*), AG193 (*ΔponA ΔmprF*), AG383 (*ΔponA ΔltaS*), AG181 (*ΔmprF*), 4285CA (*ΔltaS*), AG347 (*ΔmprF ΔltaS*).

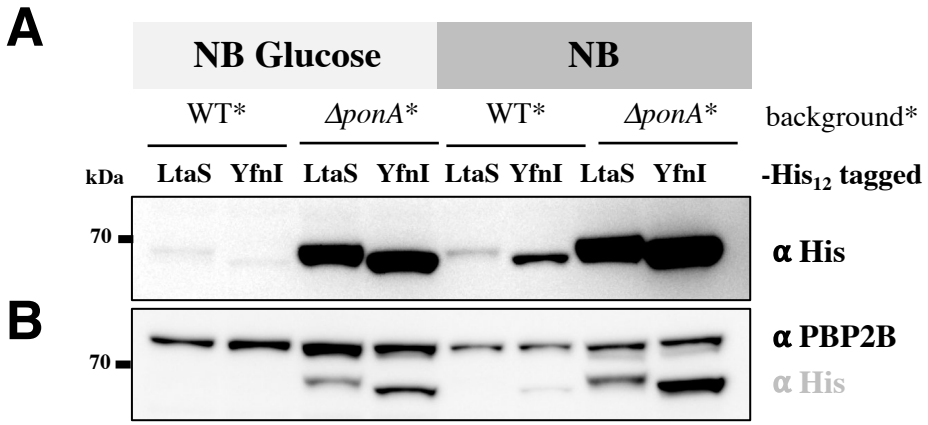

Figure EV2. Accumulation of LtaS-His and YfnI-His in *ΔponA* cells.

Strains were grown in NB and NB supplemented with glucose 0.2% until late exponential growth at 37°C. Tested once in condition similar to that of the proteins Western blot presented in this study, following a preliminary test. * Strains used here express the following his tagged protein under the control of their native promoter: either LtaS-His_{12} in a wild type-like background (AG569) or in *ΔponA* (AG588) background; or YfnI-His_{12} in a wild type-like (WT) (AG570 strain) or in *ΔponA* (AG589) background. (A) The membrane was detected for His tagged proteins with a monoclonal Penta-His and an HRP-linked anti-mouse antibodies. (B) The membrane was reused to detected PBP2B (sample loading control) with a polyclonal anti-PBP2B and HRP-linked anti-rabbit antibodies. Experiment tested on one biological set of samples.

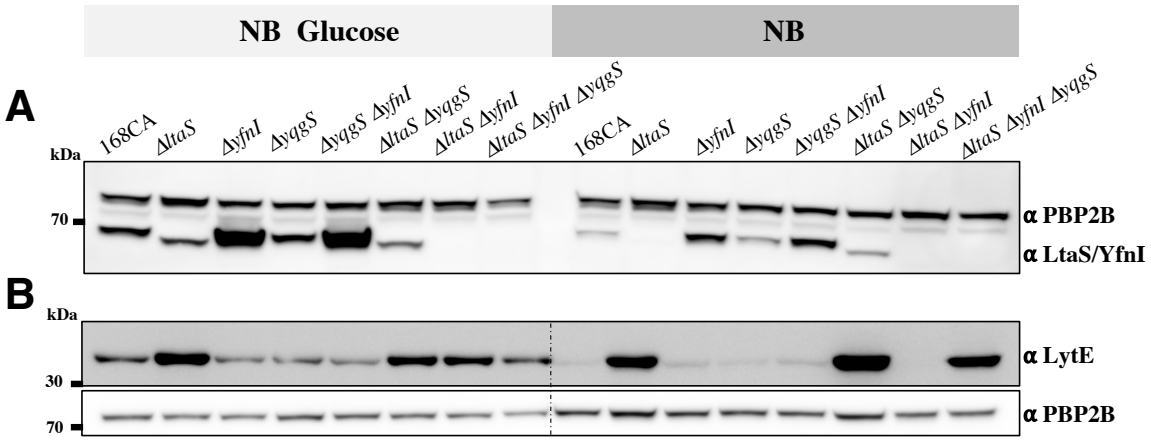

962 **Figure EV3. Accumulation of LtaS/YfnI and LytE in LTA-synthase mutants.**

963 The following strains were grown (NB ± Glc 0.2%) in condition similar to our previous assays:
964 *B. subtilis* 168CA, 4285CA (*ΔltaS*), 4289CA (*ΔyfnI*), 4292CA (*ΔyqgS*), AG595 (*ΔyqgS ΔyfnI*),
965 AG593 (*ΔltaS ΔyqgS)*, AG594 (*ΔltaS ΔyfnI)*, AG600 (*ΔltaS ΔyfnI ΔyqgS*). In this figure, the
966 Western blot experiments were carried out in same condition as other assays (polyclonal anti-
967 LtaS antibody cross reacts with YfnI, unpublished Errington's lab) (A), except for the use of
968 our newly produced polyclonal anti-LytE antibody (B). Experiment tested on one biological
969 set of samples.

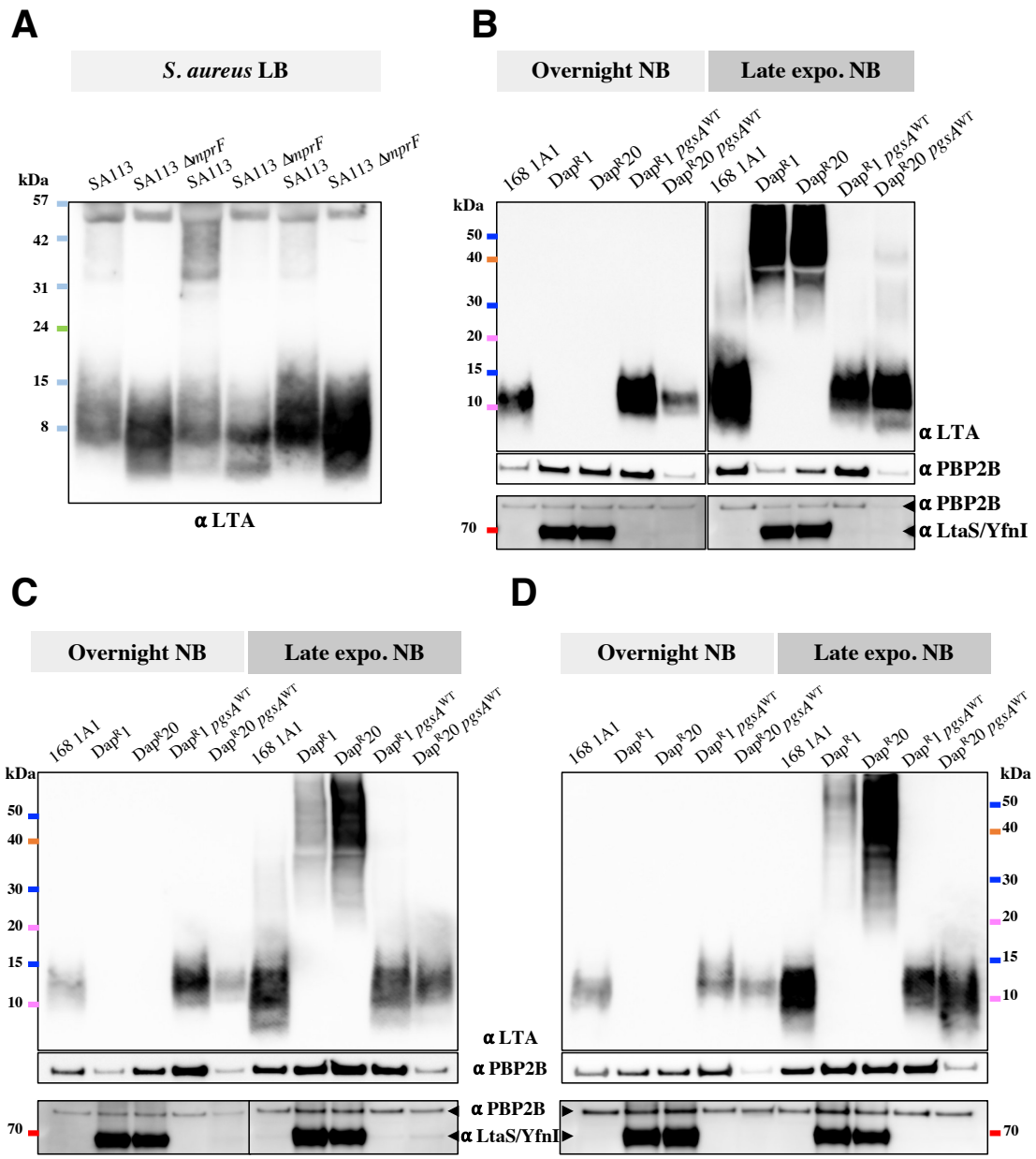

Figure EV4. Results of three independent experiments supporting Fig 5.

A Samples of methicillin-sensitive *Staphylococcus aureus* strains SA113 and SA113 *ΔmprF* (Peschel et al., 2001) were probed for LTA by Western Blot. Three independents set of cultures grown in LB at 37°C were tested simultaneously.

B-D It has been shown that a modified allele of *pgsA*(*A64V*) was the major determinant of daptomycin resistance of *B. subtilis* Dap^{R}1 and Dap^{R}20 strains selected by serial daptomycin antibiotic passages (Hachmann et al., 2011). The strains 168 1A1 (wild type, WT), Dap^{R}1, Dap^{R}20, HB15516 (Dap^{R}1 *pgsA*^{WT}) and HB15507 (Dap^{R}20 *pgsA*^{WT}) were grown in NB overnight at 30°C and at late exponential growth phase (37°C, using theses overnight cultures). For each set of samples, LTA was detected along with PBP2B productions by Western Blots. Bottom panel shows the cellular abundance of PB2B and the LTA-synthase detected with anti-LtaS antibody (also detect YfnI, unpublished Errington's lab). Samples used in the bottom panel where those of the LTA/PBP2B experiment loaded onto a new SDS-gel, after minor samples normalization based on PBP2B signal shown on the upper panel.

Expanded View Tables

Table EV1: Plasmids used in this study (by alphabetic order)

Plasmids	Relevant features[1]	Source or reference
pAM-21	*kan* P_{T7} LytE$^{(26\text{-}334AA)}$-6His *lacI*	This study
pCotC-GFP	used as matrix to amplify *cat*	(Veening et al., 2006)
pDR111	*bla amyE::(lacI* $P_{hyspank}$*, spc)*	Rudner, D., unpublished
pDR111-$P_{hyspank}$-*ltaS*	*bla amyE::(lacI* $P_{hyspank}$*-ltaS, spc)*	This study
pDR111-$P_{hyspank}$-*lytE-mprF*	*bla amyE::(lacI* $P_{hyspank}$*-lytE-mprF, spc)*	This study
pDR111-$P_{hyspank}$-*mprF*	*bla amyE::(lacI* $P_{hyspank\text{-}ATG}$*mprF, spc)*	This study
pDR111-$P_{hyspank}$-*mprF-lytE*	*bla amyE::(lacI* $P_{hyspank\text{-}ATG}$*mprF-lytE, spc)*	This study
pDR111-$P_{hyspank}$-*yfnI*	*bla amyE::(lacI* $P_{hyspank}$*-yfnI, spc)*	This study
pDR111-$P_{hyspank}$-*yqgS*	*bla amyE::(lacI* $P_{hyspank}$*-yqgS, spc)*	This study
pET28a (+)	*kan* P_{T7} *his lacI*	Novagen
pG^{+}host9::*ΔponA*	*erm*, carry flanking DNA regions of *ponA*	(Emami et al., 2017)
pG^{+}host10::*ΔpbpD*	*bla*, carry flanking DNA regions of *pbpD*	(Emami et al., 2017)
pG^{+}host10::*ΔpbpF*	*bla*, carry flanking DNA regions of *pbpF*	(Emami et al., 2017)
pIC22	used as matrix to amplify *phleo*	(Steinmetz and Richter, 1994)
pLOSS*	*bla spc* P_{spac}*-mcs* P_{divIVA}*-lacZ lacI* rep_{pLS20}*(GA→CC)*	(Claessen et al., 2008)
pLOSS-P_{spac}-*lytE*	*bla spc* P_{spac}*-lytE* P_{divIVA}*-lacZ lacI* rep_{pLS20}*(GA→CC)*	This study
pLOSS-P_{spac}-*ponA*	*bla spc* P_{spac}*-ponA* P_{divIVA}*-lacZ lacI* rep_{pLS20}*(GA→CC)*	(Emami et al., 2017)
pMarB	*bla erm* TnYLB-1::*kan Himar1* transposase	(Le Breton et al., 2006)
pMUTinHis	*bla erm* P_{spac} *mcs 12xhis lacZ lacI*	(Ishikawa et al., 2006)
pMUTin-`*lytE-his*	*bla erm* P_{spac} *mcs* `LytE-6AA-12His *lacZ lacI*	This study
pMUTin-`*ltaS-his*	*bla erm* P_{spac} *mcs* `LtaS-6AA-12His *lacZ lacI*	This study
pMUTin-`*yfnI-his*	*bla erm* P_{spac} *mcs* `YfnI-6AA-12His *lacZ lacI*	This study

[1] *cat,* chloramphenicol resistance; *bla*, ampicillin resistance; *spc*, spectinomycin resistance; *erm*, erythromycin resistance; *phleo*, phleomycin resistance; *kan*, kanamycin resistance; *lacI*, encodes lactose repressor; *mcs,* multiple cloning site; *lacZ*, encodes β-galactosidase; AA, amino acids; $P_{hyspank}$ and P_{spac} are IPTG-inducible promoters with $P_{hyspank}$ known to be stronger; rep_{pLS20}*(GA→CC)*, unstable replication in *Bacillus.*

Table EV2: Strains used in this study.

Strains	Relevant genotype[1]	Source or reference[2]
E. coli		
DH5α	F^- endA1 glnV44 thi-1 recA1 relA1 gyrA96 deoR nupG Φ80d*lacZ*ΔM15 Δ(*lacZYA-argF*)U169, hsdR17(r_K^- m_K^+), λ–	Lab. stock
BL21(DE3)	B F^- *ompT gal dcm lon* $hsdS_B(r_B^- m_B^-)$ λ(DE3 [*lacI lacUV5-T7p07 ind1 sam7 nin5*]) $[malB^+]_{K-12}(\lambda^S)$	Novagen
B. subtilis		
168CA	*trpC2*	R. Daniel Lab. stock
168 1A1	*trpC2* (BGSC n° 1A1)	(Hachmann et al., 2011)
3725CA	*trpC2 Ωneo ΔmreB*	3725 (Formstone and Errington, 2005) → 168CA cells
4261CA	*trpC2 Δmbl::cat*	4261 (Schirner and Errington, 2009) → 168CA cells
4283CA	*trpC2* Δ*ltaS::neo*	(Schirner and Errington, 2009) → 168CA cells
4285CA	*trpC2 ΔltaS::cat*	(Schirner and Errington, 2009) → 168CA cells
4287CA	*trpC2 ΔyfnI::spc*	(Schirner and Errington, 2009) → 168CA cells
4289CA	*trpC2 ΔyfnI::erm*	(Schirner and Errington, 2009) → 168CA cells
4292CA	*trpC2 ΔyqgS::spc*	(Schirner and Errington, 2009) → 168CA cells
4293CA	*trpC2* Δ*yqgS::cat*	(Schirner and Errington, 2009) → 168CA cells
4294CA	*trpC2* Δ*yqgS::erm*	(Schirner and Errington, 2009) → 168CA cells
4295CA	*trpC2 ΔyvgJ::spc*	(Schirner and Errington, 2009) → 168CA cells
4620	*trpC2* Δ*ltaS::neo* Δ*yfnI::cat* Δ*yqgS::spc* Δ*yvgJ::erm*	(Schirner and Errington, 2009)
AG105	*trpC2 ΔpbpD ΔpbpF*	pGhost10::ΔpbpF (Emami et al., 2017) → RE103 cells
AG108	*trpC2 ΔponA ΔpbpD ΔpbpF*	$pG^+host10$::*ΔpbpF* → RE104 cells
AG123	*trpC2 ΔponA ΔpbpD ΔpbpF* pLOSS-P_{spac}-*ponA*	pLOSS-P_{spac}-*ponA* → AG108 cells
AG141	*trpC2 ΔponA ΔpbpD ΔpbpF* pLOSS-P_{spac}-*ponA lacA::cat*	K532 → AG123 cells

AG157	*trpC2 ΔponA ΔpbpD ΔpbpF ΔpbpG::kan*	(Emami et al., 2017)
AG181	*trpC2 ΔmprF::phleo*	This study
AG185	*trpC2 ΔmprF::phleo Ωneo ΔmreB*	3725CA → AG181 cells
AG189	*trpC2 ΔmprF::phleo Δmbl::cat*	4261CA → AG181 cell
AG193	*trpC2 ΔponA ΔmprF::phleo*	AG181 → RE101 cells
AG200	*trpC2 ΔponA ΔpbpD ΔpbpF* pLOSS-P_{spac}-*ponA ΔmprF::phleo lacA::cat*	AG183 → AG141 cells
AG200BK#42	*trpC2 ΔponA ΔpbpD ΔpbpF* pLOSS-P_{spac}-*ponA ΔmprF::phleo lacA::cat gtaB::*TnYLB-1*(kan)*	This study
AG210	*trpC2 ΔponA ΔpbpD ΔpbpF ΔpbpG::kan ΔmprF::phleo lacA::cat* pLOSS-P_{spac}-*ponA*	DPVB45CA → AG200 cells
AG211	*trpC2 ΔponA ΔpbpD ΔpbpF ΔpbpG::kan* pLOSS-P_{spac}-*ponA*	DPVB45CA → AG123 cells
AG223	*trpC2 ΔponA ΔpbpD ΔpbpF ΔpbpG::kan ΔmprF::phleo*	AG181 → AG157 cells
AG290	*trpC2 ΔponA ΔpbpD ΔpbpF ΔpbpG::kan* pLOSS-P_{spac}-*ponA ΔgtaB::erm*	SM08 → AG211 cells
AG290NopLoss	*trpC2 ΔponA ΔpbpD ΔpbpF ΔpbpG::kan ΔgtaB::erm*	AG290 lost plasmid on 20 mM $MgS0_4$ with kan
AG292	*trpC2 ΔponA ΔpbpD ΔpbpF ΔpbpG::kan* pLOSS-P_{spac}-*ponA Ωerm ΔtagE*	SM50 → AG211 cells
AG293	*trpC2 ΔponA ΔpbpD ΔpbpF ΔpbpG::kan ggaAB::spc*	SM31 → AG229 cells
AG296	*trpC2 ΔponA ΔpbpD ΔpbpF ΔpbpG::kan* pLOSS-P_{spac}-*ponA pgcA::tet*	SSB122 → AG211 cells
AG304	*trpC2 amyE::(*$P_{hyspank}$*-mprF, spc)*	pDR111-$P_{hyspank}$-*mprF* → 168CA cells
AG311	*trpC2 ΔponA amyE::(*$P_{hyspank}$*-mprF, spc)*	AG304 → RE101 cells
AG317	*trpC2 ΔponA ΔpbpD ΔpbpF ΔpbpG::kan amyE::(*$P_{hyspank}$*-mprF, spc)*	AG304 → AG157 cells
AG322	*trpC2 amyE::(*$P_{hyspank}$*-mprF, spc) Δmbl::cat*	4261CA → AG304 cells
AG327	*trpC2 amyE::(*$P_{hyspank}$*-mprF, spc) Ωneo ΔmreB*	3725CA → AG304 cells
AG341	*trpC2 ΔponA ΔpbpD ΔpbpF ΔpbpG::kan dltAB::cat*	DLT71 (Perego et al., 1995) → AG157 cells
AG342	*trpC2 ΔponA ΔpbpD ΔpbpF ΔpbpG::kan ΔltaS::cat*	4285CA → AG157 cells
AG343	*trpC2 ΔponA ΔpbpD ΔpbpF ΔpbpG::kan ΔyfnI::erm*	4289CA → AG157 cells
AG344	*trpC2 ΔponA ΔpbpD ΔpbpF ΔpbpG::kan ΔyqgS::erm*	4294CA→ AG157 cells

AG347	*trpC2 ΔmprF::phleo ΔltaS::cat*	4285CA → AG181 cells
AG353	*trpC2 amyE::($P_{hyspank}$-mprF, spc) ΔyfnI::erm*	4289CA→ AG304 cells
AG370	*trpC2 ΔponA ΔpbpD ΔpbpF ΔpbpG::kan ΔltaS::cat ΔyfnI::erm*	4289CA → AG342 cells
AG372	*trpC2 ΔponA ΔpbpD ΔpbpF ΔpbpG::kan ΔltaS::cat ΔyqgS::erm*	4294CA → AG342 cells
AG377	*trpC2 ΔponA ΔpbpD ΔpbpF ΔpbpG::kan ΔyqgS::erm ΔyfnI::spc*	4287CA → AG344 cells
AG380	*trpC2 ΔponA ΔpbpD ΔpbpF ΔpbpG::kan ΔltaS::cat ΔyqgS::erm ΔyfnI::spc*	4287CA → AG372 cells
AG383	*trpC2 ΔponA ΔltaS::cat*	4285CA → RE101 cells
AG384	*trpC2 ΔponA ΔyfnI::erm*	4289CA → RE101 cells
AG385	*trpC2 ΔponA ΔyqgS::spc*	4292CA → RE101 cells
AG389	*trpC2 ΔponA ΔpbpD ΔpbpF ΔpbpG::kan ΔmprF::phleo ΔltaS::cat ΔyqgS::erm*	AG223 → AG372 cells
AG390	*trpC2 ΔponA ΔpbpD ΔpbpF ΔpbpG::kan ΔmprF::phleo ΔygqS::erm ΔyfnI::spc*	AG223 → AG377 cells
AG393	*trpC2 ΔponA ΔltaS::cat ΔyfnI::erm*	4289CA → AG383 cells
AG394	*trpC2 ΔponA ΔltaS::cat ΔyqgS::spc*	4292CA → AG383 cells
AG395	*trpC2 ΔponA ΔyfnI::spc ΔyqgS::spc*	4292CA→ AG384 cells
AG399	*trpC2 ΔponA ΔpbpD ΔpbpF ΔpbpG::kan ΔmprF::phleo ΔltaS::cat ΔyfnI::erm*	AG223 → AG370 cells
AG400	*trpC2 ΔponA ΔpbpD ΔpbpF ΔpbpG::kan ΔmprF::phleo ΔltaS::cat ΔyqgS::erm ΔyfnI::spc*	AG223 → AG380 cells
AG403	*trpC2 ΔponA ΔltaS::cat ΔyfnI::erm ΔyqgS::spc*	4292CA → AG393 cells
AG417	*trpC2 ΔpbpD ΔpbpF ΔpbpG::kan*	DPVB45CA → AG105 cells
AG421	*trpC2 ΔpbpD ΔpbpF ΔpbpG::kan amyE::($P_{hyspank}$ mprF, spc)*	AG304 → AG417 cells
AG441	*trpC2 ΔponA ΔltaS::cat ΔyfnI::erm ΔugtP::spc*	PG253 → AG393 cells
AG442	*trpC2 ΔponA ΔltaS::cat ΔyfnI::erm gtaB::TnYLB-1(kan)*	AG200BK#42 → 168CA → AG393 cells
AG443	*trpC2 ΔponA ΔpbpD ΔpbpF ΔpbpG::kan ΔugtP::spc*	PG253 → AG157 cells
AG444	*trpC2 ΔponA ΔugtP::spc*	PG253 → RE101 cells
AG474	*trpC2 ΔcwlO::spc*	PDC463 (Dominguez-Cuevas et al., 2013) → 168CA cells
AG475	*trpC2 amyE::($P_{hyspank}$-lytE, spc)*	Dominguez-Cuevas, unpublished → 168CA cells
AG484	*trpC2 ΔponA amyE::($P_{hyspank}$-lytE, spc)*	AG475 → RE101 cells

AG501	*trpC2 ΔponA ΔpbpD ΔpbpF ΔpbpG::kan amyE::(*$P_{hyspank}$*-lytE, spc)*	AG475 → AG157 cells
AG502	*trpC2 ΔponA ΔpbpD ΔpbpF ΔpbpG::kan ΔmprF::phleo amyE::(*$P_{hyspank}$*-lytE, spc)*	AG475 → AG223 cells
AG506	*trpC2 ΔponA ΔgtaB::erm*	SM08 → RE101 cells
AG547	*trpC2 ΔlytE::cat*	This study
AG549	*trpC2 ΔlytE::cat* pLOSS-P_{spac}*-lytE*	pLOSS-P_{spac}*-lytE* →AG547 cells
AG551	*trpC2* pLOSS-P_{spac}*-lytE*	pLOSS-P_{spac}*-lytE* → 168CA cells
AG557	*trpC2* Δ*ponA* pLOSS-P_{spac}*-lytE*	pLOSS-P_{spac}*-lytE* → RE101 cells
AG565	*trpC2* Ω*lytE-his*$_{12}$::(pMUTin-*`lytE, erm*)	pMUTinHis-*'lytE* → 168CA cells
AG569	*trpC2* Ω*ltaS-his*$_{12}$*::(*pMUTIN-*`ltaS, erm)*	pMUTinHis-*'ltaS* → 168CA cells
AG570	*trpC2* Ω*yfnI-his*$_{12}$*::(*pMUTIN-*`yfnI, erm)*	pMUTinHis-*'yfnI* → 168CA cells
AG586	*trpC2* Δ*cwlO::spc* Ω*lytE-his*$_{12}$::(pMUTin-*`lytE, erm*)	pMUTinHis-*'lytE* → AG474 cells
AG587	*trpC2* Δ*ponA* Ω*lytE-his*$_{12}$::(pMUTin-*`lytE, erm*)	AG565 → RE101 cells
AG588	*trpC2* Δ*ponA* Ω*ltaS-his*$_{12}$*::(*pMUTIN-*`ltaS, erm)*	AG569 → RE101 cells
AG589	*trpC2* Δ*ponA* Ω*yfnI-his*$_{12}$*::(*pMUTIN-*`yfnI, erm)*	AG570 → RE101 cells
AG593	*trpC2 ΔyqgS:spc ΔltaS::cat*	4292CA → 4285CA cells
AG594	*trpC2 ΔyfnI::erm ΔltaS::cat*	4289CA → 4285CA cells
AG595	*trpC2 ΔyfnI::erm ΔyqgS::spc*	4292CA → 4289CA cells
AG600	*trpC2 ΔltaS::cat ΔyfnI::erm ΔyqgS::spc*	4285CA → AG595 cells
AG614	*trpC2 ΔponA ΔpbpD ΔpbpF ΔpbpG::kan ΔmprF::phleo* pLOSS-P_{spac}*-ponA ΔgtaB::erm*	SM08 → AG210 cells
AG632	*trpC2 ΔponA ΔpbpD ΔpbpF ΔpbpG::kan ΔmprF::phleo ΔugtP::spc*	PG253 → AG223 cells
AG636	*trpC2 ΔponA ΔpbpD ΔpbpF ΔpbpG::kan ΔmprF::phleo ΔgtaB::erm*	AG614 plasmid lost on NA $MgS0_4$ 20 mM with erm
AG1460	*trpC2* Δ*pbpD* Δ*pbpF* Δ*pbpG::kan amyE::(*$P_{hyspank}$*-lytE, spc)*	AG475 → AG417 cells
AG1461	*trpC2* Δ*lytE::cat amyE::(*$P_{hyspank}$*-lytE, spc)*	AG475 → AG547 cells
AG1462	*trpC2* Δ*ltaS::cat amyE::(*$P_{hyspank}$*-lytE, spc)*	AG475 → 4285CA cells
AG1463	*trpC2* Δ*yfnI::erm amyE::(*$P_{hyspank}$*-lytE, spc)*	AG475 → 4289CA cells

AG1465	*trpC2* Δ*ponA* Δ*pbpD* Δ*pbpF* Δ*pbpG::kan* Δ*ltaS::cat amyE::(*$P_{hyspank}$*-lytE, spc)*	AG475 → AG342 cells
AG1466	*trpC2* Δ*ltaS::cat* pLOSS-P_{spac}-*lytE*	pLOSS-P_{spac}-*lytE* → 4285CA cells
AG1467	*trpC2* Δ*yfnI::erm* pLOSS-P_{spac}-*lytE*	pLOSS-P_{spac}-*lytE* → 4289CA cells
AG1469	*trpC2* Δ*ltaS::cat* Δ*yfnI::erm* pLOSS-P_{spac}-*lytE*	pLOSS-P_{spac}-*lytE* → AG594 cells
AG1478	*trpC2* Δ*mprF::phleo amyE::(*$P_{hyspank}$*-lytE, spc)*	AG475 → AG181 cells
AG1479	*trpC2* Δ*ponA* Δ*mprF::phleo amyE::(*$P_{hyspank}$*-lytE, spc)*	AG475 → AG193 cells
AG1480	*trpC2* Δ*ponA* Δ*ltaS::cat amyE::(*$P_{hyspank}$*-lytE, spc)*	AG475 → AG383 cells
AG1481	*trpC2* Δ*mprF::phleo* pLOSS-P_{spac}-*lytE*	pLOSS-P_{spac}-*lytE* → AG181 cells
AG1482	*trpC2* Δ*ponA* Δ*mprF::phleo* pLOSS-P_{spac}-*lytE*	pLOSS-P_{spac}-*lytE* → AG193 cells
AG1483	*trpC2* Δ*ponA* Δ*ltaS::cat* pLOSS-P_{spac}-*lytE*	pLOSS-P_{spac}-*lytE* → AG383 cells
AG1486	*trpC2* Δ*mprF::phleo* Ω*lytE-his*$_{12}$::(pMUTin-`*lytE, erm*)	AG565 → AG181 cells
AG1487	*trpC2* Δ*ponA* Δ*mprF::phleo* Ω*lytE-his*$_{12}$::(pMUTin-`*lytE, erm*)	AG565 → AG193 cells
AG1488	*trpC2* Δ*ponA* Δ*ltaS::cat* Ω*lytE-his*$_{12}$::(pMUTin-`*lytE, erm*)	AG565 → AG383 cells
AG1489	*trpC2* Δ*ltaS::cat* Ω*lytE-his*$_{12}$::(pMUTin-`*lytE, erm*)	AG565 → 4285CA cells
AG1490	*trpC2* Δ*ltaS::cat* Δ*yqgS::erm*	4294CA → 4285CA cells
AG1491	*trpC2* Δ*yqgS::cat* Δ*yfnI::erm*	4293CA → 4289CA cells
AG1492	*trpC2* Δ*yqgS::cat amyE::(*$P_{hyspank}$*-lytE, spc)*	AG475 → 4293CA cells
AG1493	*trpC2* Δ*yqgS::cat* pLOSS-P_{spac}-*lytE*	pLOSS-P_{spac}-*lytE* → 4293CA cells
AG1497	*trpC2* Δ*ltaS::cat* Δ*yfnI::erm amyE::(*$P_{hyspank}$*-lytE, spc)*	AG475 → AG594 cells
AG1498	*trpC2* Δ*ltaS::cat* Δ*yqgS::erm amyE::(*$P_{hyspank}$*-lytE, spc)*	AG475 → AG1490 cells
AG1499	*trpC2* Δ*yqgS::cat* Δ*yfnI::erm amyE::(*$P_{hyspank}$*-lytE, spc)*	AG475 → AG1491 cells
AG1500	*trpC2* Δ*ltaS::cat* Δ*yqgS::erm* pLOSS-P_{spac}-*lytE*	pLOSS-P_{spac}-*lytE* → AG1490 cells
AG1502	*trpC2* Δ*yqgS::cat* Δ*yfnI::erm* pLOSS-P_{spac}-*lytE*	pLOSS-P_{spac}-*lytE* → AG1491 cells

AG1535	*trpC2* Δ*ugtP::spc* Ω*lytE-his*$_{12}$::(pMUTin-`*lytE, erm*)	AG565 → PG253 cells
AG1541	*trpC2* Δ*cwlO::spc* Ω*lytE-his*$_{12}$::(pMUTin-`*lytE, erm*)	AG565 → AG474 cells
AG1581	*trpC2* Δ*mbl::zeo amyE::(P*$_{hyspank}$*-mprF, spc)*	AK045B → AG304 cells
AG1593	*trpC2* Δ*mreBH::kan*	BGSC strain* → 168CA cells
AG1594	*trpC2* Δ*ugtP::kan*	BGSC strain* → 168CA cells
AG1604	*trpC2* Δ*ponA* Ω*neo* Δ*mreB*	KS36 → RE101 cells
AG1605	*trpC2* Δ*ponA* Δ*mbl::zeo*	AK045B → RE101 cells
AG1643	*trpC2* Δ*ugtP::kan amyE::(P*$_{hyspank}$*-lytE, spc)*	AG1594 → AG475 cells
AG1663	*trpC2* Δ*mprF::kan*	BGSC strain* → 168CA cells
AG1667	*trpC2* Δ*ltaS::cat* Δ*yfnI::erm amyE::(P*$_{hyspank}$*-lytE, spc) ΔmprF::kan*	AG1663 → AG1497 cells
AG1668	*trpC2* Δ*ltaS::cat* Δ*yqgS::erm amyE::(P*$_{hyspank}$*-lytE, spc) ΔmprF::kan*	AG1663 → AG1498 cells
AG1669	*trpC2* Δ*yqgS::cat* Δ*yfnI::erm amyE::(P*$_{hyspank}$*-lytE, spc) ΔmprF::kan*	AG1663 → AG1499 cells
AG1670	*trpC2* Δ*ltaS::cat* Δ*yfnI::erm amyE::(P*$_{hyspank}$*-lytE, spc) ΔugtP::kan*	AG1594 → AG1497 cells
AG1671	*trpC2* Δ*ltaS::cat* Δ*yqgS::erm amyE::(P*$_{hyspank}$*-lytE, spc) ΔugtP::kan*	AG1594 → AG1498 cells
AG1672	*trpC2* Δ*yqgS::cat* Δ*yfnI::erm amyE::(P*$_{hyspank}$*-lytE, spc) ΔugtP::kan*	AG1594 → AG1499 cells
AG1676	*trpC2 amyE::(P*$_{hyspank}$ *mprF, spc) aprE::(P*$_{spac}$ *lytE, erm)*	PCR on gDNA PDC620 → AG304 cells
AG1677	*trpC2 amyE::(P*$_{hyspank}$ *mprF, spc) aprE::(P*$_{xyl}$ *lytE, erm)*	PCR on gDNA PDC702→ AG304 cells
AG1684	*trpC2* Δ*ponA* Ω*lytE-his*$_{12}$::(pMUTin-`*lytE, erm*) *amyE::(P*$_{hyspank}$*-mprF, spc)*	AG304 → AG587 cells
AG1685	*trpC2* Δ*ponA* Ω*lytE-his*$_{12}$::(pMUTin-`*lytE, erm*) Δ*ugtP::kan*	AG1594 → AG587 cells
AG1707	*trpC2 amyE::(P*$_{hyspank}$ *-mprF-lytE)*	pDR111 *P*$_{hyspank}$ *mprF-lytE* → 168CA cells
AG1709	*trpC2 amyE::(P*$_{hyspank}$ *-lytE-mprF)*	pDR111 *P*$_{hyspank}$ *lytE-mprF* → 168CA cells
AG1711	*trpC2 ΔponA amyE::(P*$_{hyspank}$ *-mprF-lytE)*	AG1707 → RE101 cells
AG1713	*trpC2 ΔponA amyE::(P*$_{hyspank}$ *-lytE-mprF)*	AG1709 → RE101 cells
AG1715	*trpC2 ΔltaS::cat amyE::(P*$_{hyspank}$ *-mprF-lytE)*	AG1707 → 4285CA cells
AG1717	*trpC2 ΔltaS::cat amyE::(P*$_{hyspank}$ *-lytE-mprF)*	AG1709 → 4285CA cells
AK045B	*trpC2 Δmbl::zeo* (in 168CA background)	H. Strahl's lab, A. Koh
Dap^{R}1	DAP-resistant isolate derived from 168 1A1	(Hachmann et al., 2011)

Dap^{R}20	DAP-resistant isolate derived from 168 1A1	(Hachmann et al., 2011)
DLT71CA	*trpC2 dltAB::cat*	DLT71 (Perego et al., 1995) → 168CA cells
DPVB45CA	*trpC2 ΔpbpG::kan*	DPVB45 (McPherson et al., 2001) → 168CA
HB15507	Dap^{R}20 *pgsA*^{WT}	(Hachmann et al., 2011)
HB15516	Dap^{R}1 *pgsA*^{WT}	(Hachmann et al., 2011)
K532	*trpC2 lacA::cat*	D. Claessen, unpublished
KS36	*trpC2 Ωneo ΔmreB* (in 168CA background)	H. Strahl's lab, K. Seistrup
PDC620	*trpC2 aprE::(*P_{spac}*-lytE, erm)*	(Dominguez-Cuevas et al., 2013)
PDC702	*trpC2 ΔlytE::cat::spc aprE(::*P_{xyl}*-lytE erm)*	(Dominguez-Cuevas et al., 2013)
PG253	*trpC2 ΔugtP::spc*	P. Gamba, unpublished
RE101	*trpC2 ΔponA*	(Emami et al., 2017)
RE102	*trpC2 ΔpbpF*	pG$^+$host10::*ΔpbpF* (Emami et al., 2017) → 168CA cells
RE103	*trpC2 ΔpbpD*	pG$^+$host10::*ΔpbpD* (Emami et al., 2017) → 168CA cells
RE104	*trpC2 ΔponA ΔpbpD*	pG$^+$host9::*ΔponA* (Emami et al., 2017) → RE103 cells
SM08	*trpC2 ΔgtaB::erm*	S. Moore, unpublished
SM31	*trpC2 ggaAB::spc*	S. Moore, unpublished
SM50	*trpC2 Ωerm ΔtagE*	S. Moore, unpublished
SSB122	*trpC2 pgcA (yhxB)::tet*	(Branda et al., 2004)
SWA11a	*trpC2 ΔponA ΔpbpD ΔpbpF lacA::cat mprF::TnYLB-1(kan)*	This study
S. aureus		
SA113	SA113 (wild type, methicillin-sensitive)	T. Palmer, lab collection
SA113 *ΔmprF*	SA113 *ΔmprF::erm*	(Peschel et al., 2001)

[1] Antibiotic resistance to *spc*, spectinomycin; *kan*, kanamycin; *erm*, erythromycin; *neo*, neomycin; *cat*, chloramphenicol; *tet*, tetracyclin; *zeo*, zeocin and *phleo*: phleomycin. *TnYLB-1(kan)* transposon that originates from pMarB (Table EV1). his_{12} indicates a coding sequence that corresponds to a 12 His tag at the C terminus. $P_{hyspank}$ and P_{spac} are IPTG-inducible promoters with $P_{hyspank}$ known to be stronger. Other abbreviations: Δ, deletion; Ω, insertion.
[2] Arrows indicate how the strain was constructed by transformation using either a plasmid DNA, a chromosomal DNA (strain code is then indicated) or a PCR on chromosomal DNA. BGSC* refers to the deletion mutant collection of the Bacillus Genetic Stock Center (Koo et al., 2017).

Table EV3: primers used in this study

Primer name	Sequence (in bold restriction enzyme site)	Used for[1]
oAA01	TTTTTCACCTTAATGCTTTGCATGGTATA TCTCCTTCTTAAAGTTAAACAAAATTATT TCTAGAGG	To amplify pET28a (+)
oAA02	ACCTCGGTGCGAAAAGATTCCACCACCA CCACCACCACT	To amplify pET28a (+)
oAA03	TAAGAAGGAGATATACCATGCAAAGCAT TAAGGTGAAAAAAGGCGAC	To amplify *lytE* from base 76th-1002th
oAA04	CAGTGGTGGTGGTGGTGGTGGAATCTTTT CGCACCGAGGTAACG	To amplify *lytE* from base 76th-1002th
oAA05	ACGCCGAAACAAGCGCTC	To check pET28a-*lytE-his* plasmid
oAA06	GCTAGTTATTGCTCAGCG	To check pET28a-*lytE-his* plasmid
oAG18	GTTGACTTTATCTACAAGGT	To check insert cloned in pLOSS-P_{spac}-*lytE*
oAG19	GGTACCAGTAGTTCACCAC	To check pLOSS-P_{spac}-*lytE*
oAG81	GAATCGCCTGGCTCACATCATC	To check *B. subtilis mprF::*TnYLB-1
oAG82	CGGCAAAGAACAGTCCCAAG	To check *B. subtilis mprF::*TnYLB-1
oAG103	CCTGTATGTCTGGCACTCAC	To amplify upstream *mprF*
oAG104	GC**TCTAGA**TGGTCTCTCCAATCATATTC	To amplify upstream *mprF* (*Eco*RI)
oAG105	CG**GAATTC**TAAGACGGAGTCTTTTTTTAT TTCG	To amplify downstream *mprF* (*Xba*I)
oAG106	CGGAGATGCGAGAGGGTTTC	To amplify downstream *mprF*
oAG107	TGCGGCATGCTCATATCCAG	To check *B. subtilis ΔmprF*
oAG108	TGGGCCAATCAGTGGACAAG	To check *B. subtilis ΔmprF*
oAG124	CCATCATCTGGTGCGAAAGG	(Emami et al., 2017), to check *B. subtilis ΔponA*
oAG125	CCGCAAAGCCGATTAATTGG	
oAG126	TCTATTGGCGAGTGCTTC	(Emami et al., 2017), to check *B. subtilis ΔpbpF*
oAG127	AGCATCGACTCCGTATTG	
oAG128	TTATTCGGAATGGCGATGGG	(Emami et al., 2017),to check *B. subtilis ΔpbpD*
oAG129	CCTTAATGGCTGCAGTTGAC	
oAG165	CTAACCTGGCTGACATTCAC	To check *B. subtilis gtaB::*TnYLB-1
oAG166	TGATCAGGTCTTCGCAGTTG	To check *B. subtilis gtaB::*TnYLB-1
oAG197	GC**TCTAGA**GCACCCATTAGTTCAACAAA CG	To amplify *cat* (*Xba*I)
oAG198	GC**GGATCC**AGTACAGTCGGCATTATCTC	To amplify *cat* (*BamH*I)
oAG271	GGG**GTCGAC**AAAGGAGATTCCTAGGAT GCTGATTAAAAAGAATGCT	To construct pDR111-$P_{hyspank}$-*mprF*
oAG272	GGG**GCATGC**TTGATGATATTGAAACCT	To construct pDR111-$P_{hyspank}$-*mprF*
oAG292	AGGCACTCGTGAAAGGAATC	To check plasmid by sequencing
oAG294	TTCAGCGTGCGGTATTAGTG	To check plasmid by sequencing
oAG300	CAATCACGAAACAATAATTGG	To check cloned insert in pDR111

oAG301	GTTGACTTTATCTACAAGGTG	To check cloned insert in pDR111
oAG308	GGG**GCTAGC**AAAGGAGATTCCTAGGATGAAAACATTTATAAAAGAAAGAGG	To construct pDR111-$P_{hyspank}$-*ltaS* (*Nhe*I)
oAG309	CCG**GCATGC**CCGAATGTGGAATTTGC	To construct pDR111-$P_{hyspank}$-*ltaS* (*Sph*I)
oAG310	GGG**GCTAGC**AAAGGAGATTCCTAGGATGAAGAAACTTTTTCTTACAAAC	To construct pDR111-$P_{hyspank}$-*yfnI* (*Nhe*I)
oAG311	CCG**GCATGC**TGTAATGATATGAGAGAAAGC	To construct pDR111-$P_{hyspank}$-*yfnI* (*Sph*I)
oAG312	GGG**GCTAGC**AAAGGAGATTCCTAGGATGCGAAAAACGTTTTTTCGAAG	To construct pDR111-$P_{hyspank}$-*yqgS* (*Nhe*I)
oAG313	CCGGCATGCGAAAGCCTCCCGCTCACTTC	To construct pDR111-$P_{hyspank}$-*yqgS* (*Sph*I)
oAG340	GTCACATGAAGTCAAGACTATT	To check *ΔlytE*
oAG341	ACGGTTTATCAAGGAAGGACTC	To check *ΔlytE*
oAG348	GTG**GCGGCCGC**ATGAAAAAGCAAATCATTACAG	To construct pLOSS-P_{spac}-*lytE* (*Not*I)
oAG349	CCG**GGATCC**GATTGCCCTTTATGAAAATAAG	To construct pLOSS-P_{spac}-*lytE* (*BamH*I)
oAG350	GTCTGTGCTTGAGGATAAGG	To amplify upstream *lytE* for construction *ΔlytE*
oAG351	GGG**TCTAGA**CTGCTGTCGTAGCTGTAATG	To amplify upstream *lytE* (*Xba*I) for construction *ΔlytE*
oAG352	CCG**GGATCC**GCGAAAAGATTCTAATTTTTAG	To amplify downstream *lytE* (*BamH*I), for construction *ΔlytE*
oAG353	GATCCGTTTGCGTGTTTC	To amplify downstream *lytE,* for construction *ΔlytE*
oAG354	GGG**GAATTC**GGCGGAACGACAACTTCAG	To construct pMUTin-`*lytE-his*, amplify 3' terminus `*lytE* (no stop codon)
oAG355	GGG**CTCGAG**GAATCTTTTCGCACCGAGG	To construct pMUTin-`*lytE-his*, amplify 3' terminus `*lytE* (no stop codon)
oAG360	GGC**GAATTC**GATTTATTCTCTAAAGACCACG	To construct pMUTin-`*yfnI-his*, amplify 3' terminus `*yfnI* (no stop codon)
oAG361	GGG**CTCGAG**TTTGATTTCTTTCTCCTTGCCG	To construct pMUTin-`*yfnI-his*, amplify 3' terminus `*yfnI* (no stop codon)
oAG366	GGC**GAATTC**CGAAACGGAGACTTTATTTCAC	To construct pMUTin-`*ltaS-his*, amplify 3' terminus `*ltaS* (no stop codon)
oAG367	GGG**CTCGAG**TTTATCTTCGTTATCCTTTGAC	To construct pMUTin-`*ltaS-his*, amplify 3' terminus `*ltaS* (no stop codon)
oAG368	CAAGGTGTGGCATAATGT	To check integration in pMUTinHis
oAG369	GACATCCAGAGGCACTTC	To check integration in pMUTinHis
oAG412	CACCTGGTTTTCTGCTATAGT	To check *B. subtilis ΔgtaB*
oAG413	GTTTAACTCTACAATCAGTG	To check *B. subtilis ΔgtaB*

PhleoXbaI-fw	GC**TCTAGA**TCTTCCTTCAGGTTATGAC	To amplify *phleo* from pIC22 (*Xba*I)
PhleoEcoRI-rev	C**GAATTC**CGCGCCCGATTGCTGAAC	To amplify *phleo* from pIC22 (*Eco*RI)
oAG686	AAGAGAATGCGCCGGAACATC	To amplify *aprE* locus and generate strain AG1676-1677
oAG689	TGACATTCGGCACACTCC	To amplify *aprE* locus and generate strain AG1676-1677
oAG911	TGATTGGCAAAAGCAAAAAAGACTCCGTCTAATAGTCGACAAAGGAGATTCCTAGGatgaaaaagcaaatcattacagc	To construct pDR111-$P_{hyspank}$-*mprF-lytE* (co-expression)
oAG912	GACCTCGTTTCCACCGAATTAGCTTGCATGCTTGATGATATTGAAACCTAttagaatcttttcgcaccgag	To construct pDR111-$P_{hyspank}$-*mprF-lytE* (co-expression)
oAG913	GGTACGTACGATCTTTCAGC	To check plasmid construct
oAG914	GGAGTGGCGAGGGAAATAC	To check plasmid construct
oAG915	ccttaatgctttgtgcagatg	To check plasmid construct
oAG916	GTTAACTCTAGAGCTGCCTG	To check plasmid construct
oAG917	GTGTGTAATTGTGAGCGGATAACAATTAAGCTTAGTCGACAAAGGAGATTCCTAGGatgaaaaagcaaatcattacagc	To construct pDR111-$P_{hyspank}$-*lytE-mprF* (co-expression)
oAG918	TATTGATAAAGCATTCTTTTTAATCAGCATCCTAGGAATCTCCTTTGTCGACTAttagaatcttttcgcaccgag	To construct pDR111-$P_{hyspank}$-*lytE-mprF* (co-expression)
oAG919	GATGACCATGAGCGTACG	To check plasmid construct
oAG920	ccgtctgttggtgatttcgtc	To check plasmid construct

[1] *cat,* chloramphenicol resistance*; phleo*, phleomycin cassette; P_{spac} and $P_{hyspank}$ are promoter inducible with IPTG, the latter is known to be stronger; $rep_{pLS20}(GA \rightarrow CC)$, unstable replication in *Bacillus, TnYLB-1* transposon associated to kanamycin resistance.

APPENDIX

Insights into the role of lipoteichoic acids in *Bacillus subtilis*- a new function for MprF

Aurélie Guyet[1]*, Amirah Alofi[1], Richard A. Daniel[1]*

[1]The Centre for Bacterial Cell Biology, Baddiley-Clark Building, Medical School, Newcastle University, Richardson Road, Newcastle upon Tyne NE2 4AX, United Kingdom.
*For correspondence: aurelie.guyet@newcastle.ac.uk and richard.daniel@newcastle.ac.uk
Tel. +44 1912 083239.

TABLE OF CONTENT

Appendix Figure S1. Other growth condition assays supporting Fig 1.

Appendix Figure S2. Growth of actin like mutants in 168CA background and in absence of *ponA*.

Appendix Figure S3. Additional TEM images of *B. subtilis* strains.

Appendix Figure S4. Absence of *gtaB* or *ugtP* causes severe growth defect in absence of *ponA*.

Appendix Figure S5. Cell morphogenesis changes associated with deletion of LTA-synthase genes combined with class A PBPs null mutants of *B. subtilis*.

Appendix Figure S6. Effect of LTA-synthase deletions in *ΔponA* background.

Appendix Figure S7. Results of three independent LTA Western blots supporting Fig 3A.

Appendix Figure S8. Results of three independent LTA Western blots supporting Fig 3B.

Appendix Figure S9. Results of three independent LTA Western blots supporting Fig 3C.

Appendix Figure S10. LytE overexpression is conditionally lethal in absence of PBP1 or LtaS.

Appendix Figure S11. Results of three independent experiments supporting Fig 4C.

Appendix Figure S12. Results of three independent experiments supporting Fig 4D.

Appendix Figure S13. Effect of magnesium in culture medium on the production of LytE and LtaS and accumulation of LtaS/YfnI and LytE in synthetically sick strains *ΔponA* MprF ↑ and *ΔponA ΔugtP*.

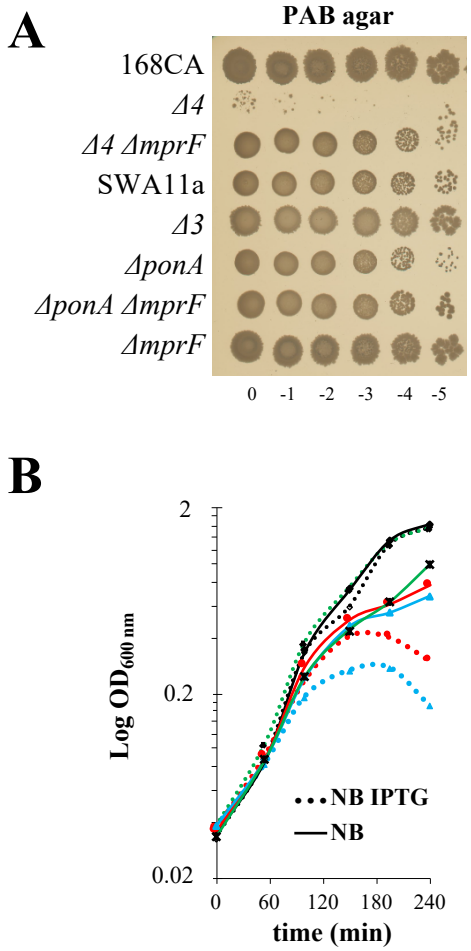

Appendix Figure S1. Other growth condition assays supporting Fig 1.

A Ten-fold spot growth assays of strains *B. subtilis* wild type 168CA, AG157 (*ΔponA ΔpbpD ΔpbpF ΔpbpG* renamed *Δ4*), AG223 (*Δ4 ΔmprF*), SWA11a (*ΔponA ΔpbpD ΔpbpF mprF::TnYLB-1 lacA*), AG417 (*ΔpbpD ΔpbpF ΔpbpG* renamed *Δ3*), RE101 (*ΔponA*), AG193 (*ΔponA ΔmprF)* and AG181 (*ΔmprF*). Serial dilutions were spotted onto nutrient agar (NA) with or without glucose 1% (**Fig 1B**) as well as on PAB agar (this figure). Plates were incubated at 37°C for 24 h and imaged.

B Overnight cultures of strains were diluted back in NB and grown at 37°C in presence or absence of IPTG (dashed or solid lines, respectively). Growth curves of strains carrying $P_{hyspank}$-*mprF* are displayed with the following code: wild-type-like MprF ↑ (black, diamond symbol, AG304 strain), *ΔponA* MprF ↑ (red, round symbol, AG311 strain), *Δ4* MprF ↑ (blue, triangle symbol, AG317 strain) and *Δmbl* MprF ↑ (green, square-cross symbol, AG322 strain).

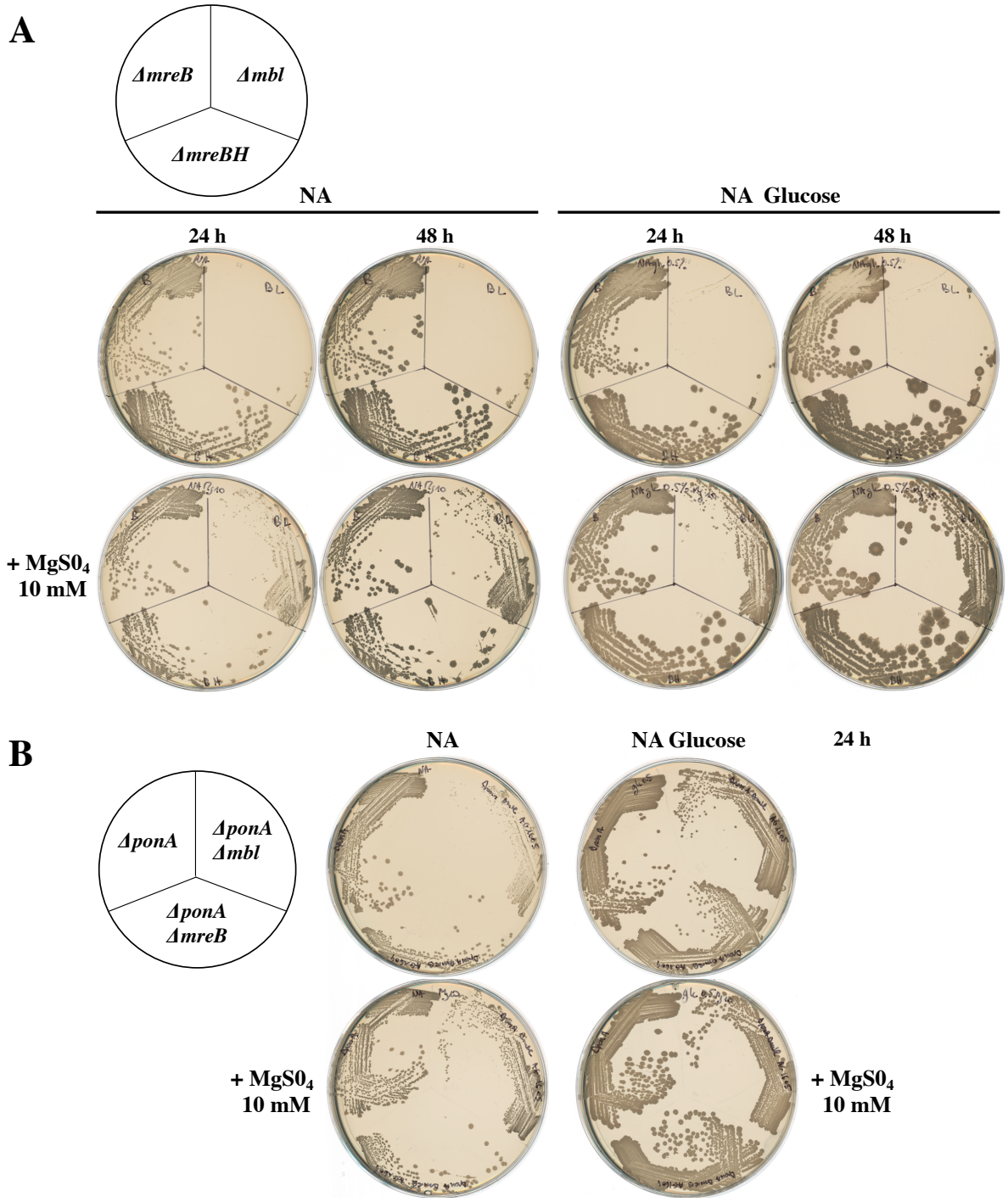

Appendix Figure S2. Growth of actin like mutants in 168CA background and in absence of *ponA*.

Strains were streaked from the glycerol stock onto NA plates supplemented with antibiotic and/or magnesium, where required. After incubation at 37°C overnight, a single colony for each strain was then streak across the set of plates (Glc 0.5%) shown above and scanned after 24 h or 48 h incubation at 37°C. The following strains obtained in 168CA background were inoculated: (A) *ΔmreB* (KS36), *Δmbl* (AK045B), *ΔmreBH* (AG1593); (B) *ΔponA* (RE101), AG1605 (*ΔponA Δmbl*), AG1604 (*ΔponA ΔmreB*).

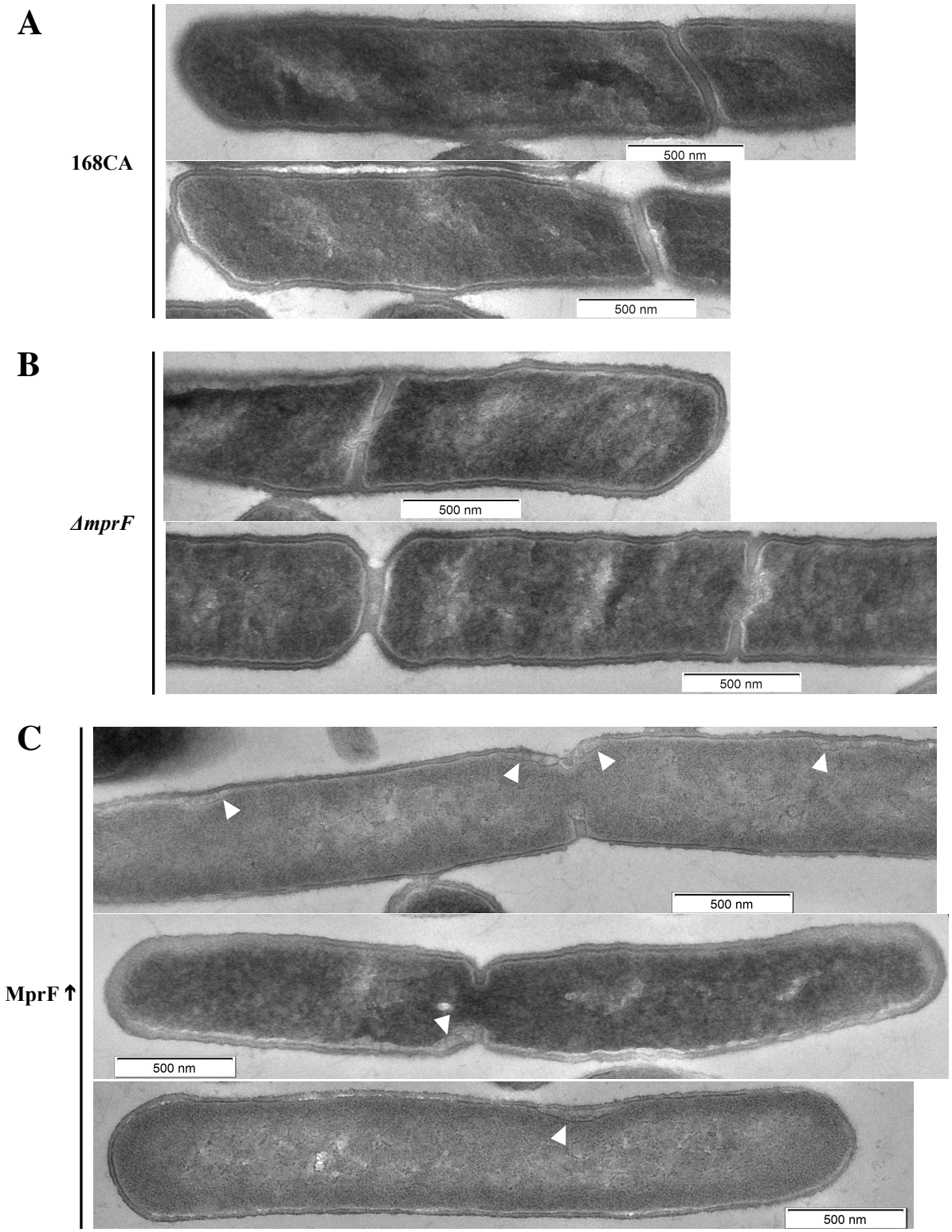

Appendix Figure S3. Additional TEM images of *B. subtilis* strains.

Figure shows images of cross-sections of *B. subtilis* 168CA (**A**), *mprF* mutant (AG181) (**B**) and strain overexpressing *mprF* (AG304) (**C**) grown in nutrient broth (with IPTG present to overexpress *mprF*). Samples were taken in mid-exponential growth. Arrows indicate abnormal cell wall structures that seem specific to the overexpression of *mprF*. All images were taken at 15,000x magnification and processed in ImageJ (Fiji) with scale bars attached.

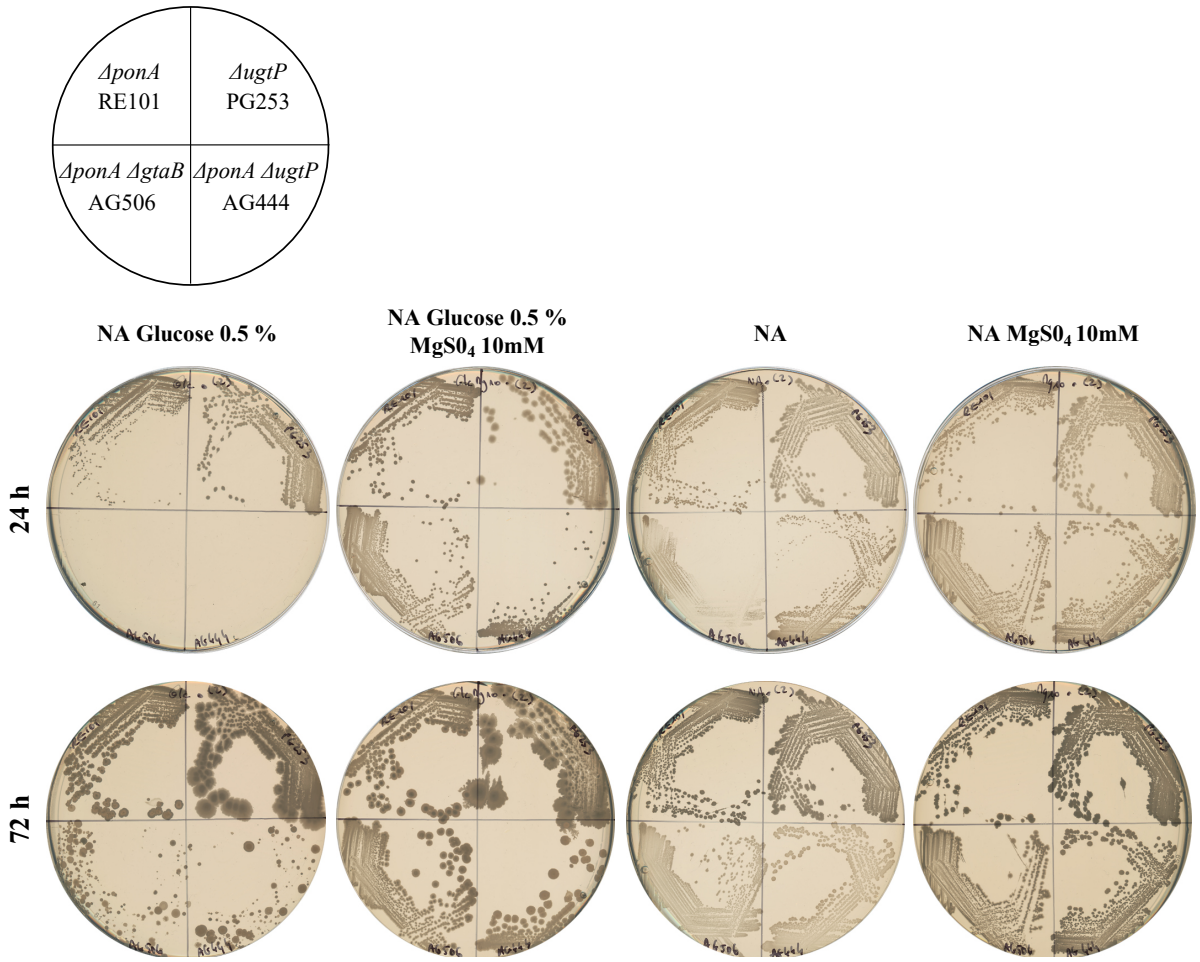

Appendix Figure S4. Absence of *gtaB* or *ugtP* causes severe growth defect in absence of *ponA*.

Strains were taken from the glycerol stocks onto NA plate supplemented with antibiotic and/or magnesium, where required. After incubation at 37°C overnight, a single colony was then streak across a set of plates shown above. The top plan indicates the strains used and their position in the pictures taken after 24 h and 72 h incubation at 37°C.

A

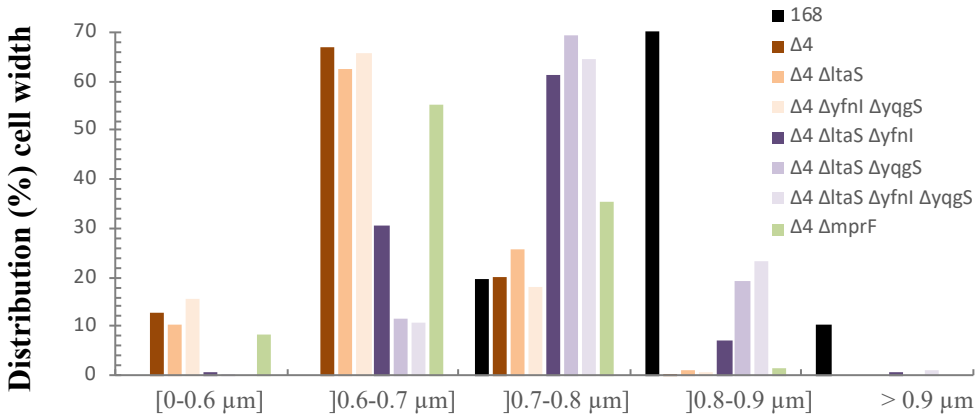

B

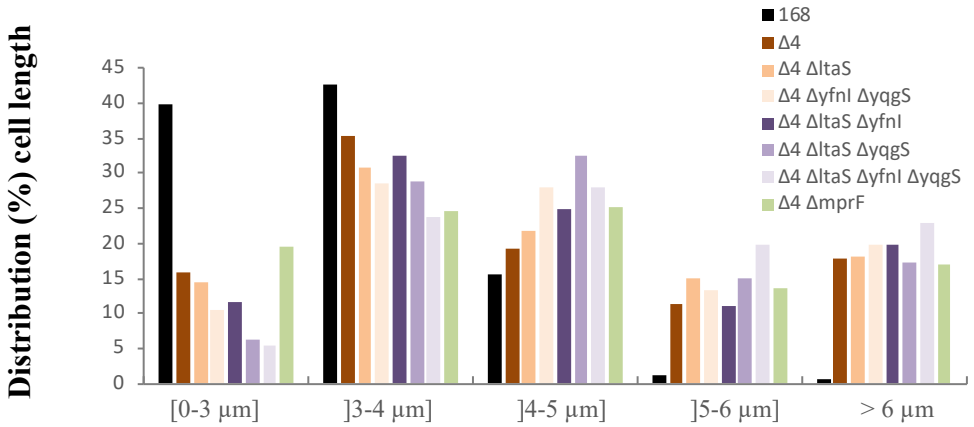

C

strains	**168CA**	***Δ4***	***Δ4 ΔltaS***	***Δ4 ΔltaS ΔyfnI***	***Δ4 ΔltaS ΔyqgS***	***Δ4 ΔyfnI ΔyqgS***	***Δ4 ΔltaS ΔyfnI ΔyqgS***	***Δ4 ΔmprF***
average cell width (µm)	0.8399	0.6595	0.6679	0.7269	0.7560	0.6538	0.7666	0.6793
stdev	0.0469	0.0492	0.0550	0.0528	0.0499	0.0513	0.0529	0.0546
average cell lenght (µm)	3.258	4.557	4.828	4.873	4.926	4.813	5.312	4.659
stdev	0.787	2.075	2.325	2.240	2.301	1.926	2.651	2.180
cells counted	437	419	414	426	420	423	416	399

Appendix Figure S5. Cell morphogenesis changes associated with deletion of LTA-synthase genes combined with class A PBPs null mutants of *B. subtilis*.

All the strains grew exponentially in NB with 10 mM $MgS0_4$, were washed and diluted in NB. Strains 168CA, AG157 (*Δ4*), AG342 (*Δ4 ΔltaS*), AG377 (*Δ4 ΔyfnI ΔyqgS*), AG370 (*Δ4 ΔltaS ΔyfnI*), AG372 (*Δ4 ΔltaS ΔyqgS*), AG380 (*Δ4 ΔltaS ΔyfnI ΔyqgS*) and AG223 (*Δ4 ΔmprF*) (**Table EV2**) grown for 120 min until mid-exponential at 37°C. Cells were stained with FM5-95 dye and microscopy images were acquired. Cells were measured using plugin ObjectJ in ImageJ. About 400 cells were counted for each strain. Content of the figure is from data acquired by one experiment only. Due to the formation of twisted cell chains, the cells measurement of *Δ4 ΔltaS ΔyfnI ΔyqgS* strain was done on the straight regions of the chain. Distributions of cell width **(A)** and cell length **(B)**. **(C)** indicates the average of cell width and cell length in the cell population analysed.

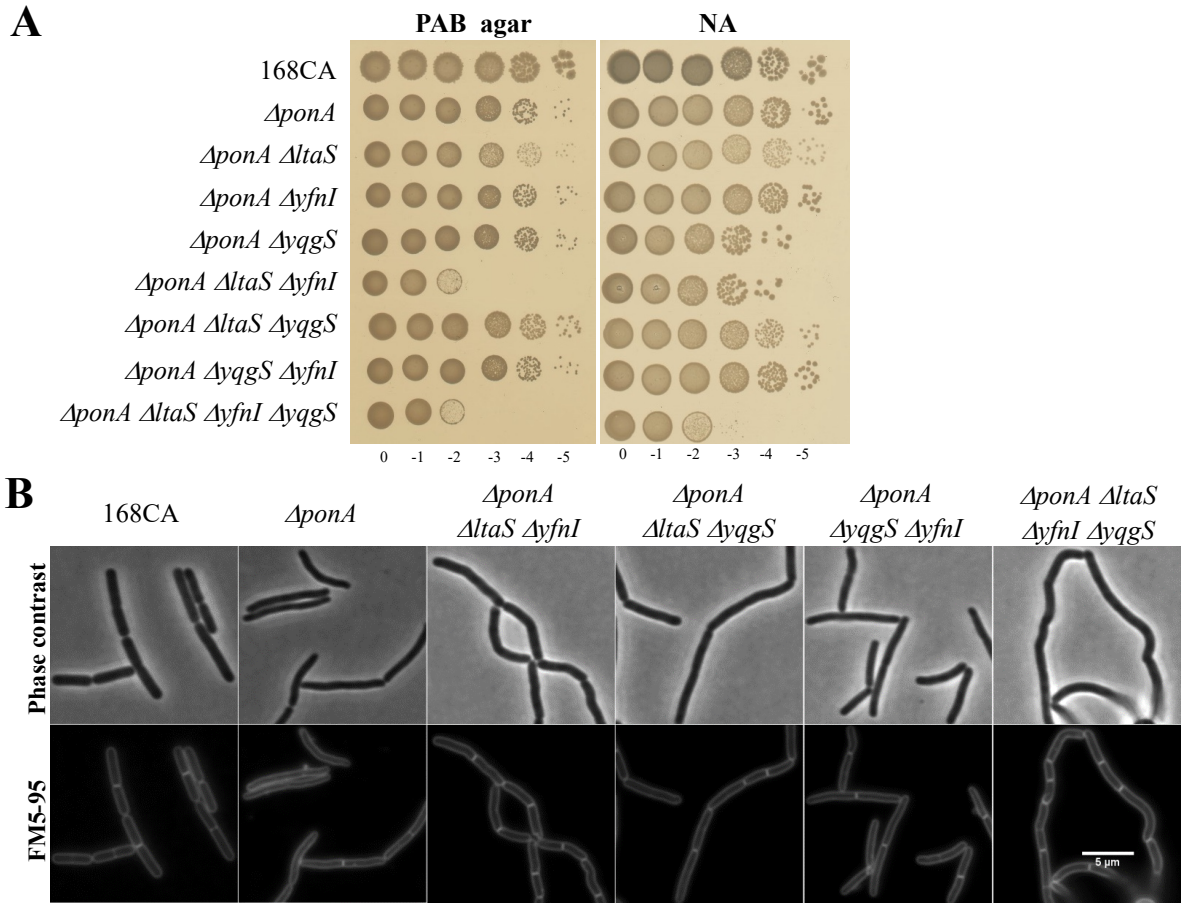

Appendix Figure S6. Effect of LTA-synthase deletions in *ΔponA* background.

A 10-fold serial dilutions were prepared in NB as in previous assays for strains 168CA, RE101 (*ΔponA)*, AG383 (*ΔponA ΔltaS*), AG384 (*ΔponA ΔyfnI*), AG385 (*ΔponA ΔyqgS*), AG393 (*ΔponA ΔltaS ΔyfnI*), AG394 (*ΔponA ΔltaS ΔyqgS*), AG395 (*ΔponA ΔyfnI ΔyqgS*) and AG403 (*ΔponA ΔltaS ΔyfnI ΔyqgS*) (**Table EV2**). Plates were incubated at 37°C and imaged at 22 h.

B Strains described in (A) were diluted in NB and grown at 37°C for 120 min. When cells reached mid-exponential phase, cell membranes were stained with a FM5-95 dye and observed under a microscope. Representative images were assembled in photoshop. Scale bar represents 5 µm.

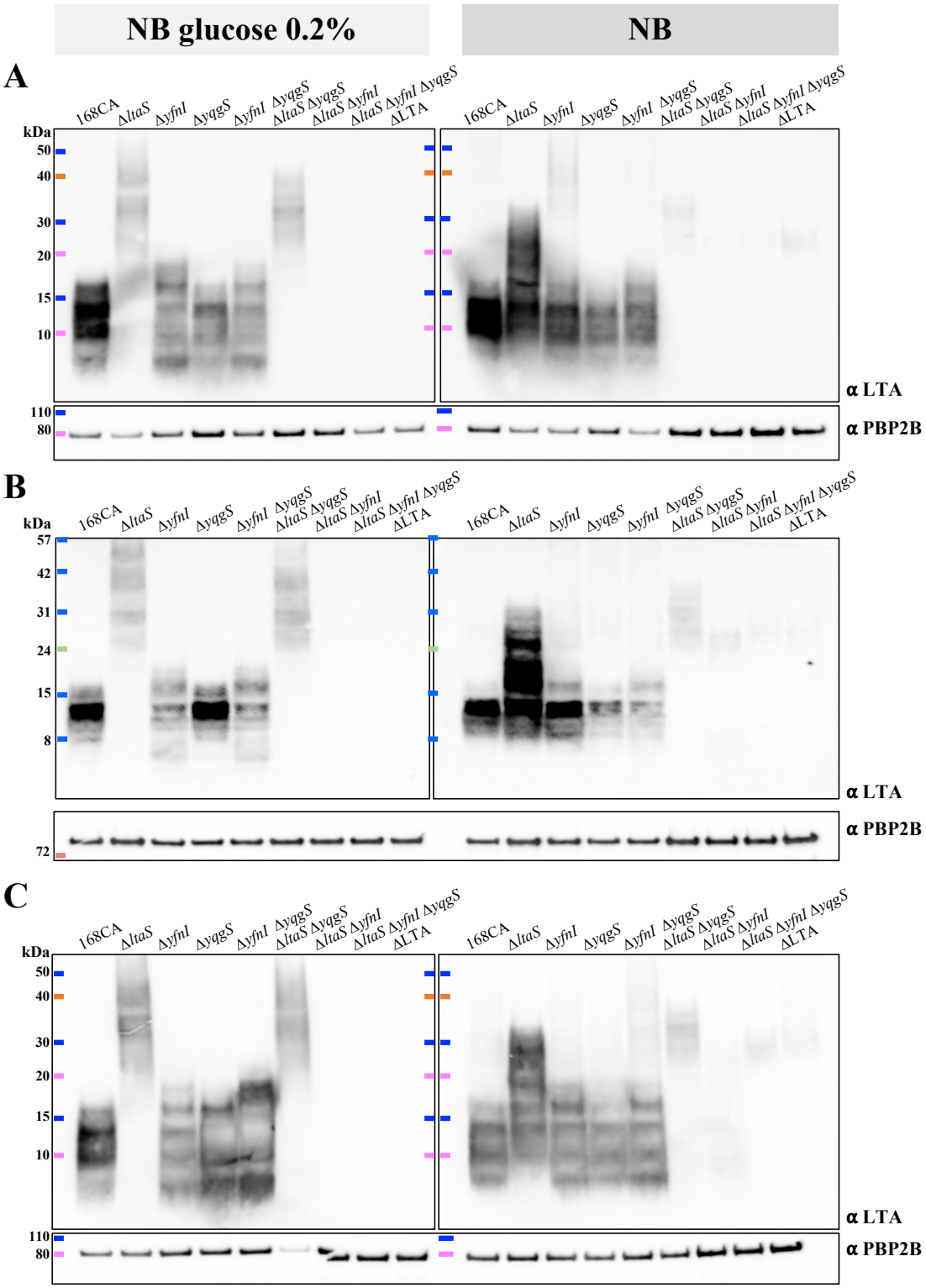

Appendix Figure S7. Results of three independent LTA Western blots supporting Fig 3A.

The lower part of the membrane was probed using a monoclonal LTA antibody and an HRP-linked anti-mouse antibody. The other membrane part was probed using polyclonal anti-PBP2B and HRP-linked anti-rabbit antibodies, to provide a sample loading control. Samples were prepared from strains *B. subtilis* wild type (168CA), 4285CA (*ΔltaS*), 4289CA (*ΔyfnI*), 4292CA (*ΔyqgS*), AG595 (*ΔyfnI ΔyqgS*), AG593 (*ΔltaS ΔyqgS*), AG594 (*ΔltaS ΔyfnI*), AG600 (*ΔltaS ΔyfnI ΔyqgS*) and 4620 (*ΔltaS ΔyfnI ΔyqgS ΔyvgJ*, noted here *Δ*LTA).

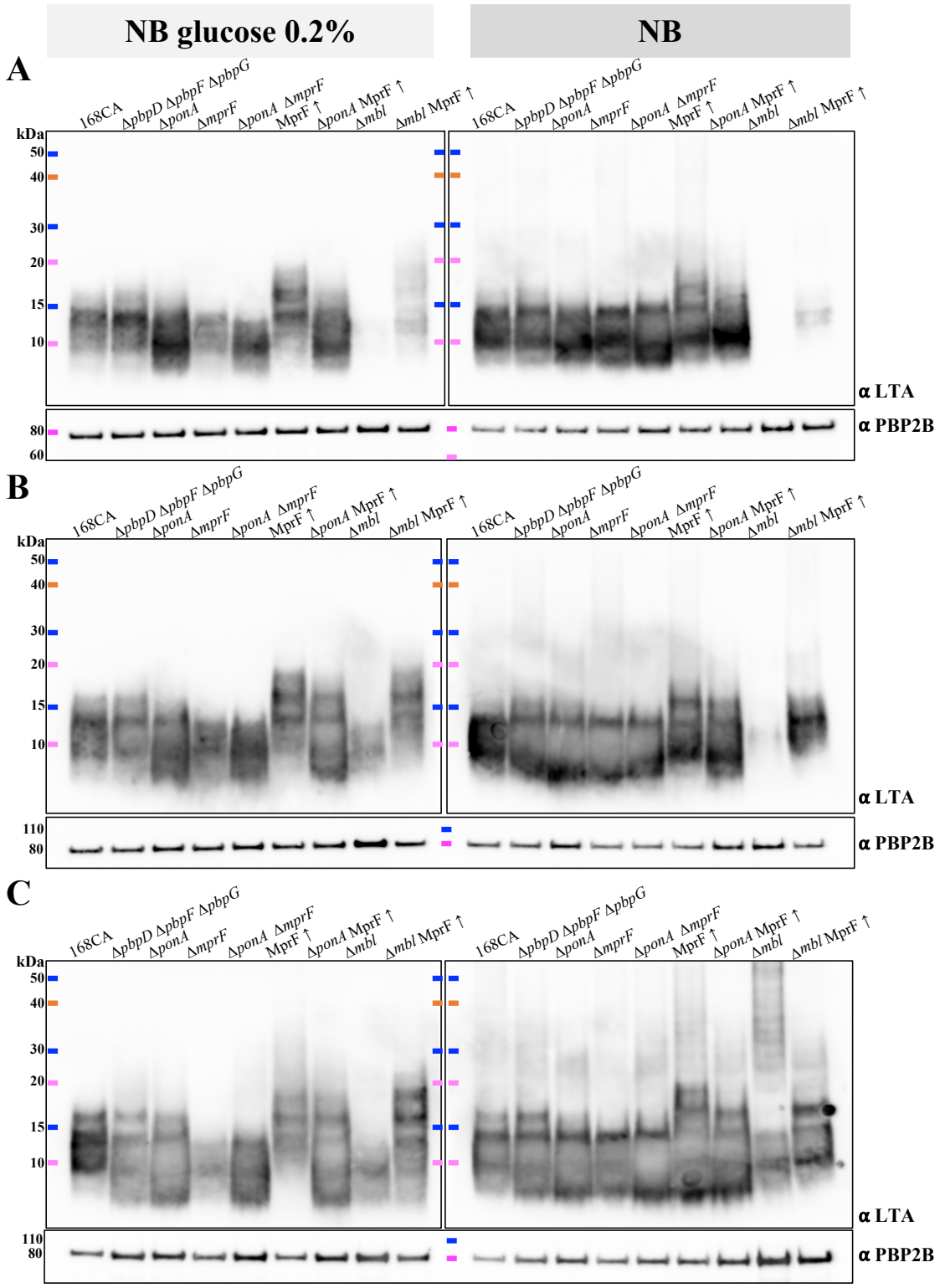

Appendix Figure S8. Results of three independent LTA Western blots supporting Fig 3B.

The lower part of the membrane was probed using a monoclonal LTA antibody and an HRP-linked anti-mouse antibody. The other membrane part was probed using polyclonal anti-PBP2B and HRP-linked anti-rabbit antibodies, to provide a sample loading control. Samples were prepared from strains *B. subtilis* wild type (168CA), AG417 (*ΔpbpD ΔpbpF ΔpbpG*), RE101 (*ΔponA*), AG181 (*ΔmprF*), AG193 (*ΔponA ΔmprF*), AG304 (MprF ↑), AG311 (*ΔponA* MprF ↑), 4261CA *(Δmbl)*, AG322 *(Δmbl* MprF ↑).

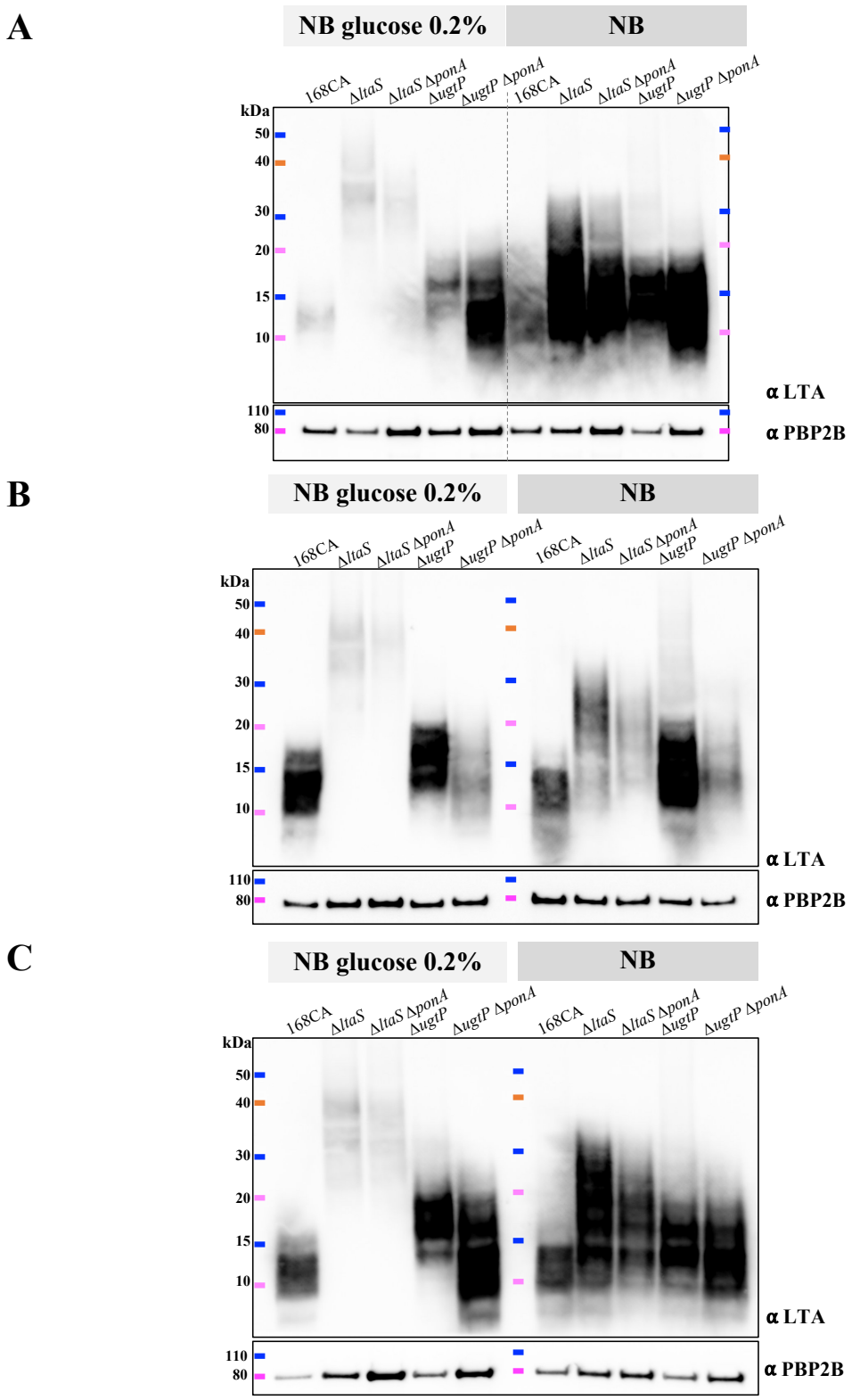

Appendix Figure S9. Results of three independent LTA Western blots supporting Fig 3C.

The lower part of the membrane was probed using a monoclonal LTA antibody and an HRP-linked anti-mouse antibody. The other membrane part was probed using polyclonal anti-PBP2B and HRP-linked anti-rabbit antibodies, to provide a sample loading control. Samples were extracted from *B. subtilis* 168CA, 4285CA (*ΔltaS*), AG383 (*ΔltaS ΔponA*), PG253 (*ΔugtP*) and AG444 (*ΔugtP ΔponA*) strains.

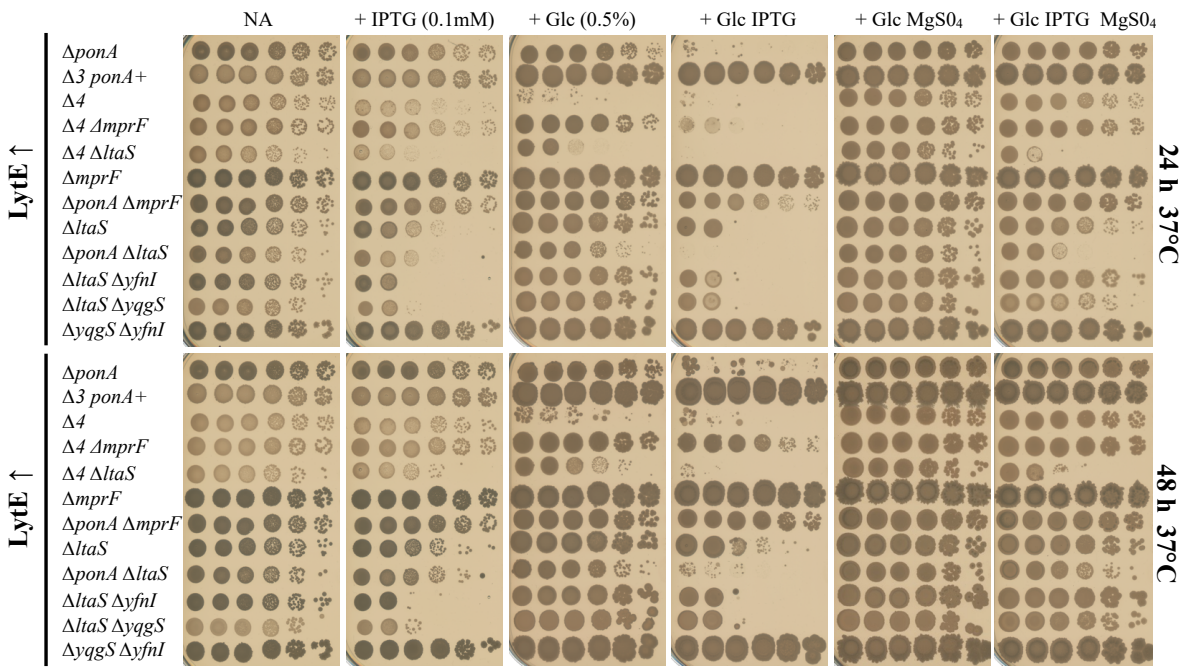

Appendix Figure S10. LytE overexpression is synthetically lethal in absence of PBP1 or LtaS.

lytE overexpression was analysed in strains which integrated at the *amyE* locus an IPTG-inducible $P_{hyspank}$-*lytE,* represented here LytE ↑. The strains tested had the following relevant features: AG484 (*ΔponA* LytE ↑), AG1460 (*Δ3 ponA*$^{+}$ LytE ↑), AG501 (*Δ4* LytE ↑), AG502 (*Δ4 ΔmprF* LytE ↑), AG1465 (*Δ4 ΔltaS* LytE ↑), AG1478 (*ΔmprF* LytE ↑), AG1479 (*ΔponA ΔmprF* LytE ↑), AG1462 (*ΔltaS* LytE ↑), AG1480 (*ΔponA ΔltaS* LytE ↑), AG1497 (*ΔltaS ΔyfnI* LytE ↑), AG1498 (*ΔltaS ΔyqgS* LytE ↑) and AG1499 (*ΔyqgS ΔyfnI* LytE ↑). The following strains that did not display any obvious phenotype are not represented here: AG475 (168CA LytE ↑), AG1461 (*ΔlytE* LytE ↑), AG1463 (*ΔyfnI* LytE ↑), AG1492 (*ΔyqgS* LytE ↑). NA plates were supplemented with IPTG (0.1 mM), glucose Glc (0.5%) and $MgS0_4$ (10 mM). Plates were incubated at 37°C and scanned after 24 h (**Fig 4A**) and 48 h.

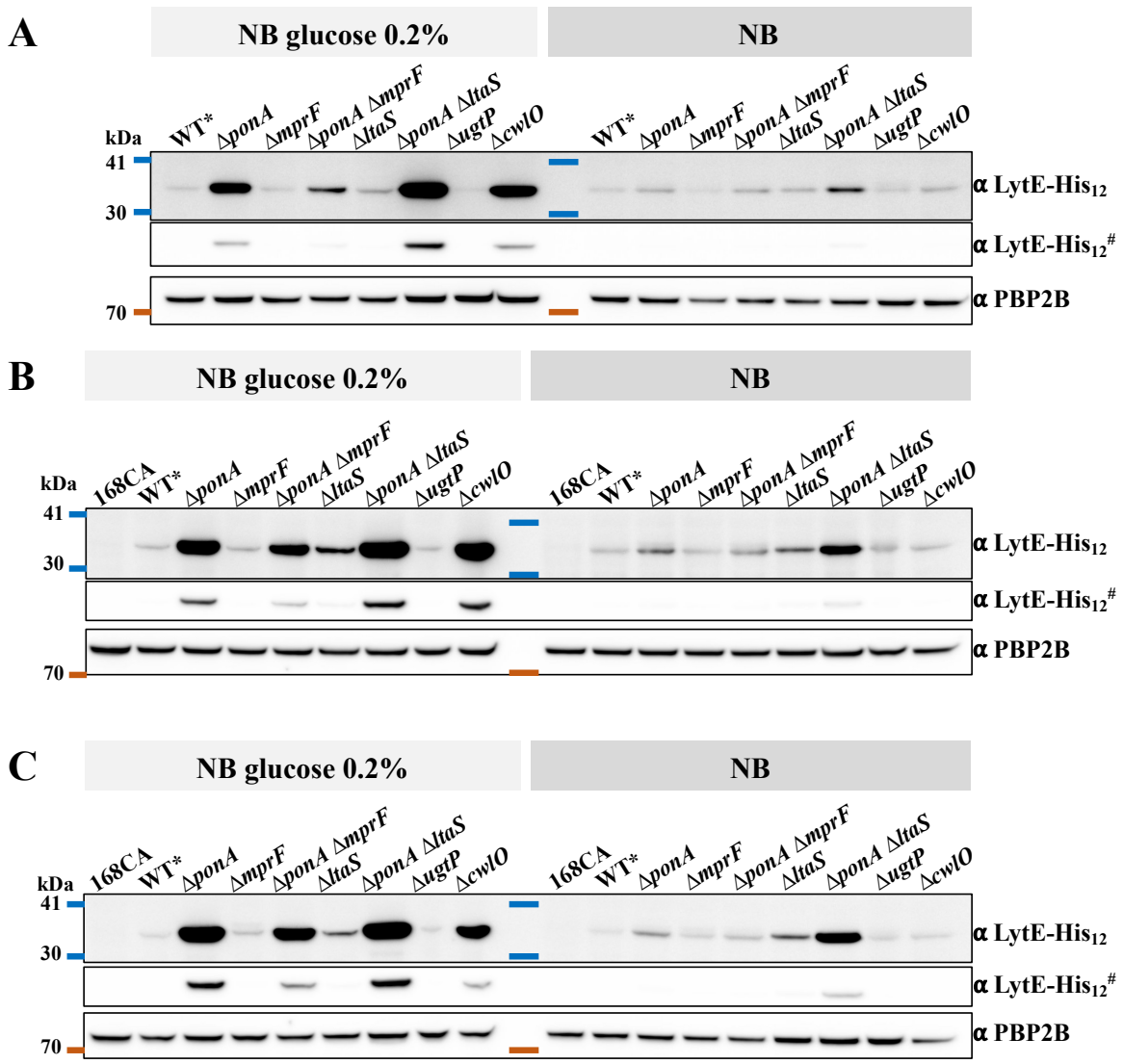

Appendix Figure S11. Results of three independent experiments supporting Fig 4C.

Relative abundance of LytE and PBP2B protein levels in mutant strains detected by Western blots. Strains expressing LytE-His_{12} under the control of its native promoter were grown in NB and NB supplemented with glucose 0.2% until late exponential growth at 37°C. For simplification on this figure only the relevant background feature is displayed for the following strains: wild type-like AG565 (WT*), AG587 (*ΔponA*), AG1486 (*ΔmprF*), AG1487 (*ΔponA ΔmprF*), AG1489 (Δ*ltaS*), AG1488 (*ΔponA ΔltaS*), AG1535 (*ΔugtP*) and AG1541 (*ΔcwlO*). In addition, the wild type 168CA (i.e. not expressing LytE-His_{12}) was grown in parallel and used here as a negative control for the LytE-blot. The bottom part of the membrane (split at ~ 53 kDa position) was incubated with a monoclonal Penta-His and an HRP-linked anti-mouse antibodies. The top membrane part was detected with a polyclonal anti-PBP2B and HRP-linked anti-rabbit antibodies. # For each section, the middle panel corresponds to the raw image of the LytE-His_{12} blot at a detection time where one of the sample signals has already reached saturation.

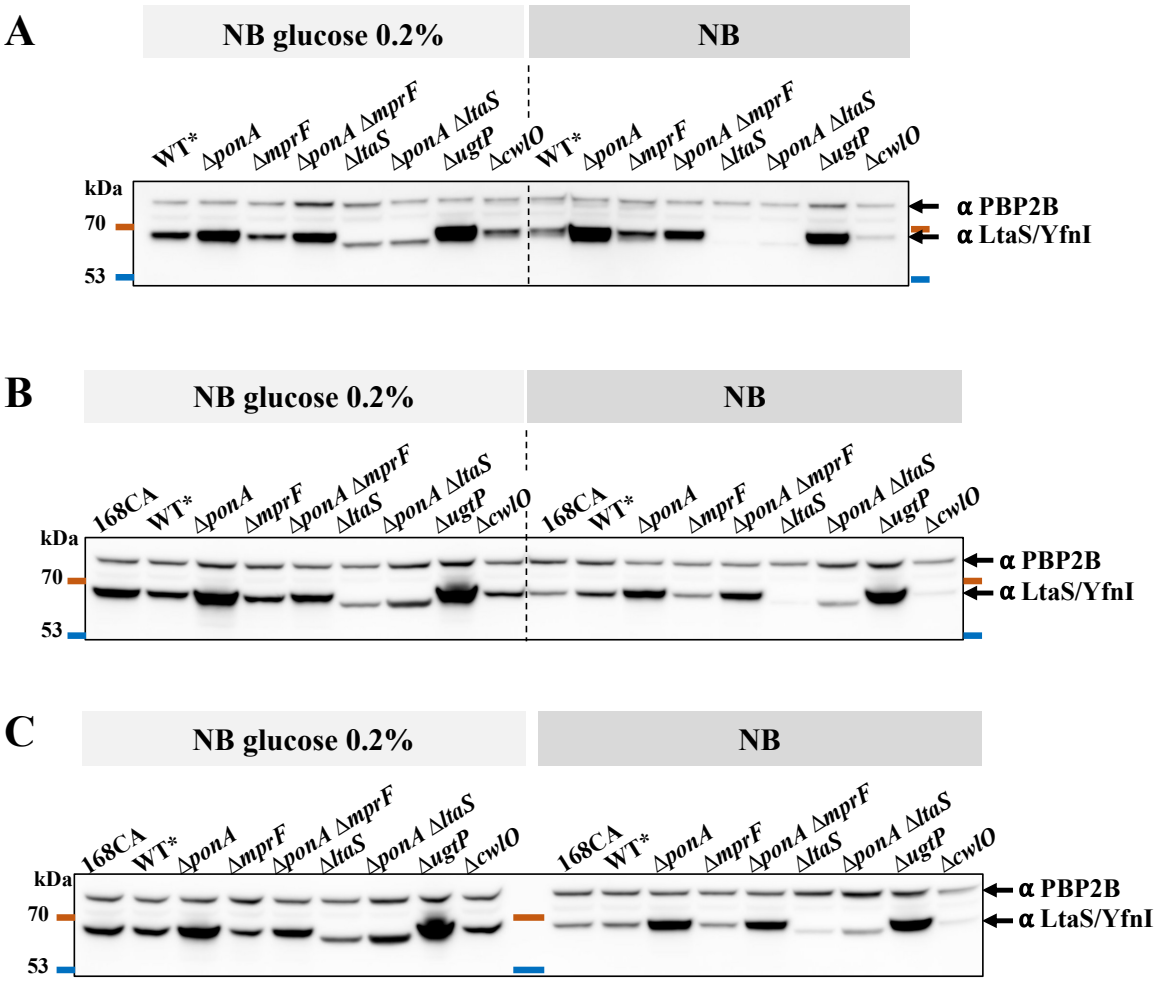

Appendix Figure S12. Results of three independent experiments supporting Fig 4D.

Relative abundance of LTA-synthases LtaS, YfnI and PBP2B protein levels in mutant strains detected by Western blots. The samples used in Appendix Figure S10 were loaded on a new SDS-gel and the Western blot was carried out with polyclonal anti-LtaS (that cross reacts with YfnI, unpublished Errington's lab), anti-PBP2B antibodies, and HRP-linked anti-rabbit antibody. A weak non-specific protein band is observed between PBP2B and LtaS and is detected by the anti-PBP2B antibody. Strains expressing LytE-His_{12} under the control of its native promoter were grown in NB and NB supplemented with glucose 0.2% until late exponential growth at 37°C. For simplification on this figure only the relevant background feature is displayed for the following strains: 168CA, wild type-like AG565 (WT*), AG587 (*ΔponA*), AG1486 (*ΔmprF*), AG1487 (*ΔponA ΔmprF*), AG1489 (Δ*ltaS*), AG1488 (*ΔponA ΔltaS*), AG1535 (*ΔugtP*) and AG1541 (*ΔcwlO*).

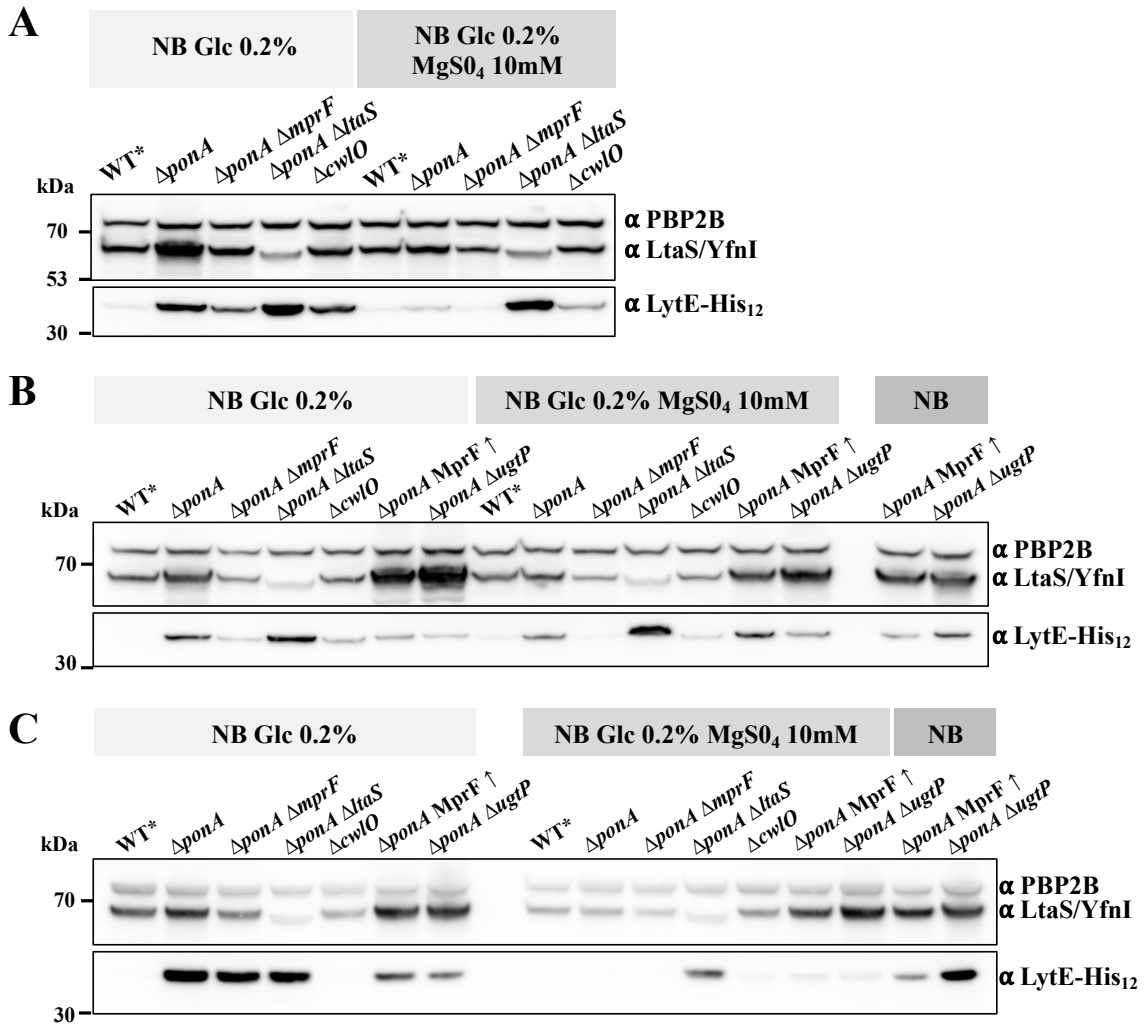

Appendix Figure S13. Effect of magnesium in culture medium on the production of LytE and LtaS and accumulation of LtaS/YfnI and LytE in synthetically sick strains Δ*ponA* MprF ↑ and Δ*ponA* Δ*ugtP*.

Detection of LytE-His$_{12}$ and PBP2B by Western blots. Strains expressing LytE-His$_{12}$ under the control of its native promoter were grown in NB supplemented with glucose 0.2% with or without $MgS0_4$ (10 mM) at 37°C. For simplification on this figure only the relevant background feature is displayed for the following strains: wild type like AG565 (WT*), AG587 (*ΔponA*), AG1487 (*ΔponA ΔmprF*), AG1488 (*ΔponA ΔltaS*), AG1541 (*ΔcwlO*), AG1684 (*ΔponA* MprF ↑) and AG1685 (*ΔponA ΔugtP*). The last two strains were also grown in parallel in NB. The top membrane part was incubated with polyclonal anti-LtaS (that cross reacts with YfnI, unpublished Errington's lab), anti-PBP2B antibodies, and HRP-linked anti-rabbit antibody.The bottom part of the membrane was incubated with a monoclonal Penta-His and an HRP-linked anti-mouse antibodies. Images were processed in ImageJ software. Results of three independent experiments are presented here.

983